Ministero dell'Universitá e
della Ricerca

Dipartimento di Scienze
Fisiche ed Astronomiche

Universitá degli Studi
di Palermo

Dipartimento di Scienze Fisiche e Astronomiche
Dottorato di Ricerca in Fisica – XX Ciclo

Insulin Fibril Formation: Growth Mechanisms and Fiber Morphologies

S.S.D. FIS/07

Vito Foderá

Palermo, Febbraio 2009

Supervisore: Prof. Maurizio Leone

Coordinatore: Prof. Antonio Cupane

Contents

Outline of the work

Aggregation processes, and in general the physical and chemical instability of proteins, are at the moment a major problem related to different scientific fields, spanning from biochemistry and biophysics to pharmaceutical and medical sciences. In fact, increased knowledge on protein aggregation may clarify different aspects related to several degenerative pathologies like Alzheimer's and Parkinson's diseases, type-II diabetes, etc. Because of this high social impact, in the last decades scientific community has addressed a lot of efforts towards the comprehension of the cause-effect relationship between the protein aggregation phenomenon and the clinical aspects of the diseases presenting such proteinaceous assemblies.

Moreover, in the pharmaceutical sciences, protein instability represents one the obstacle to be overcome for the development of reliable protein delivery systems. For this reason, a deeper understanding of the molecular mechanisms leading to aggregates formation is also necessary to improve purification, storage, and delivery of protein-based drugs. The huge number of studies on this topic has also evidenced that propensity of protein to aggregate can be generally considered as a common feature for each polypeptide chains, making this kind of studies relevant also for the scientific basic research.

In this work protein hormone insulin has been chosen as a model system. The reasons of this choice are strictly connected to the large use of this molecule in protein-based drugs as well as to its propensity to form amyloid aggregates with mechanisms similar to those of other disease-related proteins. As a consequence, insights on insulin stability in adverse conditions as well as on mechanisms of aggregate formation could have a double relevance.

The Thesis is divided in 5 Chapters, two introductive (Chapters 1 and 2) and three on the experimental results (Chapters 3, 4 and 5). Aim of this work is to focus on the aggregation processes of insulin paying particularly attention to the mechanisms involved in two different experimental conditions (Chapter 3 and 4). Moreover, efforts have been also put in clarifying and testing the reliability of a detection tool largely used in this study, i.e. fibril staining by the specific fluorescent marker Thioflavin T (ThT) (Chapter 5).

In Chapter 1, an overview of protein aggregation processes, in particular amyloid aggregation, will be provided contextualizing it in the more general scientific topic of protein folding. Moreover, the concept of nucleation-dependent process is presented together with a mathematical description of these phenomena. A description of the model system here employed, insulin, and a discussion on the literature related to insulin fibrillation process will complete the chapter.

In Chapter 2, detailed information on the employed instrumentations and experimental tools will be provided. Further, because of the wide use of the fluorescent amyloid sensitive probe Thioflavin T (ThT), the theoretical background on the optical and structural features of this dye is also discussed. Finally, the last part of the chapter is dedicated to the materials, samples preparation and treatments procedure used.

In Chapter 3, an analysis of the fibrillation kinetics of human insulin as a function of the initial protein concentration is presented, evidencing the occurrence of different mechanisms during the kinetics. Finally, process stochasticity and variability of the kinetic parameters are also taken into account. The experiments on human insulin samples have been performed in the framework of the collaboration with Novo Nordisk A/S, Denmark (January 2006) that kindly provides human insulin powder.

In Chapter 4, aggregation processes involving bovine insulin in HCl solution will be analyzed. Combining spectroscopic and imaging techniques, a highly variegated features of processes are pointed out. Different aggregation pathways, morphologies, nucleation mechanisms and spatial heterogeneity in the early stages are discussed, supplying a scenario of the interconnected events taking place in these conditions.

In Chapter 5, a characterization of the chemical and physical stability of Thioflavin T as a function of pH, temperature and dye concentration is presented. Experimental data reveal a significant effect of these parameters on the reliability of the dye as a tool for specific staining of fibrils.

Finally, a summary of the results together with suggestions to further develop specific problems raised in this Thesis constitute the *Conclusions and Perspectives* paragraph.

Chapter 1

Overview on protein aggregation

[...]man had always assumed that he was more intelligent than dolphins because he had achieved so much - the wheel, New York, wars and so on - whilst all the dolphins had ever done was muck about in the water having a good time. But conversely, the dolphins had always believed that they were far more intelligent than man - for precisely the same reasons[...]

[Douglas Adams, *Hitchhiker's Guide to the Galaxy*, 1979]

A general picture of the scientific contest in which the present work finds its place will be provided. After an introduction of the concept of protein folding, discussion will be addressed to the specific topic of protein aggregation, pointing out both the relevance of these studies and the approach generally used to describe such processes. Finally, a deep and detailed overview on the aggregation processes of the protein model chosen for this study, i.e. insulin, will be presented.

1.1 Protein *folding*, *misfolding* and aggregation

A living organism is a highly evolved system consisting of a large number of molecular networks. In such networks a key role is played by proteins. These macromolecules enable and control chemical processes that take place in the cell and they can be considered as a final result of a careful and refined pursuit provided by nature. In fact, originally each protein starts as a polypeptide, translated from a sequence of mRNA as a linear chain of amino acids without any specific three-dimensional arrangement [1]. Identification of the amino acids sequences of a large number of human-related proteins was one of the result of the Human Genome Project started at the beginning of 90's and finalized in 2003. After such mapping, one of the still open questions was related to the molecular mechanisms involved in building up a

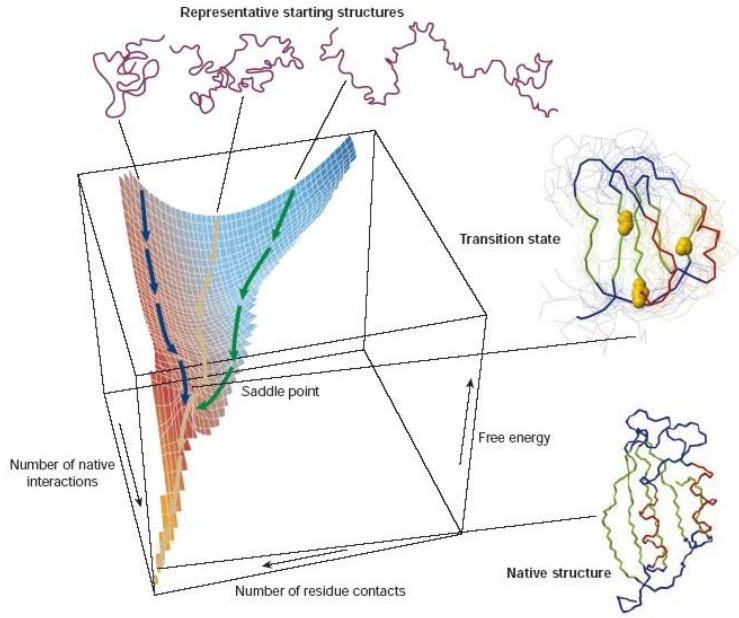

Figure 1.1: A schematic energy landscape for protein folding. The surface is derived from a computer simulation of the folding of a highly simplified model of a small protein. The surface funnels the multitude of denatured conformations to the unique native structure. The critical region on a simple surface such as this one is the saddle point corresponding to the transition state, the barrier that all molecules must cross if they have to fold to the native state. Figure and caption are adapted from the original paper [2].

protein structure able to fulfil its biological function. In fact, reaching a functional structure *via* specific interactions between single residues of the aminoacidic chains is the fundamental process at the basis of the correct functionality of the living system. Such process, referred as *folding*, has been subject of a huge number of studies since the 70's, being counted among the so called *complex systems* descriptions. As a consequence, due to the enormous number of variables affecting this process, the study of the behavior of proteins following synthesis within a living organism requires tools developed in mathematics, physics, chemistry, cell biology and medicine to gain a proper understanding of the molecular events [1].

The capability of a random sequence of a polymer to fold into a well defined structure is entirely contained within the sequence of amino acids in a polypeptide chain [3]. The connection between the sequence and the fold in polypeptides, and the stochastic manner in which the folding process enables the correct structure to be rapidly reached for any given sequence, represents a clear example of biological

complexity. Moreover, folding can be considered as a particular aspect of the more general phenomenon of the self-assembly in cell biology [1].

Native states of proteins almost always correspond to the structures that are most thermodynamically stable under physiological conditions [4]. To properly describe the folding pathway, the concept of *energy landscape* has been developed by Joseph Bryngelson and Peter Wolynes in the late 1980s and early 1990s [5, 6]. An example of this illustrative scheme is presented in Figure 1.1 [2]. A very large number of possible conformations (local minima of energy) of any polypeptide chain should be experienced before reaching the final and functional structure. Unfortunately, such a kind of process leads to a not reliable result for a standard folding process that under this assumption would take an astronomical length of time (*Levinthal's Paradox*). To overcome the Levinthal's Paradox, a reliable description of protein folding is based on the so called *principle of minimal frustration*. According to this principle, biological evolution has selected amino acid sequences with side chains, i.e. hydrophobic and polar residues [2], able to readily interact and reach the folded state. Such statement strongly reduces the number of energy minima that protein can experience or, equivalently, reduces the probability of exploring a huge number of different conformations [7–9]. With such assumption, the pathway to self-assembly in the folded state is reduced to a *preferential way* displayed as a colored surface in Figure 1.1 and not in a random search into the whole three-dimensional space. The preferential way is often referred in literature as the *funneled energy landscape*.

Clearly, details of the folding depend on the particular environment in which the process takes place, i.e. cell [2]. Along the pathway, not completely folded conformations (*intermediate states*) can temporally expose specific domains to the solvent leading to not proper interactions between residues and solvent molecules [10]. Such interactions reduce the probability to reach the native state and allow the occurrence of not functional species in the pathway. To prevent such occurrences, a sort of quality control of the folding pathway has been developed by biological evolution [10–12]. In fact, molecular chaperones are present in all the cell compartments and are not only involved in guiding later stages of the folding process, but they also interact with the chains just after the synthesis in the ribosome [11, 12].

Notwithstanding such prevention and also due to the stochasticity and the high complexity of the process, failure to correctly fold can always take place and it leads to malfunctioning of living systems and hence to diseases [13–15]. In the *funnel* picture (Figure 1.1), accessibility to this undesired states corresponds to the presence of not negligible local minima on the energy surfaces. In Figure 1.2, a scheme of the potential occurring species during the folding pathway is shown. When a specific polypeptide chain fails to fold or loses its closely-packed native state, a population of *unfolded* or *not correctly folded* states starts increasing. These new states are characterized by

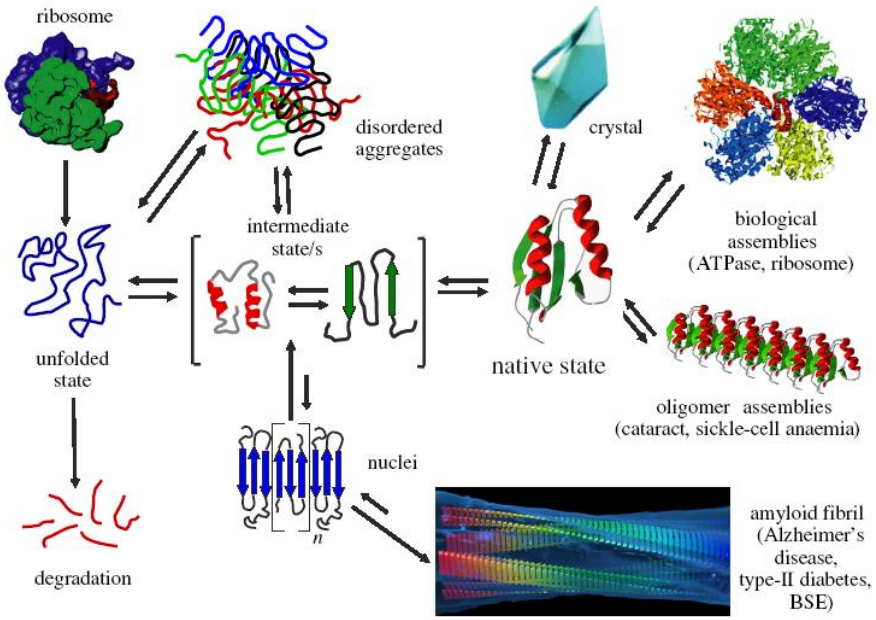

Figure 1.2: Scheme the states accessible to a protein following its biosynthesis on the ribosome. Figure and caption are adapted from the original paper [1].

a not so packed structure, so that such open arrangements of the protein molecules enhance the tendency to interact each other and assembly in oligomeric species [16]. Such interactions can lead to the formation of disordered aggregates often referred in literature as *amorphous*, or, by specific reactions, to the formation of highly ordered protein aggregates named *amyloid fibrils* (see Sections 1.2 and 1.3). Moreover, from the native state a number of other reactions can take place, giving rise to different structures as oligomer, biological assemblies and crystals [1].

The above mentioned aggregation mechanisms are not only confined at cellular level. In fact, under specific chemical and physical conditions, protein aggregation can also be induced *in vitro* starting from native protein solutions and making possible a deep investigation on the interactions involved in such phenomenon. The occurrence of aggregates deposits can be triggered by several factors, i.e. pH, temperature, ionic strength, denaturant agents [17–23]. In fact, formation of protein aggregates can be considered as a product of an interplay between protein-solvent and protein-protein interactions. Changing the physical properties of the solvent, i.e. pH far from the physiological values or high temperature, clearly affects the balance of the forces involved in the correct packing of the protein thus allowing new intermolecular interactions to take place. Several mechanisms are counted to properly explain the

molecular events, each one involved in different time and length scales.

Conformational changes leading to partially destabilized protein structures are commonly recognized as a key step in aggregation processes [24–27]. Specifically, such step includes a weakening of the tertiary interactions and simultaneously a favoring of all the secondary interactions, mainly hydrogen bonding. In these conditions, proteins misfold in molten globule-like structure, where the normally buried hydrophobic residues may become solvent-exposed. After such misfolding, aggregation can generally be formed in two steps rationalized in terms of the so-called nucleation-dependent model; the destabilized protein molecules interact with each other, forming a new high energy species referred to as the *nucleus*, from which, by subsequent addition of protein molecules, aggregates are formed.

Experimental results presented in this work are mainly focused on the formation of amyloid aggregates obtained by nucleated processes. In particular, temporal features of the fibril growth mechanisms will be analyzed in the sections of the experimental results (Chapter 3 and 4). For this reason, present knowledge on amyloid fibrils together with theoretical treatments of such processes will be briefly provided in the next two sections. For a proper introduction on the conformational changes involved in protein aggregation, specific forces involved, and for deeply reviewing this subject, it is suggested to refer to a more specialized work carried out in the biophysics research group in Palermo [28].

1.2 Ordered protein aggregates: amyloid fibrils

The term *amyloid* was introduced in 1854 by Virchow during his study on the cerebral corpora amylacea. Such term was used to indicate macroscopic deposits in the brain tissue being detectable by iodine staining [29]. In the 19th and early 20th centuries, investigations on the nature of amyloid evolved from the first macroscopic observations to the classifications of clinical symptoms in amyloid-related human diseases [30, 31]. For this reason, in the last decades, a great interest has been devoted to the understanding of the molecular mechanisms of amyloid formation [29].

Several human diseases with a high social impact as Parkinson's and Alzheimer's diseases, cystic fibrosis, diabete Type II, the spongiform encephalopathies such as Creutzfeldt-Jakob disease are characterized by the presence in the involved tissues of highly structured protein deposits. Generally, around 20 different amyloid-related proteins have been observed, being involved in human diseases (called *amyloidoses*). Although it is still not clear which is exactly the role of fibrils in the diseases and if and how amyloid deposition can be accounted as primary origin of the associated pathological conditions, a variety of experimental observations suggests that there is

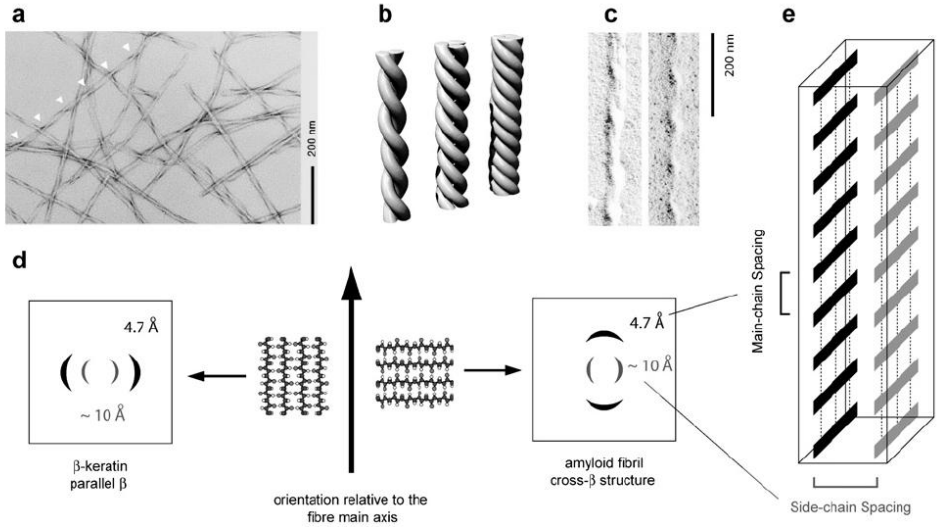

Figure 1.3: (a) Electron micrograph of Aβ(1−40) amyloid fibrils showing crossovers (arrow heads) at regular distance. (b) Schematic representation of fibrils consisting of 2, 3 and 4 protofilaments. (c) Fibril of Aβ(1−40) amyloid fibrils observed with transmission electron microscopy (TEM). (d) Schematic representation of the X-ray diffraction patterns of cross-β and parallel-β structures. (e) Protofilament structure interpretation based on X-ray diffraction (two laminated β-sheets, β-strands shown as black and grey bars; dotted lines indicate orientation of hydrogen bonds). In (b-e), the fibril main axis is aligned in the vertical direction. Figure and caption are adapted from the original paper [34].

a strong causal link between fibril formation and the onset of pathological symptoms [32, 33]. Interestingly, fibrils formation is not only a phenomenon related to human diseases. In fact, under specific and destabilizing conditions, i.e. high temperature, extreme pH value and denaturants presence, even globular proteins not related to any disease and with very different native structures can self-assembly forming regular structures similar to the ones exhibited in the amyloidoses. For this reason, such research topic seems to have a more general scientific impact.

The above reported definition of amyloid fibrils as *proteinaceous deposits in human tissues* is strictly related to the medical context in which they were firstly identified. However, studying the molecular mechanisms and the biophysical principles underlying fibrils formation requires a structure-based definition for amyloid aggregates [34]. For such reason, several *in vivo* and *in vitro* structural studies have been carried out and they revealed common features of these deposits independent of the precursor protein and/or of the specific human disease. In fact, fibrils commonly display a general template (Figure 1.3a, 1.3b and 1.3c). This type of structure has

been revealed by X-ray or electron diffraction showing a specific pattern as shown in Figure 1.3d. The characteristic distances in this pattern are interpreted in terms of a helicoidal distribution of β-sheet structure running perpendicularly around an elongation axis (*cross-β structure*). In the example shown in Figure 1.3e each sheet presents hydrogen bonds to the identical molecules above and below it in the same sheet. It must be noted that the side chains of each molecule are oriented in the same direction as those above and below, creating columns of hydrogen bonds running up and down the sheets [35]. Schematic periodicity shown in Figure 1.3d and 1.3e is revealed by transmission electron microscopy (TEM) evidencing the occurrence of fibrils several micrometers long with a diameter ranging from 5 to 25 nm [34]. Interestingly, it is generally believed that amyloid fibrils possess a well-defined twist of natural β-sheets leading to the schematic representation in Figure 1.3b where a number of metastable aggregate precursors, called *protofilaments*, interacts each others and form the final structure [17, 36, 37].
Moreover, amyloid fibrils show specific optical properties when bound in complex to proper markers, i.e. birifrangence with Congo Red and high quantum yield of fluorescence with Thioflavin T (see Section 2.1). Such specific binding can be used for amyloid diagnosis but it depends on solution and staining conditions [38–42]. Further, by means of Fourier-transform infrared (FTIR) spectroscopy specific bands centered at 1620 cm^{-1} and 1685 cm^{-1} occur in presence of amyloid β-sheets structures [43]. All such criteria for amyloid identification have been clearly reviewed together with an interesting discussion on the experimental tools to study fibrils formation *in vitro* by Nilsson [44].
Besides the structure of amyloid fibrils occurring during the fibrillogenesis kinetics, the mechanisms underlying the growth of amyloid fibrils represent one of the crucial points that need to be clarified. Studying such aspect could be a preliminary investigation for individuating fibril precursors and should represent a first step towards a reliable pharmaceutical formulation able to block the onset of mature fibrils in the human organ or tissues. Further, a study on the molecular mechanisms of fibrils formation has to be considered in the more general scientific problem related to the protein stability and protein delivery system. For these reasons, in this Thesis interest has been addressed to the analysis of the fibrillation kinetics profile to clarify the mechanism involved. To properly describe and correctly understand the experimental data related to insulin fibrillogenesis (see Section 1.4 for a background on the subject) nucleation-elongation model has been taken into account [45–48] and its main features will be presented in the next Section.

1.3 Nucleation mechanisms in protein aggregation

A main goal of a mathematical modeling of protein aggregation kinetics is to describe the time course of the reaction also predicting the dependence of the temporal features of the process on critical parameters such as temperature and protein concentration. To build up a model, a molecular mechanism need to be assumed, so that the rate constants of the process together with their dependence on the parameters can be obtained. With the aim of supporting the description and discussion of the experimental results, in the following sections a short introduction of the mathematical approach to describe the nucleation processes will be provided. The description is mostly based on the concepts and the mathematical modeling developed by Ferrone and coworkers in the 80's, working on HbS polymerization. A more detailed and deep description of these results is elegantly presented by Ferrone in a complete and exhaustive review [47].

1.3.1 Homogeneous and secondary nucleation

Amyloidogenic proteins, like other fiber-forming proteins, have been suggested to self-assembly by a nucleated polymerization mechanism and a simplified scheme of this process is presented in Figure 1.4. In a nucleated polymerization two main steps can be identified. A first sequence of reactions takes into account the unfavorable assembling of monomers to form oligomeric species proceeding with association and dissociation rate constants a and b, respectively (Figure 1.4). After subsequent monomer addition and a series on unfavorable equilibria, oligomer reaches a critical size (X_n, different in dependence on the specific polymerization) that defines the so called *nucleus*. Since this point, another sequence of reactions takes place and attachment of monomer to the nucleus is characterized by new kinetic parameters (a and c in Figure 1.4 with $c<b$) with a very high monomer-nucleus affinity that makes practically irreversible the reaction. Last step is known as elongation mechanism and proceeds up to a complete depletion of the monomer population.

Nucleated polymerization has several well-known features according to the classical model: 1) a critical concentration, below which fibrils cannot form, 2) a strong dependence of the fibril formation rate on concentration, which increases with the size of the nucleus [47–49]. Based on the scheme presented in Figure 1.4, temporal behavior of the polymerization reaction can be predicted. If c^* and J^* are the concentration of nuclei and the rate of elongation of the nucleus, respectively, a differential equation for the time-dependence of polymer concentration (c_p) can be wrote:

$$\frac{dc_p}{dt} = J^* \cdot c^* \tag{1.1}$$

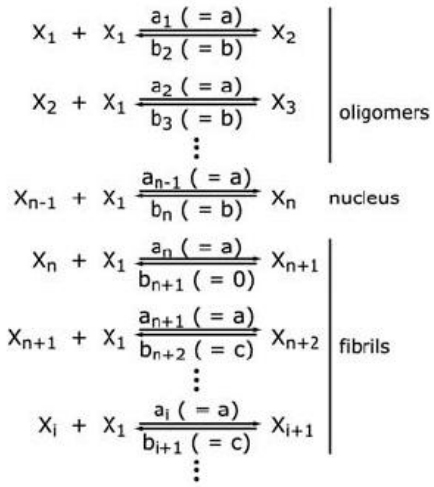

Figure 1.4: The sequence of reactions in a nucleated polymerization. Aggregates are assumed to grow by monomer addition. The association and dissociation rate constants are shown above and below the arrows, respectively. The n-mer, X_n, is known as the nucleus. Smaller species are called oligomers, whereas larger species are called fibrils. Figure and caption are adapted from the original paper [50].

Moreover, assuming that polymers can increase in mass only by attachment of monomers to their ends and each attachment proceeds with the same elongation constant J independent of the length of the polymer, a differential equation for the monomer that have gone into the polymer, $[c_0 - c(t)]$, can be established:

$$\frac{d}{dt}[c_0 - c(t)] = J \cdot c_p \tag{1.2}$$

Equations 1.1 and 1.2 together do not have an analytical solution and they can be only numerically integrated. Notwithstanding this, Ferrone developed a perturbative approach to simplify the system, consisting of the formal expansion of the equation about their initial values obtaining the analytical solution:

$$[c_0 - c(t)] = A \cdot [1 - cos(Bt)] \tag{1.3}$$

where A and B are two parameters dependent on the rate constants and nucleus concentration. Further, a more intuitive approximation could also be assuming that near the beginning of the reaction all variables take their original values ($J = J_0, c = c_0$ and $c^* = c_0^*$). Using such assumption the system composed by equations 1.1 and

1.2 straightforwardly leads to the following solution:

$$[c_0 - c(t)] = \frac{1}{2} J \cdot J^* \cdot c^* \cdot t^2 \tag{1.4}$$

that is an expansion about the initial value of the function in equation 1.1. It must be noted, however, that, because of the pertubative procedure employed, also the expression in equation 1.3 is only a good approximation for the initial part of the kinetics. Both the functions in equations 1.3 and 1.4 are shown in Figure 1.5. The lag phase is almost absent and, as expected, the two solutions are superimposed each other in the early stages. Hypothesis on the elongation mechanism leading to equations 1.1 and 1.2 includes only a tip-to-tip attachment of monomers or, better, the so called *primary* or *homogeneous nucleation*.

The above treated mechanism is not a general one. Together with the homogeneous nucleation other reactions can take place being also dependent on the ongoing polymerization. These additional processes are commonly indicated as *secondary nucleation* and they can occur with different molecular mechanisms. Generally, three possibilities are indicated: fragmentation, branching and nucleation on the already formed fibrils, the latter also called *heterogeneous nucleation*.

Fragmentation is mainly based on the breaking of a part of the polymer chain. Such part presents additional ends to start a new polymer growth with a final result of incrementing the rate constant of the overall polymerization. Slightly different, *branching* includes the addition of a monomer, or generally of a subunit, on a specific site already present in the forming polymer. Finally, the *heterogeneous nucleation* is effective when a minimum length of the polymeric chain is provided. Then, the so called *heterogeneous nucleus* is formed and a new elongation pathway is activated (Figure 1.5).

In all the above mentioned cases, the rate of polymer growth is largely enhanced compared to the simple *homogeneous nucleation*. To mathematically describe such increase, a positive term need to be added in the equation 1.1 and, reasonably, a linear dependence on the already polymerized monomer can be taken into account for all of the three possibilities. As a consequence, the following differential equation for secondary nucleations can be used:

$$\frac{dc_p}{dt} = J^* \cdot c^* + Q \cdot [c_0 - c(t)] \tag{1.5}$$

where $Q[c_0 - c(t)]$ is the term that takes into account the auto-catalytic processes. Using again the pertubative approach and coupling equation 1.5 with 1.2, the analytical solution is:

$$[c_0 - c(t)] = A' \cdot [cosh(B't) - 1] \tag{1.6}$$

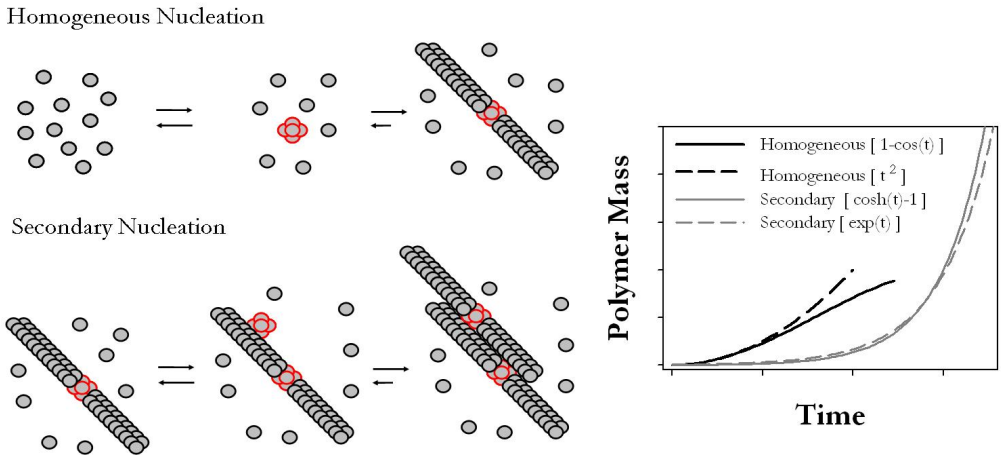

Figure 1.5: Possible mechanisms in a nucleation−elongation process: homogeneous nucleation and secondary nucleation. Circles represent monomers and red edges indicate the nucleus (X_5 in this case). In particular, nucleation on already formed polymer surfaces is shown as an example of secondary pathway. On the right, temporal behavior for homogeneous and secondary nucleation as predicted by the mathematical approach of Ferrone and coworkers (see equations 1.3, 1.4 and 1.6).

where in this case A' and B' are functions of the rate constant, nucleus concentration and Q term. In the early stages, function in equation 1.6 resembles a homogeneous nucleation and afterwards a prompt increase in the growth rate occurs. As shown in the right side of Figure 1.5, an exponential function can also describe this temporal behavior with a good approximation. Noticeably, such a kind of behavior is entirely determined by the term $[c_0 - c(t)]$ in equation 1.5.

1.4 State of the art of insulin fibrillogenesis

In this section a brief introduction of the protein molecule employed in this work is provided. Moreover, with the aim to deeper focus on the specific reaction and to give a proper background on insulin fibrillation, a summary of the main results and the improvements on this specific topic is reported. Such results will be also discussed in the framework of the mathematical modeling previously presented.

1.4.1 The model system: protein-hormone insulin

Insulin is a 51-residue protein hormone (molecular weight of 5808 Da), with a largely α-helical structure, which plays a crucial role in the carbohydrate metabolism

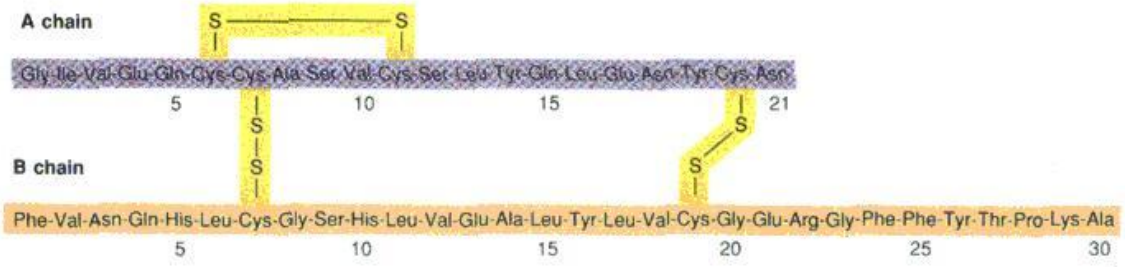

Figure 1.6: Primary structure of bovine insulin. A-chain and B-chain are connected by disulfide bond. Primary structure of human insulin differs for the position of three residues along the chains.

and several other body systems, e.g. vascular compliance, and it is naturally produced in the Islets of Langerhans in the pancreas. Several human diseases are related to a not properly working mechanism of insulin production. Besides insulinoma, metabolic syndrome, polycystic ovary syndrome, a high social impact is represented by the diabetes Type I and Type II related to the insulin deficiency and insulin resistance, respectively. Because of the large diffusion of such kind of diseases, insulin-based pharmacological formulation has attracted the interest of many researchers in the last decades. For the above mentioned medical interest, *in vitro* studying of the chemical and physical stability of this protein results to be preparatory for the realization of reliable insulin delivery systems. Moreover, *in vitro* at low pH and high temperature, insulin is very prone to form amyloid fibrils, thus constituting a suitable model system to study the molecular mechanisms of amyloid formation. In fact, this model system has recently been used to characterize the mechanical properties of individual amyloid fibrils [51] and to determine the growth rate of fibrils by monitoring in real time the increase in their mass [52].

Primary structure of bovine insulin was reported by Sanger in 1955 (Figure 1.6). 51 residues are located along two polypeptidic chains (A-chain e B-chain), connected by disulfide bonds and bovine insulin differs from the human type by changing three aminoacids in the sequences. Secondary structure of the A-chain and B-chain consists of two α-helices and a combination of one α-helix and a β-strand, respectively. Non covalent interactions between residues of the two chains stabilize the tertiary arrangement and determine the structure of the monomer with a hydrophobic core and polar residues located on the external surface (Figure 1.7). Assembling of monomers in higher hierarchical species (see Figure 1.7) is strongly dependent on physical and chemical parameters of the solution as pH, solvent composition, temperature as well as on insulin concentration. In particular, for the purposes of this Thesis, it must

Figure 1.7: Tertiary and quaternary structures for insulin. a) monomer, b) dimer and c) examer. Yellow arrows indicate the interacting β-strands that stabilize the structure.

be noted that in low pH solutions containing acetic acid, insulin occurs as monomer (see Figure 1.7a), whereas a dimer prevalence (see Figure 1.7b) takes place in presence of HCl. Thermally induced fibrillation reactions in such low pH solutions have been largely studied and in the next section the main features of this process will be described together with the proposed models.

1.4.2 Proposed models for insulin fibrillation

Since the 40's, several studies on *in vitro* thermally induced insulin fibrillogenesis are reported. First observations led to distinguish three different phases of the process in which a number of reactions takes place: formation of active centers (nuclei), growth of the nuclei and formation of floccules [53]. Although pioneristic, such studies pointed out a strong dependence of the fibrillation kinetics on temperature, pH of the solution and, clearly, protein concentration. Moreover, nucleation can be activated at high temperature whereas fibril growth can also proceed at room temperature [54].

Generally, fibrillation processes are strongly influenced by the number of protein molecules in solution. In fact for several model systems a critical concentration can exist below which native state keeps almost unvaried its structure also in adverse conditions. For insulin, protein concentration affects both the nucleation time, often referred as *lag time*, and the elongation rate. In fact temporal features of the kinetic are determined by these two steps (nucleation and elongation) as shown in Figure 1.8. In recent time the first systematic studies on time dependence of insulin fibrillation have been performed by Nielsen and coworkers, inducing fibrillation in high acidic solution at high temperature [18, 19]. These results led to a description of the progress curves in terms of three distinct phases:

Nucleation phase: native protein start undergoing structural changes leading to the formation of partially unfolded species. Such structures are able to interact each others and they form oligomer acting as nucleus of aggregation. Time necessary

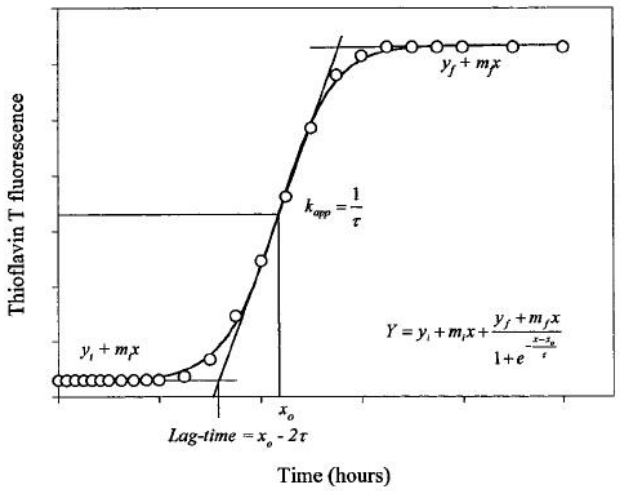

Figure 1.8: Schematic illustration of the sigmoidal fibril growth profile for insulin. Figure is adapted by the original paper [18].

for the formation of the nucleus is indicated as lag time being strongly affected by the protein concentration.

Elongation phase: after the first reaction, i.e. nuclei formation, native and unfolded protein start interacting with the nuclei present in solution. Elongation of the nucleus results thermodynamically favored, so that mature fibrils can be formed.

Equilibrium phase: finally mature fibrils and native or unfolded specie are in equilibrium and no changes on the kinetic profile are detected as obtained by several experimental tools.

It must be noted, however, that a simple nucleation-elongation scheme is not able to describe the kinetic profile shown in Figure 1.8. In fact, the hypothesis that the mature fibrils can only elongate by attachment of protein molecules to nuclei leads to take into account only a homogeneous nucleation pathway (see Section 1.3.1). In this case a quadratic time-dependence should be expected [47, 48]. On the contrary, experimental data show a pronounced lag phase and a prompt fibril growth that do not match at all with quadratic time dependence (Figure 1.8).

After 2001, to properly describe such kinetic profile, several studies have been carried out. An alternative fibrillation pathway for insulin has been firstly proposed by Librizzi and Rischel in 2005 [55]. Authors take into account several nucleation-elongation mechanisms evidencing the specific temporal behavior for each of the attempts. Kinetic data result to be rationalized in the framework of secondary nucleation pathways (see Section 1.3.1), being well described by an exponential time

curve. Such a kind of description implicates the presence of an autocatalytic reaction in which the already formed fibril in solution can act as *preferential point* for new nucleation or elongation events, determining the explosive growth after the lag phase. This idea also arises from atomic force microscopy (AFM) studies. In fact Jansen and coworkers also in 2005 [17] have monitored fibril occurrence in insulin solution looking at the morphologies of the species at different instant of the kinetics. They have observed not only a linear elongation of the nuclei, i.e. as expected for a homogeneous nucleation mechanism, but also a strong interaction between fibril and protein molecules in solution. Just in proximity of the already formed fibril a locally high-density deposition of protein occurs that starts to produce formation of subsequent fibrils. Interestingly, these autocatalytic mechanisms clearly lead to a variety of fibrils morphologies ranging among the standard thin and long filament up to thick fibers and highly compact assemblies often referred as *bundles*. Manno and coworkers largely demonstrate the occurrence of all these species during the fibrillation reaction of human insulin [56]. Moreover, different specific processes are likely to be intertwined in the overall aggregation, including both tip-to-tip elongation and lateral thickening [56]. In this regard, some recent reports result quite impressive, showing how determinant is the choice of the experimental conditions on the final fiber morphologies. In particular, varying the thermodynamic parameters, as pressure, temperature and solvent composition induces different volumetric features in the amyloid formation, even determining the species occurring in the pathway [57]. Moreover, Rogers and coworkers have observed and measured amyloid spherulites forming from heat-treated solutions of bovine insulin at low pH. The spherulites form in large numbers as semispherical dome-shaped objects, showing that surface defects or impurities, or the substrates themselves, can provide good nucleation sites for their formation [58].

Latter remark introduces to a delicate point in the study of *in vitro* insulin fibrillogenesis. New nucleation events seem to be triggered not only by the presence of already formed fibrils in solution. In fact, sample holder interfaces or in general the substrates in which the experiments are performed can represent preferential regions to originate the first nucleation events and, as a consequence, to determine the overall temporal behavior of the process. Further, surface-volume ratio of the sample seems to strongly affect the temporal features of the process (unpublished data). For these reasons, a reliable comparison of the progress curves as detected by different investigators in apparently identical sample preparation conditions can only be made if accurate and clear information on the sample holder material, surface-volume ratio and, clearly, on monodispersity of the protein solution after the preparation are provided. Interestingly, recent results strongly suggest that the capability of insulin to nucleate on exposed surfaces can definitively determine the nucleation and growth

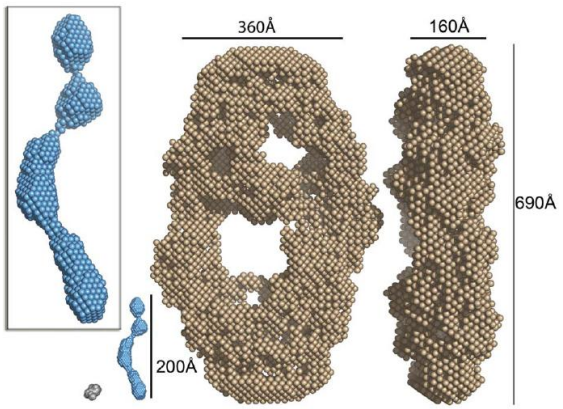

Figure 1.9: The insulin monomer is shown in grey in the lower left corner, the *ab initio* structure of the helical oligomer in blue, and the *ab initio* structure of the repeating helical unit of the fibril in beige (in front and side view). The inset shows the oligomer in a zoom box. Figure and caption are adapted from the original paper [59].

of amyloid aggregates. In particular, fibrils nucleate more quickly in the presence of hydrophobic polystyrene surfaces but the corresponding fibril growth rates decrease [51].

Most of the above mentioned results have been mainly obtained by standard spectroscopic techniques. In particular specific staining by fluorescent probes results to be still one of the most used (see Section 2.1). This method is particularly fast and allows the acquisition of the main parameters of the fibrillation reaction. On the contrary, by means of this tool direct quantitative information can not be easily obtained because of the presence of several factors that can affect in different extent the specific binding. A more accurate discussion will be provided in Chapter 2 for the amyloid sensitive probe Thioflavin T, largely used in this work.

Besides the temporal characterization of the processes as well as the attempt to elucidate the molecular mechanisms involved in insulin fibril formation, in the last decade onset and improvements of structural-determination tools have driven the interest of researchers towards the exact structural determination of the occurring species during the reaction. In particular, significant efforts were addressed to the determination of the structure of the species in the early stages of the process, i.e. nucleus and oligomers. Such a kind studies may have a great impact in the medical applications. In fact, isolating the precursor species in the fibrillation pathway could in principle indicate new methodologies to inhibit the onset of amyloid fibrillation, so that new pharmaceutical formulations can be tested in the case of fibrillogenesis associated to human diseases. In this sense, elucidation on the effect of inhibition on

prefibrillar species in bovine insulin samples have been recently provided by Smith and coworkers [60]. As for different amyloidogenic proteins, several techniques have been also employed to determine the nucleus structure for insulin. In particular, small angle X-ray scattering has been used for studying the kinetics of human insulin in acetic acid solution at 45°C [59]. The study reveals three major components along the pathway: insulin monomers, mature fibrils, and an oligomeric species. Low-resolution three-dimensional structures have been determined for the fibril repeating unit and for the oligomer, the latter being a helical unit composed of five to six insulin monomers (Figure 1.9). Such helical structure has been also proposed to be the elongation unit for mature fibrils.

Notwithstanding such huge number of studies on insulin fibrillation and the several brilliant results recently acquired, a clear picture and a general model to properly describe the evolution of fibril growth are far from being provided. Questions related to which of the secondary pathway is mainly involved in the process, which is the fibrillation-competent species and, mostly important, which event really takes place during the lag phase remain still not clear. Further, as recently shown, without a deeper knowledge and accuracy both in the method and in the experimental settings, artifacts in detecting fibril formation may occur [20, 21, 56, 59] making any evaluation of the data unreliable. For these reasons, efforts need to be put to improve the detection methodologies for a proper evaluation of the data. Such condition can lay the foundation to better investigate the still unknown dynamics preceding the onset of the sizable aggregates.

Chapter 2

Experimental approach

Curiously enough, the dolphins had long known of the impending destruction of the planet Earth and had made many attempts to alert mankind of the danger; but most of their communications were misinterpreted as amusing attempts to punch footballs or whistle for tidbits[...]

[Douglas Adams, *Hitchhiker's Guide to the Galaxy*, 1979]

Aim of this chapter is to present all the experimental tools employed in this work, even focusing on the meaningful technical aspects of the instrumentation. A key role in all the experimental results of this Thesis has been played by employing the fluorescent probe Thioflavin T. For this reason a section has been addressed to provide a proper knowledge of such tool.

The experimental instrumentation employed mainly consists of devices for absorbance and fluorescence detection. Mostly focusing on the scientific aspects that need to be clarified, these instrumentations will be accurately presented. Moreover, supporting informations have been obtained by atomic force microscopy (AFM) images and, for such reason, a brief introduction on the AFM basic principle and specific experimental settings used will be also provided. Some other experimental and computational techniques (Density Functional Theory (DFT), Dynamic Light Scattering (DLS), Nuclear Magnetic Resonance (NMR)) have been also employed to support both the study on fibril formation and the characterization of ThT properties at basic pH. Because of the not so wide use of these tools, the reader is addressed to more specialized works to provide a proper theoretical background on them.

Being the experimental results on fibril formation strongly dependent on the accuracy in samples preparation, in the final section of this chapter an overview of materials, samples preparation and treatments procedure is also provided.

2.1 Staining properties of Thioflavin T

Monitoring and characterization of folded and unfolded state of proteins are still basic approaches for the investigation on the relation between protein structure and function. For such kind of studies, extrinsic optically-active probes have been widely used for identifying protein domains involved in folding pathway for a large number of molecules [23, 25, 27, 61, 62]. Moreover, occurrence of protein self-assembly has been largely characterized using spectral properties of different fluorescent dyes, e.g. 1-anilinonaphthalene-8-sulfonate (ANS) for amorphous aggregate [27]. Even the detection of ordered association of protein molecules has been mainly performed in the past using specific dye as Congo Red and Thioflavin T, being such techniques now coupled to more advanced imaging and structural experimental tools like atomic force microscopy (AFM) and small angle X-ray scattering (SAXS). However, staining by optically-active probes still represents not only a methodology for basic research, but also a useful approach for practical problems occurring in the fields of biotechnologies and medicine, giving a fast and *on-off* response [63].

The benzothiazole dye Thioflavin T (ThT) is a fluorescent probe commonly employed in biological sciences for staining *in vivo* and *in vitro* tissues. In this Thesis, such dye has been widely used for characterizing insulin amyloid formation. Moreover with the aim of gaining new insights on photo-physical properties of the dye, the effect of varying physical parameters of aqueous solutions on ThT spectroscopic features has been also studied. In this section the background for this subject will be brought out, focusing on several aspects of ThT and ThT-fibril binding which play a crucial role for a reliable and quantitative evaluation of fibril occurrence.

2.1.1 Structural and optical features of ThT

Thioflavin T (ThT) was introduced for studying amyloid aggregates formation in 1959 [64] and its spectroscopic properties in staining different typologies of tissues, i.e. cartilage matrix, elastic fibers and mucopolysaccharides, [64, 65] cellulose matrix [66], DNA [67–69] and single-stranded polynucleotides [70], have been largely investigated in the last decades. However, detection of amyloid aggregates is still the widest employ of such dye and the application spans from *ex vivo* staining amyloid plaques in tissue to the *in vitro* monitoring of fibril formation. The molecular structure of Thioflavin T can be split into three different rather rigid fragments: the benzothiazole group, the benzene ring and the dimethylamino group (see Figure 2.1) [63, 71, 72]. The spatial orientation of these three groups is related to the two torsional angles φ and ψ (Figure 2.1) determining both the structure and the spectroscopic properties of ThT. Moreover, quantum mechanical calculations have revealed a restricted mobility

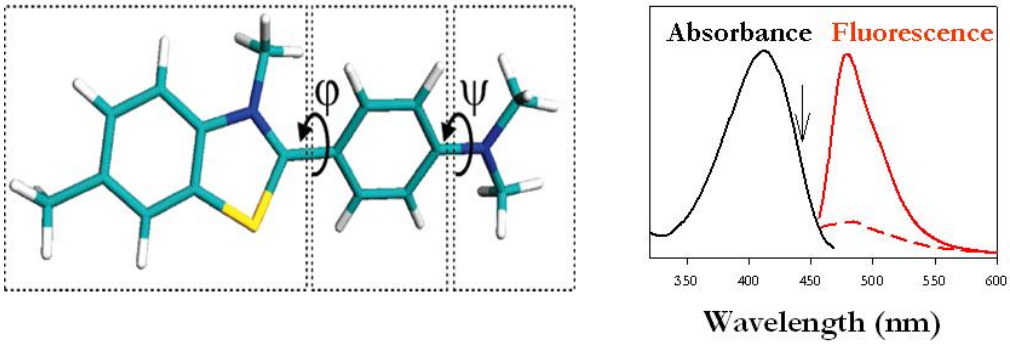

Figure 2.1: On the left, chemical structure of Thioflavin T ground state as obtained by computational methods. S, C, N and H atoms are shown in yellow, cyan, blue and white, respectively. φ and ψ are torsional angles between fragments of the molecule determining different conformations. Left, center and right dotted boxes indicate benzothiazole group, benzene ring and dimethylamino group, respectively. Adapted from [71]. On the right, optical activity of ThT: absorbance (black line) and fluorescence in presence of native protein solution (red dotted line) and in solution with amyloid fibrils (red line). Arrow indicates the excitation wavelength.

for the dimethylamino group leading to an almost no influence of the ψ angle in reaching stable conformers of ThT [72]. When ThT is dissolved in aqueous solution, the well known yellow color appears and the absorbance spectrum is characterized by two significant bands, being the most intense in the visible region at $\sim 400-450$ nm (see the right part of Figure 2.1). Interestingly, ThT shows an optical activity strongly dependent on the solvent. In particular, dissolving ThT ions in high viscosity solvent leads to variations in the position, broadening and intensity of the visible band, drastically changing its global spectroscopic features [63].

Staining properties of ThT are mainly based on its fluorescence activity. In aqueous solution and, remarkably, also in presence of native proteins with different primary and secondary structure, ThT is characterized by a low emission quantum yield [73, 74] upon excitation at $\sim 440-450$ nm (see the right part of Figure 2.1). In contrast, ThT has a high selectivity for fibrils: when bound to amyloid aggregates it shows a bright fluorescence emission in the $475-600$ nm region (see the right part of Figure 2.1). Moreover, ThT does not affect [18], or only slightly affects, the early formation of fibrils, making this method suitable for *in situ* fibrils detection.

Notwithstanding such selectivity for amyloid aggregates, one of the drawbacks of this method is the lack of a clear quantitative relationship between fluorescence activity and fibril mass, probably due to the susceptibility of the dye to optical artifacts and possible interference compound binding sites [74] as well as a poor

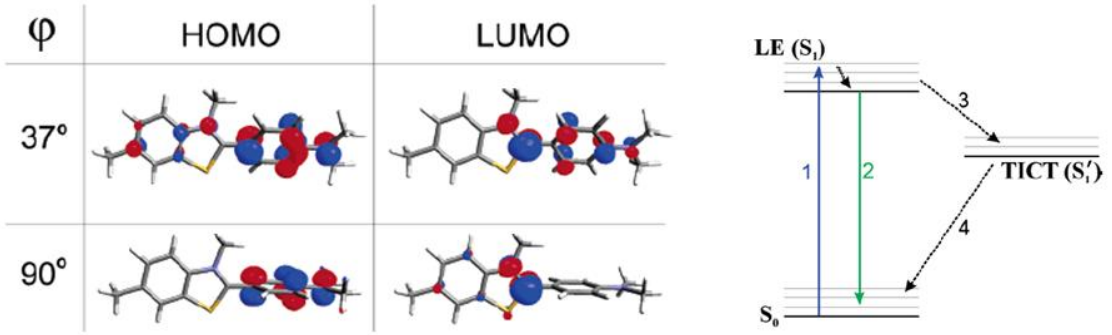

Figure 2.2: HOMO and LUMO of ThT conformers involved in the deactivation process of the excited state (left). Scheme of the excitation energy deactivation in the ThT molecule (right). Adapted from the original paper [71].

understanding of the specific ThT-fibril binding.

The mechanism of quantum yield increase in presence of fibrils is still greatly debated. Voropai and coworkers and, most recently, Stsiapura and coworkers proposed that the rotational properties of the molecule are involved in the increasing emission quantum yield when ThT is incorporated into amyloid fibrils [63, 71, 72, 75]. Based on quantum mechanical calculations, they suggest that ThT behaves as a molecular rotor. In its ground state, a dihedral angle φ of $\sim$37° between the benzothiazole group and the aminobenzene ring has been reported with a positive charge on the nitrogen (see Figure 2.2 on the left). Transition from the ground state to the excited state and the subsequent emission can be affected by the presence of another not fluorescent excited state. The general scheme proposed has been shown in the right part of Figure 2.2. Internal rotation of molecular groups is associated with intramolecular charge-transfer processes. Such process leads to a high energy state (TICT) reflecting a twisted conformation of the ThT molecule ($\varphi \sim 90°$, see Figure 2.2 on the left). After the transition from the ground state (process 1 in Figure 2.2), two different competing processes can take place: a radiative deactivation of the locally excited (LE) state (process 2) and a torsional relaxation of LE into the TICT state (process 3) followed by a not radiative deactivation to the ground state (process 4). Occurrence of the TICT clearly affects the quantum yield of fluorescence and depends on the physical properties of the enviroment, i.e. viscosity of the solvent. In low viscosity solvents, rotation of the molecule is favored and not radiative process effectively competes leading to the quencing of ThT fluorescence. In contrast, in viscous solvent, and in general in environment in which rotation is blocked, LE→TICT transition is suppressed resulting in an enhanced quantum yield of fluorescence. Such purely theoretical model could in principle explain the bright fluorescence observed

in presence of amyloid fibrils. In fact, ThT molecule seems to specifically bind to fibrils, experiencing an environment able to block the LE→TICT transition.
In the next section, a deep and detailed presentation on the ThT-fibrils molecular mechanism are reported together with a discussion on the proposed models.

2.1.2 Proposed models for ThT-fibrils binding

The rotor model for ThT presented in the previous section can provide suggestions on possible molecular mechanism only for the enhanced quantum yield, not taking into account the specificity of the ThT-fibril binding. In spite of the widespread use of ThT in detecting amyloid fibrils, several open questions are still existing on the binding mechanism, specific binding sites and ThT molecular form bound to fibrils. For this reason, in the last decade, a number of experimental studies has been addressed to this subject, each one clarifying different aspects of this scientific problem.

As discussed in Chapter 1, amyloid fibrils structure results to be rich in β-sheet polypeptide chains aligned along the perpendicular axis of the fibrils [20, 76]. By means of electron microscopy and atomic force microscopy, fibrils present a common appearance with a diameter of $\sim$ 10 nm and a variable length up to several μm [77, 78]. Moreover, a number of studies suggests a geometrical arrangements of the β-sheet chains leading to a sort of empty cavity generally referred in literature as *β-sheet channel* [20, 21, 76, 77]. Among the several proposed models on ThT-fibrils binding, a reliable description has been provided by Krebs and coworkers in 2005 [79]. Combining optical and confocal microscopy, they propose that enhanced fluorescence can only occur when ThT molecule is bound in a highly directional mode. This has been proved for ThT embedded both in PVA film and in insulin spherical aggregates. Due to the specific fibril structure and taking into account the presence of the channels, they propose the binding scheme shown in Figure 2.3. Fibril channels have been indicated as a location for ThT and the dye binds to such cavity with its long axis parallel to the elongation axis of the fibril (Figure 2.3B). Clearly, some geometrical restriction can modulate the binding. As pointed out by Groenning and coworkers, proper cavity size (8-9 Å of diameter) and length of the binding locations need to detect a significant enhanced fluorescence signal and, in general, accessibility of such cavity results to be a turning point for a reliable fibril evaluation [20]. Proper size and accessibility of binding locations guarantee for interaction of ThT and side chains, resulting in a physical confinement of the dye. Krebs and coworkers also suggest that ThT incorporated into amyloid fibril is forced into one conformation also in its excited state, without any change in the spatial orientation of the fragments. This configuration leads to a suppression of the intramolecular charge-transfer pro-

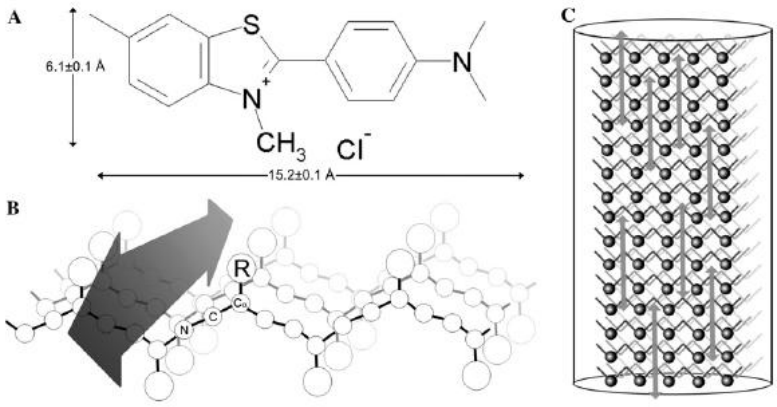

Figure 2.3: β-sheet channels for binding ThT as suggested by Krebs and coworkers (2005). (A) ThT chemical structure and molecule size are shown and (B) double headed arrow indicates one of the binding channels where ThT long axis can be located . (C) Schematic representation of protofilament with three β-sheet. Figure is adapted from the original paper [79].

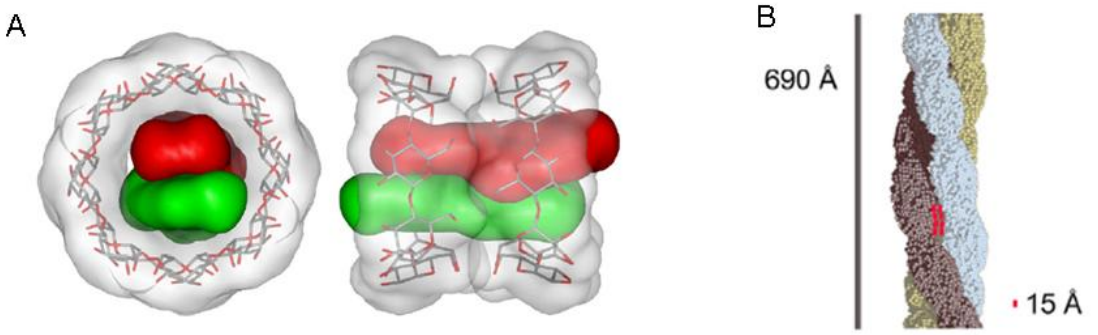

Figure 2.4: ThT binding modes as as suggested by Groenning and coworkers [20, 21]. (A) Two γ-cyclodextrin (γ-CD) in complex with two ThT (green and red) as obtained by molecular modelling and stoichiometry studies. Complex is shown in two views rotated of 90. (B) Binding of ThT (red rectangles) between three protofibrils on the repeated subunit of insulin fibril as obtained by SAXS. Figures are adapted from the original papers [20, 21].

cesses and a consequent increase of the quantum yield, as theoretically suggested by Stsiapura and coworkers (see Section 2.1.1). Moreover, Groenning and coworkers propose that restriction of rotation could be not sufficient to explain the increased fluorescence. In fact, smaller cavities able to bind and block one single ThT ion may also be unable to provide a proper environment for the characteristic fluorescence (for example β-sheet-rich channels of transthyretin). Based on such evidence and also on stoichiometry studies on several β-sheet-rich and non β-sheet-rich cavities, authors argue that formation of a ThT dimer complex could be crucial for obtaining an increase in the fluorescence signal and for this reason a minimum size for cavity is required (Figure 2.4A on the left). Moreover, the cavity needs also to be long enough to cover the entire length of the ThT ions, otherwise no increased fluorescence can be detected (Figure 2.4A on the right). Interestingly, the same authors have also investigated the specific ThT binding to insulin amyloid fibrils. Recently, insulin amyloid structure has been deeply elucidated and insulin mature fibrils result to be formed by three intertwining protofibrils with each protofibril consisting of two protofilaments (Figure 2.4B)[59]. Besides a detailed stoichiometry on ThT-fibrils interaction, they also propose two possible specific locations for the dye. Probably, ThT can bind with its long axis parallel to the elongation axis of the fibril between the protofilaments forming the protofibrils or between the protofibrils forming the mature fibrils, being the latter case illustrated in Figure 2.4B. In any case, both of these models fully agree with the previous report of Krebs and coworkers and they suggest a binding mode strongly dependent on the accessibility of interface between protofilaments/protofibrils. Such aspect has been further discussed in a recent report, focused on the binding of ThT with amyloid fibrils formed by a larger protein domain called HET-s(218-289) [80]. Such domain can form fibrils with different morphologies dependent on the pH. After incubation at 65°C and pH 2, dispersed fiber filaments have been observed by means of electron microscopy, whereas increasing the pH up to 7, filaments bring together forming dense assemblies of fibrils. Investigating kinetics of ThT-HET-s(218-289) association at the two different pH, data clearly show a much slower ThT binding to fibrils formed at pH 7. Authors suggest that a fraction of the fibrils could show a reduced accessibility to the dye in the large clumped fibrils assemblies formed at pH 7, determining a slowed down binding kinetics. Furthermore, different morphologies of amyloid fibrils can not only lead to different ThT binding kinetics, but they may also induce different ThT fluorescence quantum yields. For glucagon fibrillation [81], it has been reported that ThT fluorescence could lead to a not reliable detection of fibril mass concentration. In fact, they proved that glucagon fibrillation can occur leading to different morphologies of fibrils, being dependent on the initial concentration of the protein. ThT staining results in a much higher fluorescence for fibril formed from $\geq$1g/L of native glucagon (type A glucagon fibrils)

compared to the ones formed starting from lower concentration (type B glucagon fibrils). Such experimental evidence brings about a warning in using ThT staining as a tool for quantitative evaluation of fibril concentration. As pointed out by Manno and coworkers, in general ThT fluorescence can not be considered straightforwardly related to the fibril mass, so that capability and specificity of ThT-fibrils binding need to be verified for each specific system [56]. In particular, taking into account the available accessible fibrils surface is a crucial point for evaluating the goodness of the ThT assay. For example, in the case of thin and dispersed fibrils, the relation between fibril surface and mass is more direct and ThT signal can be easily related to the fibril concentration. In contrast, when fibrils start to assemble forming bundles, ratio between mass and available surface of fibrils dramatically increases, leading to an erroneous evaluation of fibril concentration [56]. Other possible drawbacks for a proper ThT staining can be due to the electrostatic interaction between solvent and ThT. Pedersen and coworkers also show that ThT quantum yield can also change dependent on different concentration of GdmCl in the solvent, being such effect possibly due to the charge screening by chloride ions between the positive charged ThT ions and fibril [81]. Interestingly, it must be noted that such positive charge has been also indicated to have a role in the self-association of ThT molecule. In fact, in aqueous solution, ThT ions may undergo a phase transition producing an association between ThT molecule in micelles form. In micelles phase a dramatic change in the physical properties of the dye takes place involving electrical conductivity, surface tension, osmotic pressure, refractive index and fluorescence anisotropy [80]. Such phenomenon was firstly studied by Khurana and coworkers in 2005 [82]. By means of conductivity measurements, they were able to determine a critical micellar concentration (cmc) for ThT of $\sim 4\mu$M. Occurrence of micelles in binding fibrils has been also visualized by atomic force microscopy and they suggest a binding mode *via* micelles formation. Conversely, Sabaté and coworkers recently reported a cmc much higher ($> 8\mu$M) compared to the one measured by Khurana and coworkers. Moreover, they show that ThT bound to the HET-s(218-289) fibrils results in a strong fluorescence intensity even in the lower ThT micromolar range ($<1\mu$M), when micelles formation does not occur [80]. Last evidence strongly suggests that ThT molecules do not need to be in micelles form for binding to and proper staining amyloid fibrils.

2.2 Optical and UV spectroscopies

In this section, an overview of the optical spectroscopy instrumentation employed in this Thesis will be provided. ThT fluorescence was mainly measured by means of three different detection systems each one employed to clarify a specific aspect of the

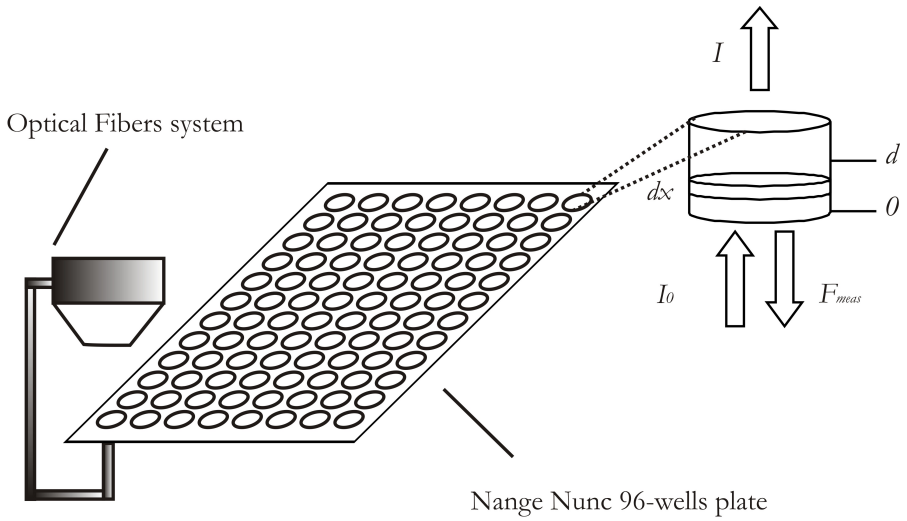

Figure 2.5: Illustration of the experimental setting in a typical plate reader detection. In this work, fluorescence measurement are performed in bottom-bottom configuration.

scientific problem.

2.2.1 Plates reader: absorbance and fluorescence

Microplates reader (FluoStar Optima and PolaStar, BMG Lab Technologies) is a widely used instrumentation for the spectroscopic detection on small volume samples (up to 500 μl) in liquid phase. The peculiarity of such scientific instrumentation is the simultaneous detection of biological, chemical and physical events on a huge number of samples, such number being dependent on the plate employed. Common detection modes for plate assays are absorbance, fluorescence intensity, luminescence, time-resolved fluorescence, and fluorescence polarization.

In the present work, plates reader system is widely employed for the characterization of thermally induced insulin fibrillogenesis by ThT fluorescence and absorbance (turbidity) (Chapter 3) and also for studying the photo-physical properties of Thioflavin T (Chapter 5). In particular, due to the stochastic nature of insulin fibrillation, simultaneous detection on several samples allows to estimate the intrinsic degree of uncertainty of the kinetic parameters. In Figure 2.5 a simplified scheme shows the experimental setting used in a typical microplates measurement. Sample is positioned in cylindrical microwells made on a plate as shown in Figure 2.5. Plate with samples is positioned in a plate-holder generally equipped with a temperature control system (up to 45°C for Fluostar, up to 60°C for PolaStar). A high-intensity flash lamp illuminates the sample by an optical fibers system and the movement of

the plate allows the scanning along all the wells and the detection of the signal of interest. Scanning time, excitation and emission wavelength, number of flash and temporal features are all controlled by software.

Experimental Settings. On the right side of Figure 2.5, the specific configuration used for fluorescence (bottom-bottom configuration) and absorbance (bottom-top configuration) detection are shown. The plates were covered with non-sterile Polyolefin sealing tape (Nalge Nunc) to avoid evaporation of the sample during the fluorescence measurements at high temperature. For the absorbance experiments, to prevent artifacts in the detection, the plates were covered with non-sterile advanced Polyolefin sealing tape (Nalge Nunc). In all the experiments here reported (fluorescence and absorbance experiments), a volume of 200 μl has been used.

To quantitatively study the dependence of the fluorescence signal on the chromophore concentration, the absorption of the excitation beam along the sample volume [83] and its effect on the detected fluorescence intensity (F_{meas}) have been taken into account for the specific experimental setting (bottom-bottom configuration) by considering the expression for the light crossing the sample (see Figure 2.5):

$$I(x) = I_0 \cdot e^{-\varepsilon \cdot c \cdot x} \tag{2.1}$$

where I_0 is the intensity of incident light, c is the concentration of the fluorophore, ε is the extinction coefficient of fluorophore at the excitation wavelength and x is the path length of light in the sample. Fluorescence signal is linear dependent on fluorophore concentration as well as on absorbance value, so that for a small portion dx an expression for the fluorescence can be easily written down:

$$dF_{meas} \propto I(x) \cdot c \cdot dx \tag{2.2}$$

Inserting eq. 2.1 into the eq. 2.2 and integrating on the entire path, the following expression is obtained:

$$F_{meas} \propto \int_0^d I(x) \cdot c \cdot dx = \int_0^d I_0 \cdot c \cdot e^{-\varepsilon \cdot c \cdot x} \cdot dx = \frac{I_0}{\varepsilon} \cdot (1 - e^{-\varepsilon \cdot c \cdot d}) \tag{2.3}$$

Knowing the value of ε, c and d, the correction factor for the fluorescence data is calculated and the deviation of eq. 2.3 from a linear concentration dependence has been evaluated:

$$F_{corr} = F_{meas} \cdot \frac{\varepsilon \cdot c \cdot d}{1 - e^{-\varepsilon \cdot c \cdot d}} \tag{2.4}$$

For the fluorophore employed in this work (ThT), no effect is expected from the self-absorption of fluorescence emission because of its weak absorption in its emission region.

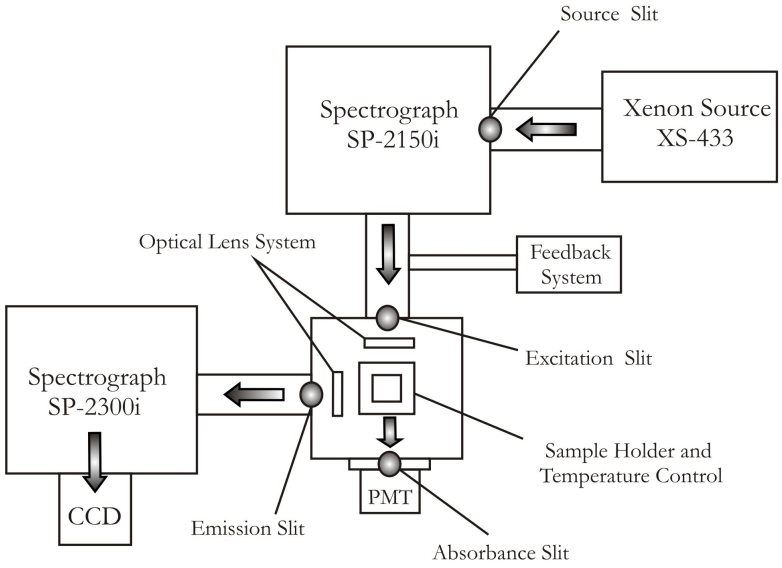

Figure 2.6: Component of the ACTON system for the detection of absorbance and fluorescence signals. In this case, fluorescence measurements are performed in right-angle configuration.

2.2.2 ThT fluorescence detected by CCD camera

Besides the detection of ThT fluorescence by plate reader, another high sensitive system has been employed for the fluorescence detection. A general picture of such instrumentation is illustrated in Figure 2.6. A Xenon lamp has been employed as a source. Light beam comes inside the excitation spectrograph (SP-2150i), where a dual grating turrets select the emission wavelength. Spatial resolution on the select wavelength depends on the type of grating employed, being much precise as bigger is the number of the lines on the grating. By software, single wavelength or wavelength scan can be controlled and then a mirror addresses the beam towards the sample holder. Intensity gain of the light beam can be set using the micrometer adjusting knob (gray circle in Figure 2.6) and afterwards an optical lens system further focalizes the beam on the sample. After the interaction with the sample, absorbance and fluorescence signal can be simultaneously detected. Transmitted light can be measured by a PMT detector, whereas fluorescence signal is detected by a CCD detector. Emission intensity is revealed in right-angle configuration, focalized by a lens system in the emission spectrograph (SP-2300i). Even in this case, the micrometer adjusting knob allows to set the intensity gain. SP-2300i spectrograph is equipped by three different gratings and with a system analogous to the SP-2150i, emission light

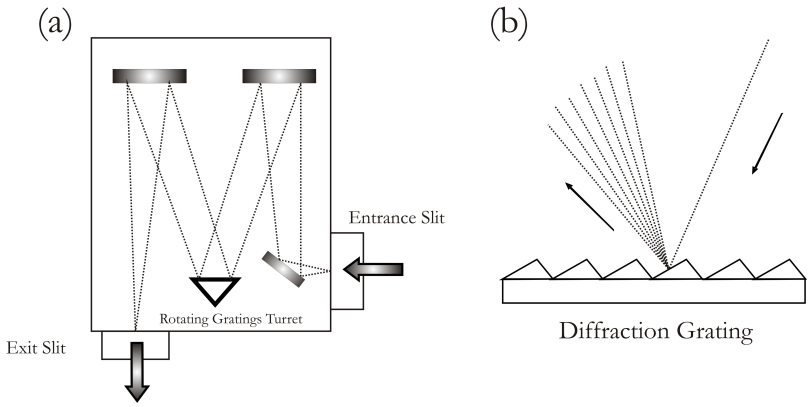

Figure 2.7: (a) General illustration of the SpectraPro spectrograph system. SP-2150i and SP-2300i models are equipped by a dual and triple indexable gratings, respectively. (b) Scheme of the gratings.

is addressed to the exit on a CCD detector. Moreover, to take into account unpredictable intensity fluctuations of the source, a feedback system has been employed in the measurements performed. Properly connected to the detection systems, the feedback system allows the correction of such effect. In the rest of this subsection, particular interest will be devoted on two components of such system (spectrographs and CCD detector), illustrating the technical aspects of these devices together with the specific experimental setting.

Spectrograph SP-2150i and SP-2300i. The SpectraPro SP-2150i and SP-2300i are a 150 mm and 300 mm focal length monochromator/spectrographs, respectively. They feature an astigmatism-corrected optical system, indexable gratings and interchangeable grating turrets. The SpectraPro systems include a direct digital grating scan mechanism with full wavelength scanning capabilities, plus built-in RS-232 and USB computer interfaces. A general scheme is presented in Figure 2.7a. Light beam coming from the source is addressed to the gratings turret by a mirror system. Such diffraction gratings separate the polychromatic white light into individuals wavelength. Light impinges on the grating and it is dispersed, so that each wavelength reflects from the grating at different angle. Afterwards, the spectrograph system readdresses the desired wavelength to the exit slit. Clearly, spatial resolution on the wavelength selection is dependent on the number of the grooves in the grating surface (see Figure 2.7b). Groove density affects the mechanical scanning range and the dispersion properties of the system and, in general, it is an important factor in determining the resolution capabilities of the monochromator. As a consequence, higher groove densities result in greater dispersion and higher resolution capabilities.

Another important parameter is the angle at which the grooves are formed with respect to the grating normal, called *blaze angle*. Efficiency at particular wavelengths is mainly a function of the blaze wavelength. Selecting the right blaze wavelength allows the optimization of the response in the desired spectral region. In the measurements performed, a 150g/mm with a blaze at 500 nm and a 300g/mm with a blaze at 500 nm have been employed for the SpectraPro SP-2150i and SP-2300i, respectively.

Charge Coupled Device (CCD). Such CCD detector system (PIXIS 400 Princeton Instruments, ACTON) results particularly powerful and useful for its high sensitivity. This device is thermoelectrically air-cooled down to -75°C to provide the lowest dark charge. The 1340 x 400 array with 8-mm chip height and 27-mm spectral coverage is ideal for multistripe spectroscopy and maximum light collecting area. This detector delivers much higher resolution and sensitivity than standard 1024-pixel sensors. Another exclusive feature is the integration of two software selectable amplifiers to achieve the highest sensitivity for low signal levels. For such reasons, this system provides an excellent tool for detecting low ThT signal during the lag phase. Furthermore, CCD is able to detect the whole emission spectrum with a very high temporal resolution. Proper triggering by software of the exposure time and the delay time between measurements leads to a reliable acquisition up to 1 spectrum per second. This temporal characteristic was very important for detecting changes in the ThT emission spectra during the early formation of aggregates at the end of the lag phase (Chapter 4).

Experimental Settings. Fluorescence measurements have been carried out in standard mono-use cuvette with 1 cm pathlength (PMMA material, Kartell) and a total sample volume of 1.1 ml has been used. Removable optical lens system allows to tune the size of the beam impinging on the cuvette (from mm to cm), changing the portion of illuminated volume. Using lens on the excitation light, a highly focalized beam is produced leading to an illuminated volume of $\sim$ 0.4% of the total sample volume, whereas taking off the lens system, a portion of $\sim$ 60% of the total volume results illuminated. For the experiments performed, entrance slit (source and excitation) were set at 300 μm and the exit slit at 500 μm. Home-made sample holder was connected to a temperature controller, having a confidence of $\pm$0.2°C.

2.2.3 ThT fluorescence detected by PMT device

Fluorescence measurements were also carried out by a Jasco FP-6500 spectrofluorometer. The general settings of this instrumentation is similar to the one shown in Figure 2.6. Source is a xenon discharge lamp. Light beam is dispersed by a first

monochromator (excitation) allowing the selection of an excitation wavelength (range $220-750$ nm, bandwidth 1-20 nm). A beamsplitter allows the generation of two different beams, one directed on the sample, the other going directly to a photomultiplier. The emitted light is collected in the right-angle configuration by a monochromator (emission) that selects a wavelength (range $220-750$ nm, bandwidth $1-20$ nm) and then signal is detected by an other photomultiplier. Moreover, a Jasco ETC-273T peltier temperature controller has been used with a confidence of $\pm 0.2°$C. Compared to the ACTON system described in Section 2.2.2, such spectrofluorometer results to be less sensitive than a CCD device with a lower S/N. Notwithstanding such drawback, this system is particularly useful for detecting fibrillation kinetics because of a very versatile integrated software able to easily control all the experimental parameters (bandwidths, scan-speed, integration time, data pitch, delay time).

Experimental Settings. Such instrumentation has been employed for preliminary study on insulin fibril formation (Chapter 4) as well as for studying the effect of ThT hydroxylation in detection of fibril (Chapter 5). In the hydroxylation study, fluorescence measurements have been carried out in standard quartz cuvette with 1 cm path length and a total sample volume of 3 ml has been used. The emission spectra of ThT were obtained with emission and excitation bandwidths of 3 nm, scan-speed of 100 nm/min, integration time of 1 s and recorded at 0.5 nm intervals using an excitation wavelength of 440 nm. To study the fluorescence intensity dependence on ThT concentration, corrections for the inner-filter effect (absorption of the excitation beam along the sample volume [83]) were made for the specific experimental setting (right-angle configuration in the approximation of *centered illuminated* cuvette [83]) by means of the following expression:

$$F_{corr} = \frac{F_{meas}}{e^{-\varepsilon \cdot c(t) \cdot \frac{d}{2}}} \tag{2.5}$$

where $c(t)$ is the ThT concentration as a function of the time, ε is the extinction coefficient of ThT at 440 nm, d is the path length of light in the entire sample, F_{meas} is the detected emission intensity and F_{corr} is the corrected emission intensity. Again, knowing the value of ε, $c(t)$ and d, the correction factor for the fluorescence data is calculated when different concentrations of ThT have been used.

2.3 Atomic Force Microscopy (AFM)

Scanning probe microscopes (SPM) define a broad group of instruments used to measure properties of material, chemical, and biological surfaces. SPM images are

obtained by scanning a sharp probe across a surface while monitoring and compiling the tip sample interactions to provide an image. In this section a very brief introduction on theory and experimental aspects related to atomic force microscopy (AFM) is presented. Such section has the aim of supporting the reader to a proper understanding of the images presented in Chapter 4, illustrating specifically the experimental setting employed (*tapping mode*). The reader is addressed to specialized works for a more complete and thorough overview of this technique [84].

2.3.1 Theoretical background and imaging mode

The theory and operation of an atomic force microscope [84] is similar to a stylus profiler. The probe forces on the surface are much smaller than those in a stylus profiler and smaller probes can be used, with a much higher resolution. The general scheme is presented in Figure 2.8. The sensitive element consists of a cantilever where a micrometric tip is applied. Such lever is coupled with a laser beam and after aligning laser and lever, scan can be started. Three piezoelectric components allow a three dimensional scanning. During the X-Y scan, interaction between the tip and the sample can induce a deflection on the cantilever leading to changes both in the beam X-Y position on the photodiode matrix and on the mutual distance between tip and sample. One of the setting used in an AFM measurement is to maintain a constant Z distance between the probe and sample while the probe is raster scanned across the surface. In fact, after interaction, a feedback system is able to apply the proper voltage to the Z piezoelectric component to keep constant the tip-sample distance. This applied voltage is subsequently translated in a geometric information on the height of the scanned surface. Such information together with the changes in the X-Y position on the photodiode matrix provides the topography of the investigated surface (see Figure 2.8).

Several modalities can be employed in an AFM measurements. Scan techniques are generally divided in *contact* and *non contact - intermitted contact* mode. Contact mode operates by scanning the tip across the sample surface while monitoring the change in cantilever deflection. A feedback loop can maintain a constant deflection, force or height between the cantilever and the sample by vertically moving the scanner at each X-Y data point. In particular, for the investigation on biological samples, such experimental setting results to be too invasive. In fact, tip-sample interaction is very strong leading to a degradation of the surfaces and an unreliability of the method.

To avoid sample degradation an *intermitted contact mode* (also called *tapping mode*) has been used in the measurements presented in this work. Cantilever is forced to oscillate close to its resonance frequency with an amplitude ranging from 20 nm to 100 nm, so that tip is not in contact with the sample but it oscillates across

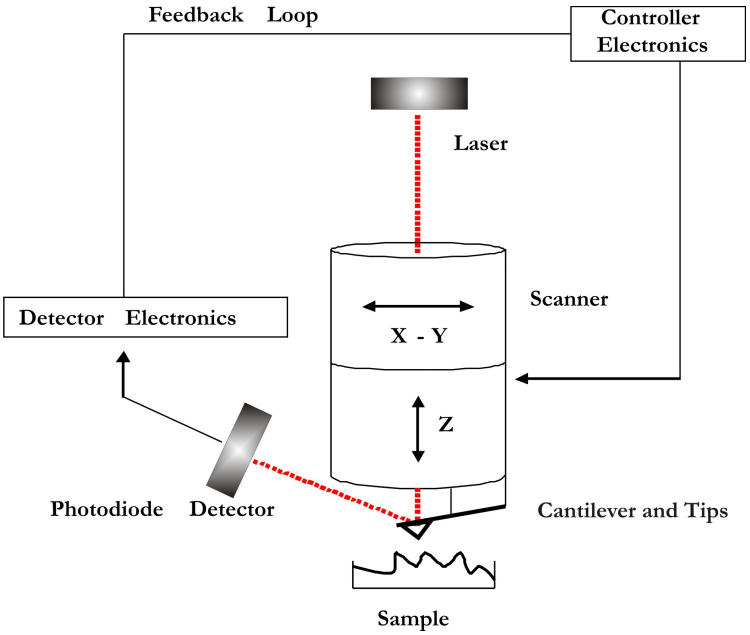

Figure 2.8: Main components of an atomic force microscope.

the surface. During the scanning, cantilever's resonant frequency is modulated by the force between tip and sample. The magnitude of amplitude damping and the amount of phase change of the cantilever depend on the chemical composition and the physical properties of the surface. Thus, on an inhomogeneous sample, contrast can be observed between regions of varying mechanical or chemical composition. During the scan, photodiode detects changes in the oscillation and a feedback loop maintains both the amplitude and the phase constant moving the piezoelelectric vertically along the Z axis during X-Y scan. Voltage necessary to keep constant the oscillation allows to build up a topographic image of the scanned surface.

AFM images result to be particularly useful for the detection of the fibril morphologies. Fibril length, thickness and shape can be easily visualized. For this reason, such tool has been employed for the characterization of different species along the insulin fibrillation pathways (Chapter 4).

Experimental Settings. Dynamic scanning force microscopy (SFM) [85] was carried out in air using a commercial instrument (Multimode Nanoscope V workstation, Veeco, Santa Barbara, CA). Etched-silicon probes with a pyramidal-shape tip having a nominal curvature of 8 nm and a nominal internal angle of 25° were used. During scanning, the 125-μm-long cantilever, with a nominal spring constant in the range of 20-80 N·m, oscillated at its resonance frequency (286 kHz). Height and phase

images were collected by capturing 512x512 points in each scan and the scan rate was maintained below 1 lines per second. During imaging, temperature and humidity were about 20°C and 40%, respectively. SFM measurements have been carried out during fibrillation kinetic of 4 mg/ml of bovine insulin in HCl 25 mM, NaCl 0.1 M pH 1.6 at 60°C. During the kinetics, aliquots have been taken out and dilute 200 times in water solution of 25 mM HCl without salt. Afterwards, 8 μl of such solution have been positioned on previously cleaned mica surface. A nitrogen flux has been used for 5 minutes to dry the protein solution on the mica before performing SFM measurements. Such procedure has been used for the acquisition of 6 images during the kinetics. To properly investigate the entire sample surface, several images were acquired from different sample areas.

2.4 Materials, samples preparation and treatments

Care and clarity on sample manipulation is a crucial point in fibrillation studies. Moreover, a deep description on how protein solutions have been prepared before inducing fibril formation may help for a reliable comparison between experimental results on the same process as obtained by different investigators. For these reasons, detailed presentation of compounds, preparation procedures and the experimental setting are provided in this section.

2.4.1 Fibril formation in human and bovine insulin samples

Human insulin was obtained from Novo Nordisk A/S, Copenhagen Denmark[1]. The zinc content was 0.4% (w/w), corresponding to approximately two Zn^{2+} ions per insulin hexamer. Samples at different concentrations were singly prepared immediately prior to each experiment. Protein concentration was determined by UV absorbance at 276 nm using an extinction coefficient of 1.0 for 1.0 mg/ml [86]. All the human insulin samples used in this study were prepared by dissolving insulin in 20% acetic acid with 0.5 M NaCl (pH 1.8). To avoid formation of salt crystals, the solvent was freshly prepared before each experiment and filtered through 0.22 μm filters (MS 16534, Sartorius), before adding human insulin. Both ThT fluorescence and turbidity experiments on human insulin were carried out using a plate reader system (Fluostar, BMG Labtech, see Section 2.2.1) with 96-microwell polystyrene plates (Nalge Nunc). Each well was filled with 200 μl of solution and four replicates

[1]The experiments on human insulin samples have been performed in the framework of the material transfer agreement (MTA) stipulated with Novo Nordisk A/S, Denmark (January 2006), for providing human insulin powder. For such reason, Novo Nordisk A/S has the copyright of the scientific results presented in Chapter 3.

for each sample were measured to determine the reproducibility of the results. For the statistical investigation at each concentration, the protein stock solution was prepared and split into aliquots of 200 μl in 44 wells, each containing 20 μM ThT. Fibril formation was simultaneously induced and detected on the 44 samples. The plates were incubated at 45°C without any mechanical shaking of the samples.

Bovine insulin was purchased from Sigma Aldrich and used without further purification. As for acetic acid solutions, to avoid formation of salt crystals, the solvent used for this study (HCl 25 mM, NaCl 0.1 M pH 1.6) was freshly prepared before each experiment and filtered through 0.22 μm filters (MS 16534, Sartorius), before adding bovine insulin. Samples at different bovine insulin concentrations were freshly prepared, centrifuged (3000 rpm 10 min) and filtered through 0.22 μm filters (MS 16534 Sartorius) prior to each experiment. Also in this case, protein concentration was determined by UV absorbance at 276 nm using an extinction coefficient of 1.0 for 1.0 mg/ml [86]. Fluorescence experiments were performed at 60°C inducing fibrillation on a sample volume of 1.1 ml in 1 cm path PMMA UV-Grade cuvette (Kartell) with 20 μM of ThT. Prior to each experiment, cuvettes were carefully washed by milli-Q water and then dried in nitrogen atmosphere to minimize presence of unpredictable impurities. To study the early stages of fibril formation in the low concentration regime (0.5, 0.75, 1, 1.5 and 2.5 mg/ml), emission spectra (λ_{exc}=450 nm) were detected by an ACTON Spectrograph system, Princeton Instruments (see Section 2.2.2).

ThT was purchased as the chloride salt from Sigma-Aldrich Chemie GmbH (Schnelldorf, Germany). The purchased ThT was recrystallized three times in demineralised water and the dye concentration in water was estimated by absorbance spectroscopy using a molar extinction coefficient of 36,000 M^{-1} cm^{-1} at 412 nm [20]. For *in situ* ThT fibrils monitoring, stock solutions of ThT in milli-Q water were prepared (0.125 mM, 0.25 mM, 0.5 mM, 1 mM, 2 mM and 4 mM) and stored a 4°C protected from light to avoid photobleaching. ThT at the desired concentration was added to each well or cuvette before incubation.

2.4.2 Thioflavin T hydroxylation and amyloid detection

For the study on the optical properties of ThT at high pHs (Chapter 5), stock solutions of 1 mM of ThT in milli-Q water were prepared (see 2.4.1 for details on ThT powder). K_2HPO_4 and KH_2PO_4 salts were properly mixed to give a final concentration of 0.1 M in milli-Q water and they were used to obtain buffer solutions at different pH values (pH range 5.2-8.9, 25°C). 20% acetic acid 0.5 M NaCl in milli-Q water was used to obtain a solution with a pH value of 1.7. ThT solutions with various dye concentration (10-100 μM) at different pH values were prepared and then

incubated at the desired temperature (35-55°C). OH^- concentrations at different temperatures were indirectly estimated by measuring pH and taking into account the well known temperature dependence of the ionization constant of water ($f(T)$) by means of the following equation

$$[OH^-] = f(T) \cdot 10^{pH-14} \tag{2.6}$$

Absorbance spectra were carried out on a Shimadzu PC201 spectrophotometer with a peltier cell. All samples were positioned in a 1 cm path cuvette and, 3 minutes after thermal equilibration to a certain temperature, spectra were collected in the range 220-500 nm. Single-wavelength kinetics were carried out using a plate reader system (Polarstar, BMG Labtech, see Section 2.2.1) with a sample volume of 200μl.

With the aim of studying the effects of ThT hydroxylation on amyloid aggregates detection, Succinil Concanavalin A (hereafter S-Con A) was employed as a model system for the growth of fibrillar aggregates, because of its capability to form fibrils under experimental conditions in which ThT hydroxylation may occur. At basic pH and at temperatures ranging between 37°C and 45°C, S-Con A rapidly forms amyloid fibrils and the rate of aggregate formation increases with temperature, without any change in the aggregation mechanisms [23].

S-Con A was purchased from Sigma-Aldrich and used without any further purification. All the measurements were performed in 0.1 M phosphate buffer at pH 8.9. A S-Con A solution at 0.5 mg/ml was freshly prepared and filtered (0.22 μm MS 16534, Sartorius) immediately before the incubation.

For fibril preparation, the sample was incubated at 50°C for 5 hours and then split into two identical aliquots. Afterwards, a freshly prepared ThT solution was added to one of the aliquots and ThT incubated at 50°C for 5 hours was added to the other. In both cases, the final ThT concentration was 40 μM. For the *in situ* fibrillation kinetics (absorbance and fluorescence), 0.5 mg/ml native S-Con A with freshly prepared ThT (5, 15 and 40 μM) was incubated at 50°C and both the absorbance and the fluorescence (λ_{exc}= 440 nm and λ_{em}= 480 nm) were recorded for a period of ∼13 hours. For the *ex situ* fibrils detection, 33 ml of 0.5 mg/ml S-Con A were split into 12 cuvettes, which were subsequently stored at 50°C. At different incubation times, each cuvette was taken out and stored in an ice bath. After waiting for thermal equilibrium at room temperature, ThT (40 μM) was added and fluorescence spectra were recorded at 25°C. Samples were positioned in a 1 cm path quartz cuvette and fluorescence measurements were carried out on a Jasco FP-6500, equipped with a Jasco ETC-273T peltier temperature controller (see Section 2.2.3).

Chapter 3

Heterogeneous pathways in insulin amyloid formation

[...]The last ever dolphin message was misinterpreted as a surprisingly sophisticated attempt to do a double-backwards-somersault through a hoop whilst whistling the "Star Sprangled Banner", but in fact the message was this: so long and thank for all the fish.

[Douglas Adams, *Hitchhiker's Guide to the Galaxy*, 1979]

It is now generally accepted that insulin fibrillation is affected by secondary nucleation pathway, leading to a characteristic kinetic profile. Notwithstanding this, several molecular mechanisms can produce such autocatalytic process like fragmentation, branching and nucleation at the surface of already formed fibrils. Aim of this chapter is to deeply investigate which of these mechanisms is mostly involved in the fibrillogenesis of human insulin.

3.1 Introduction and purposes

As previously discussed in Chapter 1, at low pH and high temperature, insulin is very prone to form amyloid fibrils [18, 19, 53, 87]. The fibrillation process exhibits a strong time dependence, with a pronounced lag phase, followed by a very fast growth of fibrils. This time dependence can be described in terms of the secondary nucleation mechanisms [55], in agreement with time lapse Atomic Force Microscopy observations [17]. In such a process, a key role is most likely played by the surface of the fibrils [56, 88], as previously suggested by Waugh [54, 89]. Notwithstanding this, clear experimental proof and a proper discussion of the specific secondary mechanism involved are not present in literature yet.

In this Chapter, the fibrillation process of human insulin in a wide range of protein concentrations has been studied. Thioflavin T fluorescence was used to selectively detect amyloid fibrils, by mechanisms which involve the interaction between the dye and the accessible surface of the fibrils (see Section 2.1). Temporal features of the process has been analyzed as a function of the initial insulin concentration. Based on the ThT-fibril binding peculiarity and also on the well known polimorphysm occurring in the insulin fibrillation pathway, experimental data lead to a suggestion on the mechanism involved in the insulin fibrillogenesis. Moreover, because of the intrisically uncertain nature of the fibrillation kinetics, a statistical study of the fibrillation progress curves has been also performed. For this study, solutions containing acetic acid have been used to dissolve the protein. In this conditions (20% acetic acid 0.5 M NaCl) native insulin is monomeric. Fibrillation was thermally induced at 45°C in a plate reader system (see Section 2.2.1).

3.2 Experimental results and discussion

Investigation on insulin fibrillogenesis here presented has been performed using ThT assay. Temporal analysis and characterization of the kinetics, ability of ThT to bind to fibrils and reproducibility of the kinetics have been taken into account.

3.2.1 Characterization of fibrils formation

The ThT fluorescence as a function of incubation time is shown in Figure 3.1 for samples at seven different insulin concentrations in the range 1-20 mg/ml, at 45°C with a fixed ThT concentration of 20 μM. All kinetics present a characteristic sigmoidal profile with a pronounced lag time, in which apparently nothing happens, followed by an abrupt increase of the fluorescence signal. In the whole concentration range, there is no evidence of the biphasic fibrillation behavior observed by Grudzielanek and coworkers at analogous pH values for bovine insulin, when the protein is dissolved in aqueous solution (without acetic acid) [57]. In that case, authors proposed an oligomeric transition state as an alternative aggregation pathway leading to several species occurring during the kinetics. Conversely, kinetic profiles in Figure 3.1 confirm a recent report in which measurements have been performed exactly in the same experimental setting here employed [59]. In accordance with previous studies [18, 19, 55], Figure 3.1 shows that lag time values decrease by increasing insulin concentration, at least in the range 1-5 mg/ml. Analogous fibrillation kinetics were observed with ThT concentrations of 5 and 40 μM (not shown) without any changes in the temporal features of the reactions. Two parameters were used to describe the process: 1) ThT fluorescence final value (FFV, see Figure 3.2a), and 2) the

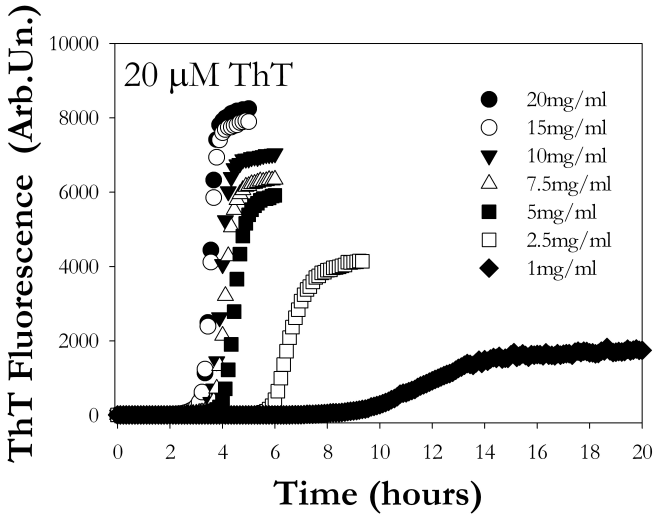

Figure 3.1: Kinetics of human insulin fibrillation in 20% acetic acid, 0.5 M NaCl, 45°C (λ_{exc}=450nm λ_{em}=480nm). The ThT fluorescence is shown as a function of incubation time at different insulin concentrations.

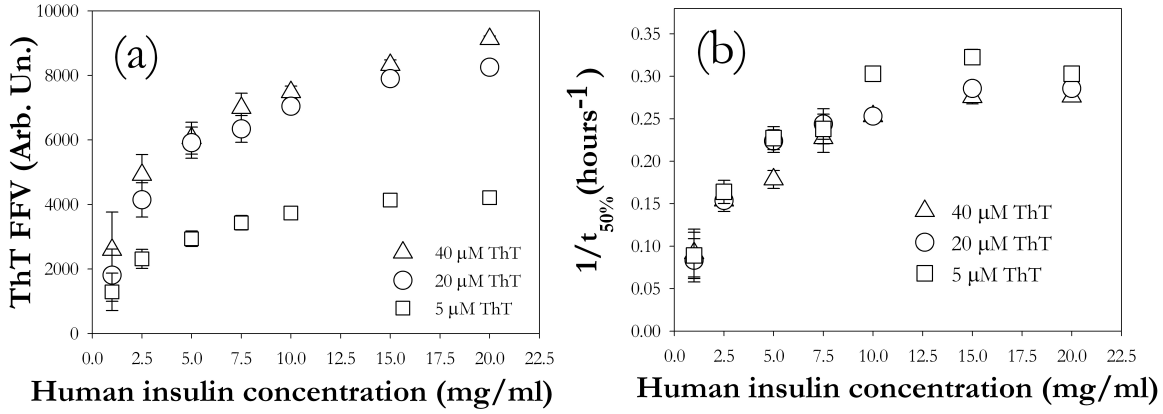

Figure 3.2: (a) ThT fluorescence final value (FFV) as a function of protein concentration at three different ThT concentrations. (b) Inverse of the time at which the fluorescence signal reaches 50% of the FFV ($1/t_{50\%}$) as a function of protein concentration at three different ThT concentrations. Error bars represent absolute deviations observed on four replicates.

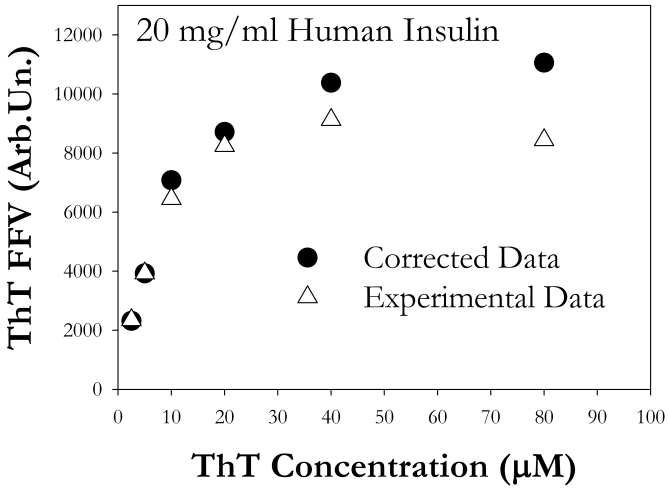

Figure 3.3: FFV as a function of ThT concentration for samples at 20 mg/ml protein concentration after fibrillation. (△) Experimental data and (•) data corrected for the inner-filter effects (see Section 2.2.1).

reciprocal of the time necessary to reach 50% of FFV ($1/t_{50\%}$, see Figure 3.2b). ThT fluorescence intensity should be in principle related to the amount of fibrils occurring in solution, so that a rough estimation of amyloid concentration can be obtained. The other parameter, $1/t_{50\%}$, contains information on the length of the lag phase and on the growth rate of the fibrillation reaction and it represents a sort of overall rate constant of the process. The values obtained for these two parameters are shown in Figure 3.2a and 3.2b as a function of protein concentration, for three different concentrations of ThT (5, 20 and 40 μM). Both parameters display a sort of saturation effect for protein concentrations above ∼5 mg/ml. Concerning FFV (Figure 3.2a), the saturation level clearly depends on the amount of ThT in the sample, but the saturation effect by itself can not be ascribed to experimental artifacts such as insufficient ThT in solution, at least for ThT concentrations > 20 μM. In this respect, a series of measurements were performed at high protein concentration (20 mg/ml) and ThT concentrations spanning from 2.5 to 80 μM. The dependence of FFV on ThT concentration for these measurements is shown in Figure 3.3; the results (open triangles) display a linear increase of FFV from 2.5 μM up to 10 μM and then, starting from 20 μM of ThT, the FFV value is almost unaffected by further addition of ThT. It is worth to note that optical artifacts were also taken into account (see Section 2.2.1); in particular, the effects of the absorption of the fluorescence excitation beam at different ThT concentrations were estimated and corrected data are also shown in Figure 3.3 (full circles). The experimental data are only slightly affected by absorp-

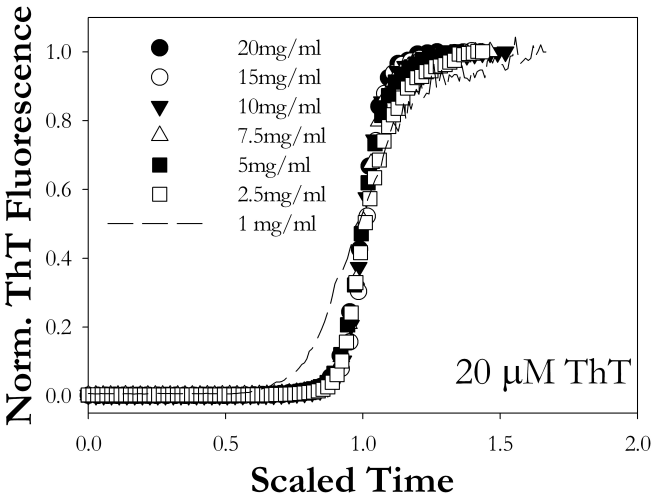

Figure 3.4: The same kinetics as in Figure 3.1 were scaled for the FFV in the ordinate axis and for $t_{50\%}$ in the abscissa.

tion of the excitation beam, confirming that the attenuation effect at higher ThT concentration has to be related to the peculiarity of fibril-dye binding. Moreover, at the end of the fibrillation kinetics at various concentrations, after centrifugation of the sample, no significant amount of protein in the supernatant was detected (<5%), confirming that in these experimental conditions insulin fibrillation proceeds by an essentially total conversion of native protein into amyloid aggregates [59]. In view of these data, the saturation effect shown in Figures 3.2a and 3.2b, at least for 20 μM and 40 μM ThT, is most likely a property of the fibrillation process by itself. The data in Figure 3.2a thus indicate that, above a protein concentration of 5 mg/ml, the number of binding sites in the fibrils for ThT yielding the characteristic fluorescence remains almost constant. The values of $1/t_{50\%}$ (Figure 3.2b) are barely affected by the amount of ThT in solution. Similar values were also obtained in the absence of ThT, by measuring the progress of the fibrillation process by sample turbidity (data not shown). On average, increasing the ThT concentration results in a slightly slower fibrillation process, without changing the main features of its protein concentration dependence and of the above mentioned saturation effect. It is interesting to note that the four replicates for each measurement indicate that the reproducibility of the fibrillation process significantly improves at high protein concentration (see the error bars in Figures 3.2a and 3.2b and Section 3.2.3). In Figure 3.4, the same kinetics shown in Fig. 3.1 are reported after scaling fluorescence intensity and incu-

bation time for FFV and $t_{50\%}$ values, respectively. All the kinetics in the range 2.5-20 mg/ml scale well, especially for the first half of the trace. Data obtained at 1 mg/ml do not match with the others and also show a low reproducibility, indicating the presence at this concentration of some unpredictable effects, probably enhanced by the long duration of the experiment ($\sim$ 20 hours). The scaling properties shown in Figure 3.4 are not trivial. In fact, the kinetics of fibril formation are described by two parameters, which are not necessarily related to each other: the duration of the lag phase, and the rate constant of fibril growth. The scaling of the data suggests there actually is a correlation between these two parameters; as recently reported, such a correlation may be a common property in the formation of amyloid aggregates [90]. In this regard, however, it must be noted that the lag phase values and rate constants of fibril growth may not be absolute; rather, they are highly dependent on the experimental setting (e.g. plate or cuvette material, surface-volume ratio of the sample, stirring and small unpredictable impurities in solution). Regarding the effect of experimental methods on nucleation events, several insights have been recently provided for insulin amyloid formation [56, 58], in particular, it has been observed by differential interference contrast (DIC) optical microscopy that glass surface defects or not properly cleaned glass surfaces catalyze the formation of amyloidogenic spheroid structures with the result of affecting dramatically both the subsequent nucleation and elongation mechanisms [58]. Furthermore, it was recently shown for islet amyloid peptide that the first nucleation events seem to be fully controlled by interactions between the protein molecules and liquid-liquid or liquid-solid interfaces, which act as nucleation points *via* a surface-assisted process [91]. This suggests that different experimental settings may induce different protein-surface interactions, thus resulting in a significant variability in the process parameters as determined by different investigators.

3.2.2 Accessible surfaces as nucleation points

The scaling properties displayed in Figure 3.4 indicate that one kinetic parameter suffices to describe the fibrillation process, and that the value of $1/t_{50\%}$ (Figure 3.2b) can be used as a measure of its velocity (a sort of overall rate constant). In Figure 3.5, this parameter is reported as a function of the FFV. Quite interestingly, as shown in the Figure 3.5 for 20 μM and 40 μM ThT concentrations, a linear relation exists between these two parameters, while neither of them is simply linearly dependent on protein concentration (see Figures 3.2a and 3.2b). This correlation, again, is not obvious at all, and the fact that it is observed at different ThT concentrations strongly suggests that it is not accidental. On the contrary, it indicates the existence of some meaningful physical quantity in the process, which determines both of the

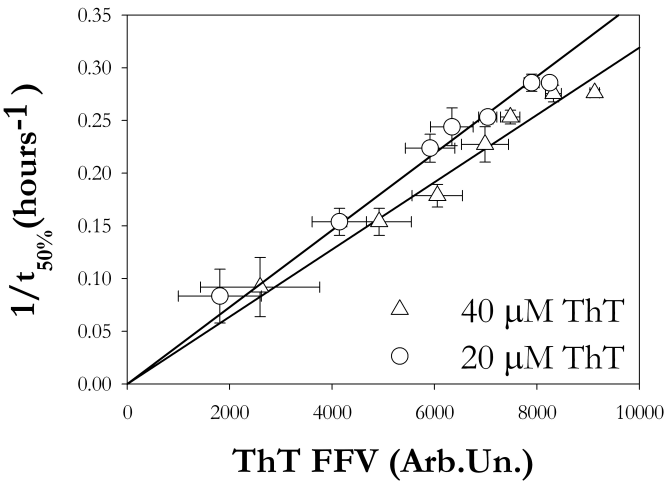

Figure 3.5: $1/t_{50\%}$ as a function of FFV for all the investigated protein concentrations at two different ThT concentrations. Error bars represent absolute deviations observed on four replicates.

parameters, and therefore the overall profile of the kinetics. This quantity is likely to be the accessible surface of fibrils, in agreement with the existence of secondary nucleation for insulin [17, 55, 56, 88] and with the recently proposed mechanisms for ThT binding to fibrils [20, 21, 79]. In fact, secondary nucleation theory predicts that the accessible surfaces of fibrils support the growth of new fibrils [47], the classical case being sickle cell hemoglobin polymerization [45, 46, 92]. Concerning the effects of surfaces on amyloid formation, it is also worth to note that an enhanced rate of fibrillation has recently been observed for β_2-microglobulin in the presence of nanoparticles characterized by large exposed surfaces [93]; the interaction between the exposed surface of the nanoparticles and the protein molecules may generate a locally high protein concentration and/or induce protein conformational changes, thus promoting a faster fibril formation. Further, in the case of insulin, an enhanced nucleation rate has been observed in the presence of hydrophobic polystyrene surfaces [51]. In this scenario, the surface of the early stable aggregates in insulin samples may act exactly in the same way: a larger accessible surface brings about a larger number of nucleation sites, promoting an enhanced growth of new fibrils. Moreover, at the same time, larger accessible surfaces mean a larger accessibility for ThT to binding sites. Accordingly, both the overall rate constant of the process ($1/t_{50\%}$) and the ThT fluorescence intensity (FFV) should be proportional to the accessible surface of fibrils and therefore linearly related to each other (Figure 3.5). Concerning

the concentration dependencies of the parameters shown in Figures 3.2a and 3.2b, it must be noted that, in general, different aggregate morphologies may occur in protein amyloid aggregation [56–58, 94]. For example, for insulin fibrillation, different environmental factors, i.e. solvent properties [19, 56] cosolvents addition [22, 57, 94, 95] and pressure [57] may affect the overall aggregation pathway [22, 94], the spatial arrangement of mature fibrils [56, 58, 95, 96] and even the presence of different cytotoxic species [94]. Different fiber morphologies may result in different ratio of fiber accessible surface and mass; this makes critical to determine a reliable estimation of the amyloid aggregates mass by ThT assay [56]. Several different structures of aggregates have been observed during the various phases of insulin fibrillation [56, 58, 96]. As clearly pointed out by Manno and coworkers [56], fibrils of different thickness can be formed and assembly in bundles, with a reduced accessible surface with respect to thin filaments. Concerning the data here presented, above ∼5 mg/ml fibril formation may be affected by a sort of molecular crowding effect, favoring the formation of less accessible objects at these concentration values. Such scenario may explain the concentration saturation effect shown in Figures 3.2a and 3.2b for both FFV and $1/t_{50\%}$. A role could be also played by the observed tendency of morphologically distinct templates to replicate themselves in an autocatalytic way [22, 97, 98]. Such explanation is also in full agreement with a recent and detailed report on the ThT binding mode to fibrils in which ThT has been used for the detection of two different morphologies of fibrils [80]. Authors proved that the ThT binding kinetics results dramatically slowed down when bundles of fibrils (e.g. less accessible binding surfaces) need to be stained compared to the kinetics of thin filaments detection (e.g. larger accessible binding surfaces).

It is worth to note that the saturation effect shown in Figure 3.2b for $1/t_{50\%}$, i.e. the weakening of the concentration dependence of the rate observed for fibril formation and growth, may have other alternative explanations. In particular, Powers and Powers (2006) showed that it can be brought about by the fact that above a *supercritical* concentration oligomers population may become significant with respect to the total protein concentration [50]. When this happens, and when aggregates can only grow by monomer addition, the rate of fibril growth may become almost independent of protein concentration because of monomer conversion to oligomers. This explanation however does not seem applicable in the case of insulin in the experimental conditions here used. Although small angle X-ray scattering measurements have shown the existence of a large population of oligomers, they were found to constitute both a structural nucleus and an elongation species in the growth of fibrils [59]. Therefore, in the case of insulin, fibrils may grow not only by monomer addition, but also by oligomer addition. As a result, oligomer formation does not explain that the lag phase no longer decreases at high protein concentration. However, the

rate of formation of these oligomers may also be affected by secondary nucleation mechanism, i.e. by the accessible surface of the fibrils.

The role of fibril surface was first noticed several decades ago by Waugh [54, 89], who proposed a model in which the rate of growth of fibrillated material was proportional to the fibril surface area [89]. However, in secondary nucleation processes what is proportional to the surface of fibrils is not the rate of growth of fibrillated material, but, instead, the rate of formation of new fibrils. The two models are conceptually different, and lead to distinct differential equations for the description of the kinetics [47, 89].

3.2.3 Stochasticity in insulin fibrils formation

In order to study the effects of protein concentration on the reproducibility of the process, a statistical investigation on samples at three different insulin concentrations has been carried out (1, 2.5 and 5 mg/ml, see Section 2.4.1). When incubated at 45°C, apparently identical insulin samples do not show exactly the same kinetic profile (Figure 3.6). In order to fully characterize such variability, in Figure 3.7 the statistical distributions of both FFV and $1/t_{50\%}$ are presented; both parameters are normalized for their average value and the relative spread of the data clearly depends on insulin concentration, being larger at lower protein concentration. Generally, the formation of the early aggregates in solution may be considered an inherently stochastic event

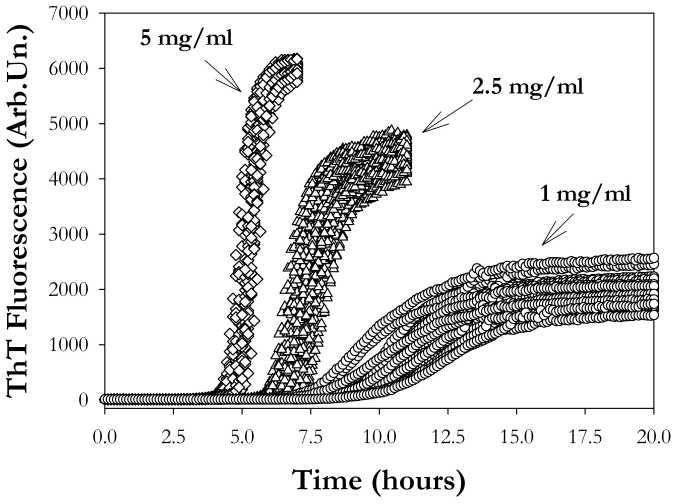

Figure 3.6: Kinetics of human insulin fibrillation at three different insulin concentrations (5, 2.5, 1 mg/ml). For each concentration, a stock solution was split in 44 wells and fibrillation was simultaneously induced in these samples.

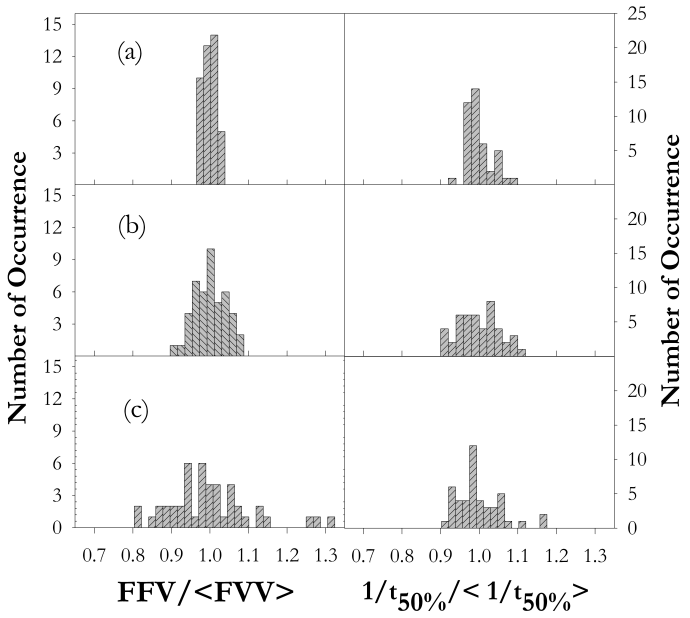

Figure 3.7: Statistical distribution of FFV and $1/t_{50\%}$ normalized for their average value. (a) 5 mg/ml, (b) 2.5 mg/ml and (c) 1 mg/ml of human insulin.

[47], resulting in some level of variability of the process parameters. In particular, the spread of $1/t_{50\%}$ in our data is mainly determined by a variation in the lag phase values and not in the elongation rate (analysis not shown), suggesting a process initially controlled by stochastic events. As recently observed for the aggregation kinetics of β-amyloid peptide [99], the kinetic reaction appears to be more reproducible at high protein concentration and, in general, in conditions favoring intermolecular association. A large variability in the lag phase of the HbS polymerization process has been observed by Hofrichter (1986), who proposed that the early stages of the kinetics are fully determined by a single nucleation event and by a subsequent fast growth of polymers, explained, as for insulin, by secondary nucleation mechanisms [100]. In this sense, insulin fibrillation seems to resemble HbS polymerization: a single nucleation event may happen in a given sample region and then the first stable aggregates determine the further growth of fibrils. However, it is important to stress again that the nature of the lag phase strongly depends on the environmental conditions. In fact, in other solvents, ThT fluorescence shows that the lag phase may be entirely suppressed [56], and even a biphasic fibrillation pathway may occur [57], with an essentially immediate pre-transition.

3.3 Conclusions

An experimental study on insulin amyloid fibril formation has been presented in this chapter. Using ThT fluorescence final value (FFV) and the inverse of the time at which the fluorescence signal reaches half of the final value ($1/t_{50\%}$), the kinetics in a wide range of concentrations have been described. Both the parameters show a sort of saturation as a function of the protein concentration. Such saturations have been interpreted as an effect of the different fibrils morphologies that can occur changing the insulin concentration. Probably at higher concentration not only thin fiber filaments can occur but fibrils can also associate forming highly compact bundles. Such compactness leads to a reduced accessible surface of fibrils with a simultaneous attenuation effect both on the detected fluorescence (dependent on ThT-fibril binding) and the rate constant (dependent on surface-catalyzed process). Moreover, the linear relationship between FFV and $1/t_{50\%}$ further confirms that both the parameters are related to the same physical amount, indicating that the fibrillation process is essentially determined by a fibril surface-catalyzed mechanism, through secondary nucleation pathways. Finally, data show that, at least in early stages, the process is inherently stochastic and is characterized by an intrinsic variability of the kinetic parameters.

Chapter 4

Spatial heterogeneity in insulin amyloid formation

In fact there was only one species on the planet more intelligent than dolphins, and they spent a lot of their time in behavioural research laboratories running round inside wheels and conducting frighteningly elegant and subtle experiments on man.

[Douglas Adams, *Hitchhiker's Guide to the Galaxy*, 1979]

Results presented in Chapter 3 focused only on the growth mechanism after the lag phase evidencing the crucial role of the heterogeneous nucleation pathway. Early stages of the process, i.e. lag phase and initial fibrils growth, need to be deeply investigated even considering different solvent composition. Aim of this chapter is to take into account the effect of insulin concentration on the fibrillation kinetics in HCl solution. Such solvent composition has been chosen because of the still not clear initial processes taking place in these experimental conditions. Initial stages, involved mechanisms and occurring species will be the main subjects of this investigation.

4.1 Introduction and purposes

As seen in Chapter 3 fibrillogenesis pathway for insulin results in a highly diversified scenario both for the involved mechanisms and the occurring species. Moreover, it is worth of note that also the kinetic profile can be affected by different experimental conditions, diverging from the classical three-steps curves (as shown in the previous Chapter) and showing a range of different species in solution. Regarding the species occurring in the fibrillation path, several studies have shown that different amyloid morphologies can occur being dependent on the solvent composition as well as on hydrostatic pressure. As pointed out in Section 1.4.2, great interest

has been recently addressed also to the effects of the experimental conditions and intrinsic uncertainty on *in vitro* insulin fibril formation [58] underlying a high degree of stochasticity for this process.

Addressing the efforts towards the above reported problematics, here it is presented an experimental study of thermally induced fibrils formation on bovine insulin in HCl solution. Progress curves for fibril formation at different insulin concentration were detected using Thioflavin T fluorescence. A double-sigmoidal ThT increase were obtained in a narrow range of insulin concentration and the occurring morphologies were revealed by atomic force microscopy. Moreover, ThT assay together with dynamic light scattering have been used for the study of the early stages pointing out a pronounced spatial heterogeneity in the formation of the early stable aggregates of the process. Fibrillation was thermally induced at 60 °C in a standard 1 cm path length cuvette (see Section 2.2.1 for details).

4.2 Experimental results and discussion

Dependence of the fibrillation profile on insulin concentration and the topographic characterization represent the preliminary results for the present study on fibril formation in HCl solutions. Further, applying the mathematical modeling reported in Section 1.3, a rationalization of the early stages of the process together with the description of the events at the end of the lag phase is also provided.

4.2.1 Amyloid morphologies in the fibrillation pathway

Figure 4.1 shows the progress curves of ThT fluorescence as a function of the incubation time for ten insulin concentrations, ranging from 0.5 to 10 mg/ml, incubated at 60°C with 20 μM of ThT. At low insulin concentrations ($<$ 3 mg/ml), the kinetics present the well known sigmoidal, three steps behavior with a pronounced lag phase, a subsequent very fast growth of amyloid aggregates, and a final saturation as revealed by ThT intensity. Interestingly, in solutions at analogous low pH and in presence of acetic acid, both human insulin (see Chapter 3) and bovine insulin [55] present a classical three-steps curve being such profile a common feature in a wide range of protein concentration (1-20 mg/ml). Contrarily, as shown in Figure 4.1, in presence of HCl increasing insulin concentration produces drastic changes in the kinetic profile. ThT emission shows a biphasic temporal behavior in the intermediate range of concentration investigated (3.5 and 4 mg/ml) and an almost absent lag phase at higher concentration (5-10 mg/ml).

It is worthy of note that, when bovine insulin is dissolved in aqueous solution at low pH (without acetic acid), the appearance of a double process has been al-

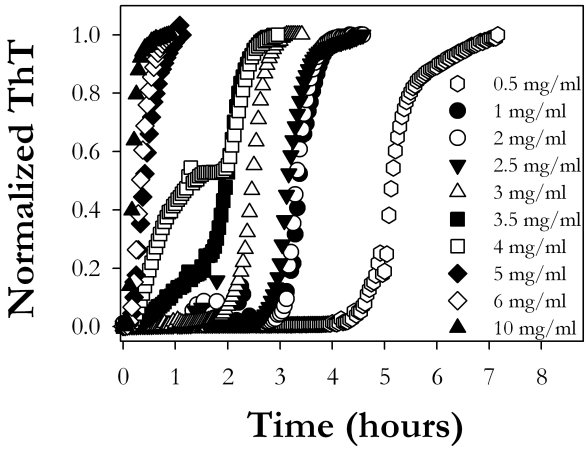

Figure 4.1: Kinetics of bovine insulin fibrillation in 25mM HCl, 0.1 M NaCl, 60 °C with 20 μM ThT (λ_{exc}=450 nm and λ_{em}=480 nm). ThT normalized to the plateau value are shown as a function of incubation time at different insulin concentrations.

ready reported by Grudzielanek and coworkers [57]. In that study, the occurrence of two concurrent aggregation pathways has been triggered by tuning the pressure and by adding proper cosolvent. The authors proposed a scheme in which formation of oligomers rich in β-sheet structures may determine the first increase of ThT intensity (pre-transition) and afterwards the standard cooperative mechanism leads to the formation of mature fibrils (main transition). In HCl solutions, data suggest that the occurrence of the so-called *pre-transition* and *main transition* phase may also be dependent on insulin concentration. In particular, they simultaneously occur only in the range of insulin concentration of 3-4 mg/ml. With the aim of further studying such double process, an investigation on the different species occurring during the fibrillation pathway at 4 mg/ml has been carried out by means of an atomic force microscope. At this concentration pre-transition accounts for $\sim$ 50% of the overall ThT fluorescence increase and AFM measurements have been performed at the different incubation times as indicated by the arrows and roman numerals in Figure 4.2a. Scans are displayed in Figure 4.2b. Image on sample at 25°C before incubation (Figure 4.2b, I) does not show sizable objects in solution. Only species with a height of 1-2 nm are revealed, indicating the presence of only native protein molecule, as also obtained by dynamic light scattering analysis (black line in Figure 4.3). Interestingly, such insulin molecule size is in agreement with previous AFM observations [17] and small angle X-ray scattering data [18] that indicate a major presence of insulin monomers and dimers in solutions with HCl. After 40 minutes of incubation (Figure

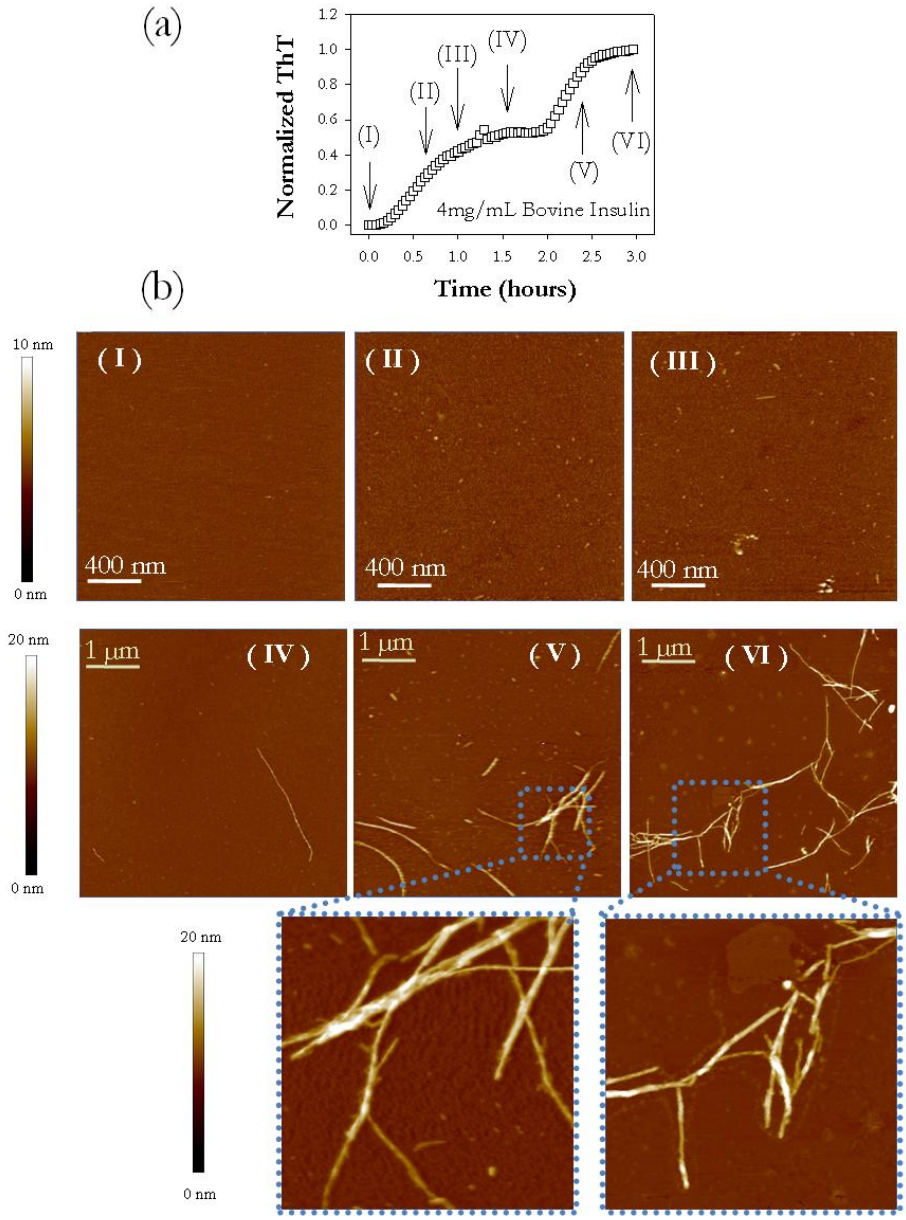

Figure 4.2: Fibrillation kinetics of bovine insulin at 4 mg/ml in 25 mM HCl, 0.1 M NaCl, 60 °C. (a) ThT fluorescence curve during the process (b) AFM images at different time point of the kinetics. Roman numerals indicate samples at different incubation time as shown in Figure 4.2a. (I) 0 min, (II) 40 min, (III) 60 min, (IV) 90 min, (V) 140 min, (VI) 180 min. In the blue dotted boxes, zooms on the fibrils morphologies in the final part of the kinetics are reported.

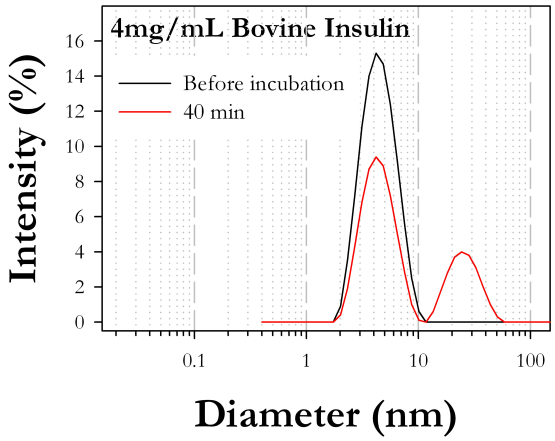

Figure 4.3: Fibrillation kinetics of bovine insulin at 4 mg/ml in 25 mM HCl, 0.1 M NaCl, 60 °C. Diameter size distribution before incubation (black) and after 40 min at 60 °C (red) as obtained by analysis of dynamic light scattering data.

4.2b, II) and in correspondence of the first growth of the ThT intensity (see Figure 4.2a), small protein assemblies occur in solution. Interestingly, a clear presence of such population has been also revealed during the kinetics by dynamic light scattering measurements and a hydrodynamic diameter of $\sim$ 30 nm has been estimated for this species (red line in Figure 4.3). Such assembled molecules are not elongated and seem to resemble the β-sheet-rich oligomers ThT-positive observed by Grudzielanek and coworkers. After $\sim$ 60 min, together with oligomers, thin filaments (2-5 nm in height) start occurring in solution. Such fibers display a quite regular shape and a length of 50-300 nm without any evidence of branching (Figure 4.2b, III). Because of the presence of such sizable assembly, since this instant, scattering data result poor for a reliable analysis of the size distribution. When ThT signal reaches the first plateau (90 min, Figure 4.2b, IV), elongation proceeds leading to fibers of 0.5-3 microns in length with an almost unvaried height. After 140 min (Figure 4.2b, V), i.e. when the second ThT increase starts, branched fibers start to appear evidencing the activation of elongation pathway in proximity of already formed fibrils (see zoom of Figure 4.2b, V) producing a noticeable increase in the thickness up to 9 nm. Such process results more pronounced in the subsequent instants of the reaction up to the formation of a highly branched and widely distributed network of fibrils at the end of the kinetics ($\sim$ 180 min, Figure 4.2b, VI). Further, besides the branching, in the last part of the kinetics interaction *via* fibrils surfaces may produce formation of thick fibrils with detected height up to $\sim$ 12 nm (see zooms of Figures 4.2b, V

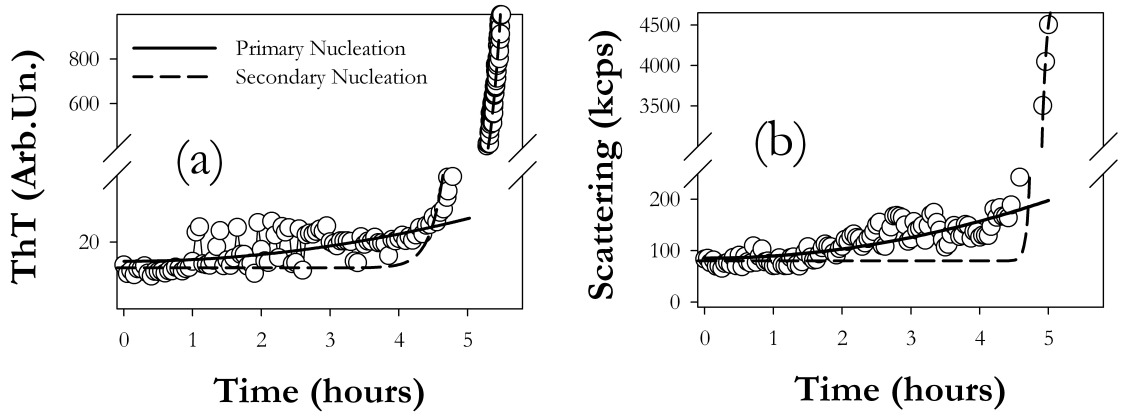

Figure 4.4: (a) ThT fluorescence and (b) DLS intensity as a function of the incubation time during the early stages of fibrillation of 0.5 mg/ml bovine insulin in 25 mM HCl, 0.1 M NaCl, 60 °C. Solid lines are quadratic fitting curves of data during the lag phase (homogeneous nucleation). Dashed lines are exponential growth fitting curves of the whole data set (secondary nucleation).

and VI), confirming the diversity of fiber morphologies along the fibrillation pathway [17, 55, 56, 89].

4.2.2 Lag phase in the low concentration regime.

At high concentration (> 4 mg/ml), besides the absence of the lag time, the biphasic behavior does not take place or, probably, the occurrences of the two processes could be too fast to be clearly detected. For the other concentrations investigated ($<$ 3 mg/ml), a standard three-steps mechanism seems to take place with a decreasing lag phase as protein concentration is increased and without any evidence of biphasic behavior (Figure 4.1).

Early stages of the process have been studied starting with the analysis of the lag phase during fibrillation at low protein concentration (< 3 mg/ml). Lag phase is generally indicated as the time in which apparently nothing happens and no significant changes in the signals are detected as also evidenced, for example, in the measurements at 0.5 mg/ml in Figure 4.1 (~ 4.5 hours).

To deeply study such aspect, we detected both ThT intensity, using a high sensitive CCD camera (see Section 2.2.2 for details), and light scattering signal. As shown in Figure 4.4a for the kinetics at 0.5 mg/ml of bovine insulin, ThT signal is not exactly constant during the *nominal* lag phase and shows a very slight increase since the

first instants up to ∼4.5 hours of incubation. Such intensity increase, even if very low, results highly reproducible on several independent attempts. Afterwards, i.e. when secondary nucleation mechanism takes the control of the reaction, an enhanced ThT intensity of several orders (up to ∼ 100 times of the initial value) occurs. Moreover, light scattering progress curve shows the same temporal behavior (Figure 4.4b). Remarkably, the above reported slight increases in the early stages have been obtained for kinetics up to 2.5 mg/ml of insulin concentration. Such data could indicate that the so called nucleation takes place in early stages of the kinetics and it does not have a length of several hours as roughly indicated in Figure 4.1. Further, at least at the beginning of the fibril formation, elongation of small fibrils from the nuclei can be considered as a sequence of a tip to tip addition of unfolded or native species to the nuclei. Such reaction can be rationalized in term of the homogeneous nucleation leading to a quadratic time dependence [47]. Both in Figures 4.4a and 4.4b a fitting ($y = a + bx^2$) has been performed on data during the lag phase showing a satisfying agreement. Afterwards, when fibrils size increases, exposed fibril surfaces allow the onset of the secondary nucleation [17]. As theoretically predicted by Ferrone (1999), since such event occurs, an exponential growth function (dashed lines in Figure 4.4a and 4.4b) very well describes the kinetic profile. However, it must be noted that the initial signal increase in Figures 4.4a and 4.4b could be also ascribed to a residual formation of β-sheet oligomers, as those observed at higher concentration (Figures 4.2a and 4.2b). In fact, a very low concentration of such species could also contribute to the initial slight increase of the signals in the kinetics at insulin concentration $<$ 2.5 mg/ml, and their formation, even if not clearly detected, can not be excluded. Interestingly, increase of the ThT signal since the early stages of the process has been also observed by Manno and coworkers, confirming that the period before the onset of sizable fibrils is far from being *flat* [56] at least in HCl solutions.

4.2.3 Spatial heterogeneity in the low concentration regime.

ThT fluorescence spectra during the fibrillation kinetics in HCl detected by PMT system display the profile of Figure 4.5. As can be seen, some of the spectra result remarkably distorted. These distorted spectra were recorded immediately at the end of the lag phase (see inset in Figure 4.5). With the aim to further characterize such peculiarity, we detected the early stages of ThT intensity growth using a CCD camera (see Section 2.2.2 for details). The time acquisition of this detector up to 1 μs enabled to perform a quantitative detection of the intensity fluctuations of the emission spectra as a function of the protein concentration ($<$ 2.5 mg/ml).

By a highly focalized beam (λ_{exc}=450 nm), a portion of the sample volume has been excited and emission spectra have been detected. As an example, Figure 4.6

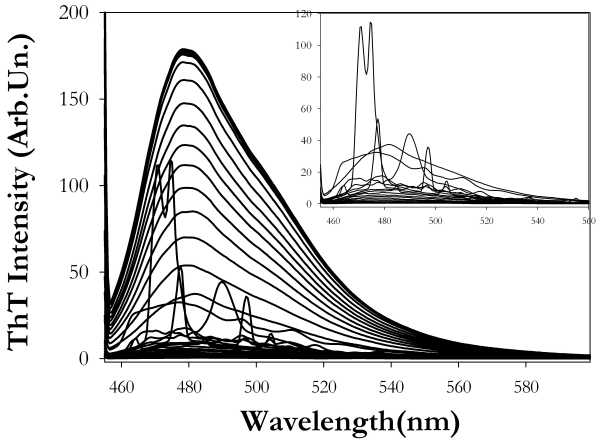

Figure 4.5: ThT fluorescence (λ_{exc}=450 nm) during fibrillation of bovine insulin in 25 mM HCl, 0.1 M NaCl at 60 °C (20 μM ThT). Inset shows the signal evolution at the end of the lag phase as detected by a PMT scanning detector.

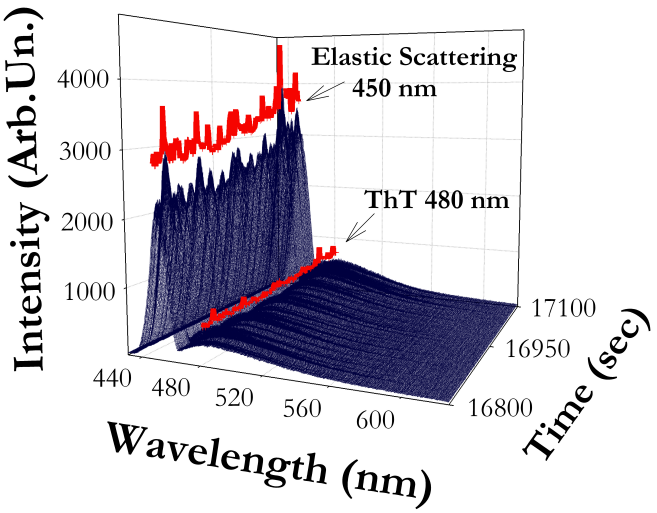

Figure 4.6: 300 emission spectra (λ_{exc}=450 nm) as detected for 300 seconds at the end of the lag phase (16800-17100 seconds of incubation) of 0.5 mg/ml of bovine insulin in 25 mM HCl, 0.1 M NaCl at 60 °C (20 μM ThT). Red lines are indicated to better visualize the evolution of elastic scattering (λ_{em}=450 nm) and ThT intensity (λ_{em}=480 nm).

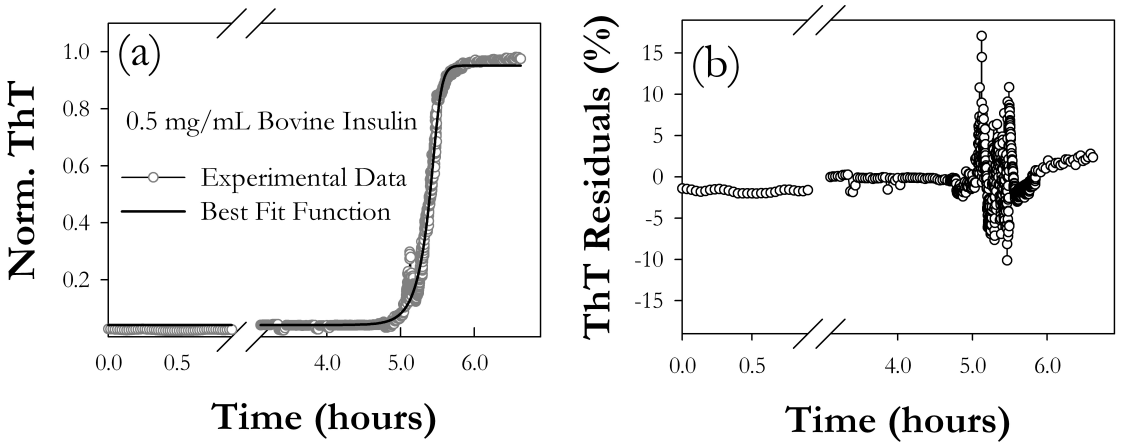

Figure 4.7: (a) Normalized ThT intensity during kinetics of 0.5 mg/ml bovine insulin in 25 mM HCl, 0.1 M NaCl, 60 °C (λ_{exc}=450nm λ_{em}=480nm). Solid line represents the best fit function. (b) Temporal profile of percentual residuals as obtained by fitting of the experimental data in Figure 4.7a.

shows the temporal evolution of the emission spectra just at the end of the lag phase (0.5 mg/ml of bovine insulin after ∼4.5 hours of incubation) detected with an acquisition time of 1 sec per spectrum for a period of 5 minutes. Spectra present a narrow band at 450 nm (elastic scattering, being its intensity related to the molecule size in solution [101]) and a lower intensity and broader band centered at 480 nm due to the ThT fluorescence, i.e. occurrence of fibrils. In the temporal window considered, both of the signals start to increase and show large intensity fluctuations in correspondence of the two peaks being such fluctuations evidenced by the red lines in Figure 4.6. This phenomenon has been considered for both of the signals and it results better visualized considering the single-wavelength kinetic profile both for ThT (Figure 4.7a) and elastic scattering (data not shown) as a function of the incubation time. At the end of the lag phase and during the initial growth phase, intensity starts to sensibly increase displaying local large deviations from a standard three-steps curve (see best fit function in Figure 4.7a). Such behavior produces the time evolution of residuals shown in Figure 4.7b. During the lag phase no significant oscillations of the signal have been detected whereas fluctuations up to the ∼15% of the fluorescence final value occur during the initial growth of fibrils (Figure 4.7b). Afterwards, ThT intensity linearly increases reaching a plateau at the end of the reaction without any further jump in the emission signal.

Formation of stable aggregates in a given region of the sample, i.e. a single nucleation events, can be considered intrinsically stochastic [47], being spatially localized in

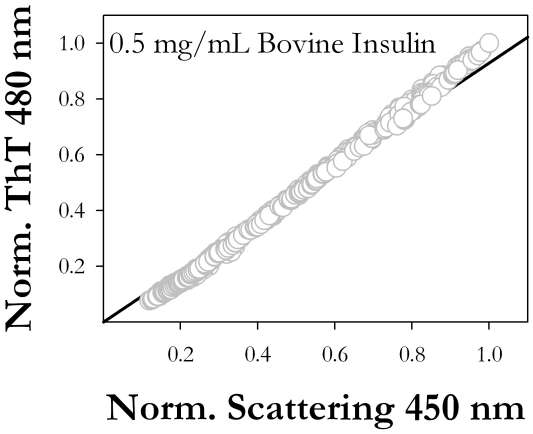

Figure 4.8: Normalized ThT intensity (λ_{exc}=450nm λ_{em}=480nm) as a function of the normalized elastic scattering intensity (λ_{exc}=450nm λ_{em}=450nm) during the kinetics of fibril formation of 0.5 mg/ml bovine insulin in 25 mM HCl, 0.1 M NaCl, 60°C. Solid line represents a linear fitting of 1300 experimental data points. ThT and elastic scattering were simultaneously measured.

the sample and temporally independent each others [100]. Experimental data suggest that already at the end of the lag phase large aggregates are present in some part of sample volume (*spatial heterogeneity*). Such objects diffuse in the solution and, crossing the incoming beam, they produce fluctuations both in the elastic scattering and ThT signal. Interestingly, elastic scattering and ThT signal show a linear correlation for the entire duration of the incubation (Figure 4.8). As a consequence, all the sizable objects crossing the volume and producing fluctuations in the scattering signal seem to have an amyloidal origin or at least a high β-sheets content. Moreover, such fluctuations result to be mostly suppressed by properly triggering the ratio between beam size and total sample volume, i.e. using small sample volume (∼100 μL) or taking out the focalizing lens system as shown in Figure 4.9 for the kinetics at 1 mg/ml. In such measurement, the sample volume has been kept constant. The focalizing system has been removed so that the beam size increases as well as the ratio between beam size and total sample volume. Such result supports the hypothesis of the *diffusing aggregates* already existing at the end of the lag phase.

The same kind of measurements as shown in Figure 4.7a has been carried out for 4 different insulin concentrations up to 2.5 mg/ml. Increasing the protein concentration, both the length and the amplitude of the fluctuations decrease. For quantitatively estimating the fluctuations the total amplitude of square residuals ($\Delta^2_{\%}$) for each concentration in the initial growth phase has been considered and the fluctua-

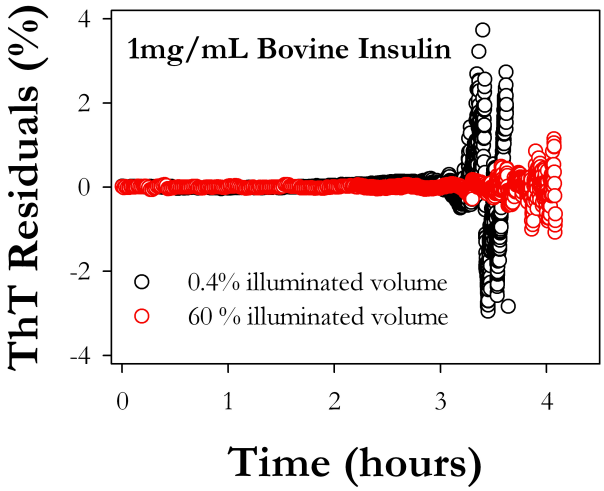

Figure 4.9: Temporal profile of ThT percentual residuals obtained by analog procedure as in Figure 4.7a. Data are stored during the kinetics of fibril formation of 1 mg/ml bovine insulin in 25 mM HCl, 0.1 M NaCl, 60°C. Temporal evolution in two different experimental settings are shown (see Section 2.2.2).

tion (F) has been calculated using the following equation:

$$F = \Sigma(\Delta^2_{\%}) \tag{4.1}$$

extending the summation in equation 4.1 over the entire length of intensity jumps after the end of the lag phase. Figure 4.10 clearly shows that above 1 mg/ml no significant fluctuations occur, whereas for lower concentrations (< 1 mg/ml) diffusion of early stable aggregate seem to be one of the main events at the beginning of the growth phase.

Data in Figure 4.10 can be explained in the framework of the secondary nucleation mechanisms proposed for insulin fibrillation [17, 55]. In presence of such process first stable fibrils can act as nucleation sites, i.e. by accessible surface of fibrils for the protein molecules in solution (heterogeneous nucleation) [55]. As a consequence, after the first nucleation events and during the diffusion of early aggregates, heterogeneous pathway takes the control of the kinetics determining the overall growth of amyloid aggregates in the whole sample volume. Increasing initial protein concentration results in a much higher probability both of primary (homogeneous) nucleation and interaction between already formed fibrils and protein molecules and, as a consequence, in a faster establishment of a spatially homogeneous distribution of amyloid fibrils along the entire sample volume. Such mechanism determines a slowed down

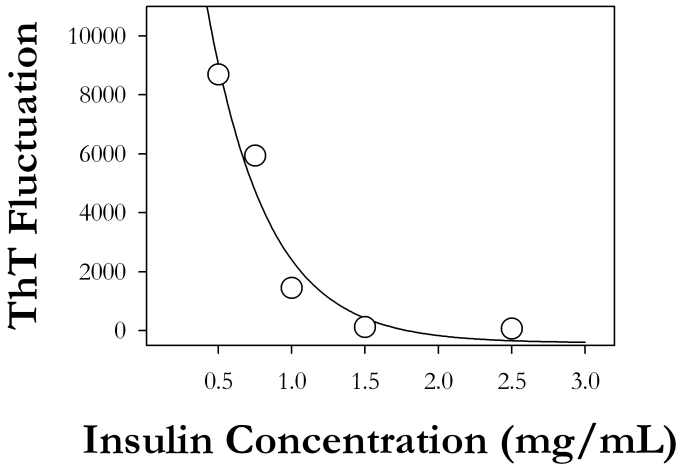

Figure 4.10: Thioflavin T fluctuations as a function of the insulin concentration. Fluctuations were estimated by means of equation 4.1. Solid line is a guide for eyes.

diffusion of early aggregates through the solution and, consequently, a damping both in the amplitude and in the temporal length of the intensity fluctuations at higher protein concentration (Figure 4.10). Further, in agreement with the statistical investigation for human insulin fibrillation in acetic acid (Chapter 3) and with the aggregation kinetics of β-amyloid peptide [99], a higher reproducibility of the fibrillation kinetic profiles, i.e. lag phase and growth rate, at higher protein concentration has been registered also for insulin in HCl solutions (data not shown). Reasonably, this evidence can be determined by the same mechanism that leads to the damping of fluctuations, so that spatial heterogeneity in the formation of early stable aggregates, i.e. single stochastic nucleation events, represents the main factor determining the reproducibility of the kinetic parameters confirming once more the hypothesis presented in Section 3.2.3. In this scenario spatial heterogeneity can be generally considered as an intrinsic aspect for the insulin fibrillation processes being related to the degree of uncertainty on the detected temporal parameters of the process. These results also show how crucial could be the knowledge of the ratio between illuminated volume and total volume for a reliable comparison of the temporal features of the reaction as obtained by different investigators.

4.3 Conclusions

An experimental study on insulin amyloid fibril formation in presence of HCl has been performed. Using ThT fluorescence, the kinetic profiles in a wide range of bovine insulin concentration were characterized and the occurrence of a biphasic behavior in the intermediate range of concentration investigated (3.5-4 mg/ml) has been shown. By means of AFM images the occurring morphologies in such double-sigmoidal process were reported, showing that the presence of β-sheet-rich oligomers ThT-positive in the first step of the reaction is also concentration dependent and not only pressure dependent as previously reported [57]. Moreover, presence of secondary pathways for fibrils elongation and its effect on fibers morphologies were also revealed in the second step of the reaction. Further, a deep investigation of the early stages of the process in the low concentration regime (< 2.5 mg/ml) was carried out. During the lag phase, both the ThT and light scattering signal are not exactly constant. In fact, they display a slight increase in the intensity that should be described in the framework of the homogeneous nucleation. Moreover, after the end of the lag phase, processes are characterized by a large intensity fluctuations both in the ThT and elastic scattering intensity followed by an increase of the signals of several orders. Such fluctuations result more pronounced at lower concentrations and this phenomenon could be ascribed to the spatial heterogeneity in the formation of the first stable aggregates: after their formation they start diffusing through the solution and they likely promote the formation of new fibrils into the whole sample volume. Interestingly, the specific concentration-dependence for fluctuations can be straightforwardly related to the existence of secondary nucleation mechanisms confirming once more the crucial role of these mechanisms in insulin fibrillogenesis.

Chapter 5

Fibril staining: Optical and UV characterization of Thioflavin T

[...]The fact that once again man completely misinterpreted this relationship was entirely according to these creatures' plans.

[Douglas Adams, *Hitchhiker's Guide to the Galaxy*, 1979]

Thioflavin T assay is generally used in several experimental conditions with a huge variety of chemical and physical properties of the environments. For these reasons, its staining and optical properties, peculiarity and specificity could in principle be affected by the specific environment, leading to an erroneous evaluation of the assay. Due to the large use of ThT in detecting thermally induced fibrils formation in a wide range of pH, efforts have been addressed to the combined effect of these two parameters (pH and temperature) on the ThT properties. Experimental results here presented would appear as a preliminary study to avoid artifacts in the quantitative evaluation of fibrils concentration.

5.1 Introduction and purposes

Generally, as shown for a large number of fluorescent dyes in water, changing physical and chemical parameters of aqueous solutions may result in a variation of their optical properties, also in the case of probes commonly employed in unfolding and aggregation studies. For example, also for another amyloid-selective dye, Congo Red [102], optical properties as well as staining features result to be strongly affected by alteration of pH in aqueous solution, making such dye a suitable pH indicator for *in vivo* studies [103]. Also for ThT, recent reports have focused on the effect of different solvents on ThT spectroscopic features [63, 71, 72, 75] and on the effects

of pH and ionic strength on ThT affinity and stoichiometry in binding fibrils [80]. Moreover for ThT, a color transition occurring in water solution at high pH and a change in its absorption properties have been observed as early as twenty-five years ago by Cundall and coworkers [70]. Such study is mostly focused on several factors that can influence photo-physical properties of ThT in binding a number of different polynucleotides. As a consequence, in that study the color transition at high pH is only marginally pointed out. They argued that a hydroxylation process takes place and proposed a theoretical ThT structure dominant in basic solutions (pH 10-12) [70]. Recently, Sabaté and coworkers observed that, at pH 8-9, ThT absorbance and fluorescence strongly decrease and authors indicate such effect as a progressive and irreversible degradation of the molecule. Moreover, from a practical point of view, they suggest to avoid using ThT in alkaline conditions for fibril staining. As a tool for detecting fibrils in aqueous solution, ThT has been employed in a wide range of physical and chemical conditions, varying e.g. ionic strength, pH, temperature [18–21, 23, 81]; as a consequence, in order to prevent artifacts in estimating the concentration of amyloid aggregates, a deeper understanding on the stability of ThT in various experimental settings has to be obtained.

With the aim of better clarify the reaction pointed out by Cundall and coworkers, an experimental study on the effect of pH and temperature on the spectroscopic properties of ThT in phosphate buffer solution has been performed. Using UV-Vis absorbance, a change in the ThT absorbance spectrum occurring at basic pH and in a wide range of temperature has been carefully followed. Moreover, supported by NMR measurements and density functional theory (DFT) calculations, a two-species model of ThT in solution have been proposed, reporting also the molecular structures involved. Finally, by means of fluorescence spectroscopy, the effects of the changes in the spectroscopic properties of the dye on its ability to detect amyloid fibrils have been also investigated. In particular amyloid aggregation of succinyl Concanavalin A (S-Con A) at basic pH has been followed by *ex situ* and *in situ* ThT experiments, underlining a warning on using ThT assay for *in situ* amyloid monitoring in alkaline conditions.

5.2 Experimental results and discussion

Experimental investigation on ThT hydroxylation has been addressed to three different aspects: characterization of the temporal and thermodynamic properties of the process, experimental and computational investigation on the involved chemical structures and, finally, the effect of such process on the amyloid detection.

5.2.1 Thermodynamics of hydroxylation process

The absorbance spectrum of 20 μM ThT in buffer solution (pH 8.6, 25°C) shows an intense peak maximum at ∼405-420 nm (Figure 5.1a). It has been reported previously that this intense band is strongly dependent on the solvent properties [63, 71, 72]. For example, the peak maximum shifts to longer wavelengths when solvent polarity is decreased [71, 72]. Under certain conditions, solutions at low pH have been reported also to affect the UV signal of ThT, showing an increasing absorption at ∼310 nm [66]. In this study, immediately after the sample preparation, at the same ThT concentration and at 25°C, no significant differences have been observed on position, broadening and intensity of the absorption bands in solutions with pH ranging from 5.2 to 8.9 (data not shown). When ThT solution (pH 8.6) is incubated at 50°C, its absorbance spectrum drastically changes as a function of incubation time (Figure 5.1b). A large change in the intensity of the bands is evident and is visualized in the differential absorbance spectra (Figure 5.1c). The band at ∼ 405-420 nm decreases in intensity and a linearly correlated broad absorbance signal in the UV region (∼260-340 nm) starts growing up with an isosbestic point at ∼ 338 nm. Moreover, during the reaction, the standard yellow color of the ThT solution starts to disappear and, at the end of the process, a totally clear solution is obtained. ThT absorbance spectra as a function of the incubation time have been measured in a wide pH range (1.7 - 8.9). In Figure 5.2a the single-wavelength kinetics (100 μM ThT at 50°C) are reported as a function of time for all of the pH values investigated. The kinetic profiles show a decrease in intensity at 405 nm occurring in solutions at pH 7.3 and the process becomes faster at higher pH values, i.e. the OH^- concentration in the solvent increases. Moreover, the intensity decrease as a function of incubation time can be described by an exponential decay. In contrast, at pH<7.3, no changes in intensity are detected and the entire absorbance spectrum is preserved.

The decrease of absorption was found to be reversible and, after the end of the reaction, the yellow color is mostly recovered, when the pH of the solution is lowered well below pH 7. In this respect, reversibility has been tested on four samples of 100 μM ThT at pH 8.6 after a period of incubation of ∼ 6 hours at 50°C (Figure 5.2b, data before axis break). The pH of the four solutions have been adjusted by addition of HCl to the values of 7.7, 7.0, 6.4 and 5.3, respectively, and these samples were again stored at 50°C. Incubation at 50°C and lowering of the pH (< 7.7) result in an increase of the absorbance intensity at 405 nm (Figure 5.2b, data after axis break) and a simultaneous recovery of the yellow color. The reverse reaction strongly depends on pH; both the rate and the final percentage of recovered signal are increased at lower pH values, reaching a maximum of ∼ 90% of the initial absorbance signal when the pH is lowered to 5.3. A further decrease in the pH (up to 1.7) does not result in

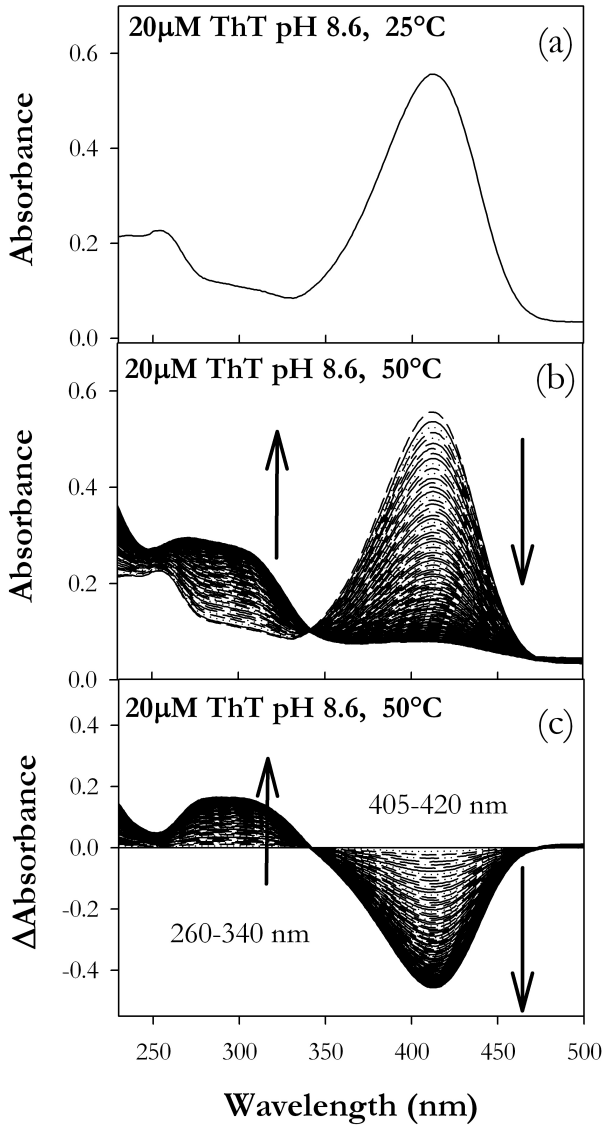

Figure 5.1: UV-Vis absorbance spectrum of 20 μM ThT in 0.1 M phosphate buffer (pH 8.6) at 25°C (a) and during incubation at 50°C (b). (c) Differential absorbance spectra of ThT during incubation. The arrows indicate the time course.

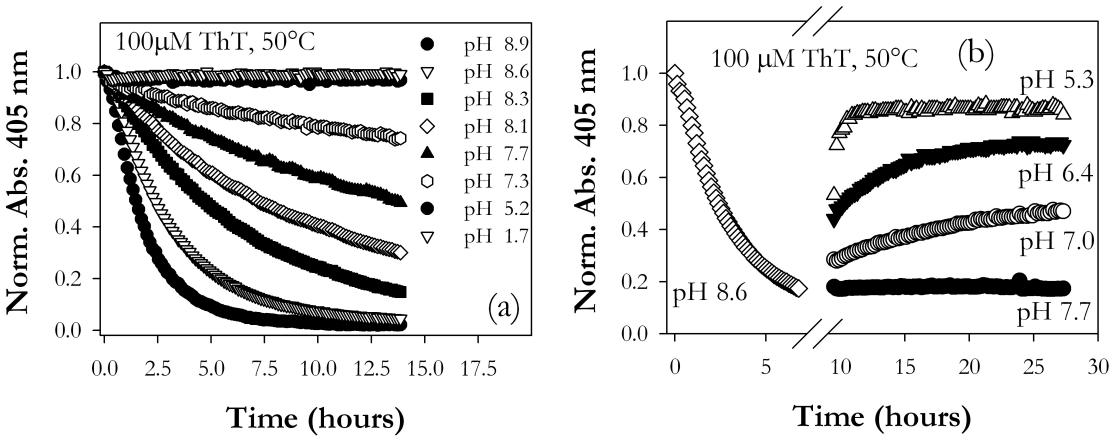

Figure 5.2: (a) Absorbance signal at 405 nm of 100 μM ThT in 0.1 M phosphate buffer at 50°C as a function of incubation time. The kinetics are measured in the pH range 1.7 to 8.9. (b) Absorbance signal at 405 nm of 100 μM ThT in 0.1 M phosphate buffer at 50°C. After $\sim$ 6 hours of incubation at pH 8.6, the pH was adjusted to a value of 7.7, 7.0, 6.4 or 5.3 and the samples were again stored at 50°C. Absorbance values are normalized to the intensity at the beginning of the reaction (405 nm).

further increased recovery of absorbance intensity (data not shown). The loss of color could in principle be dependent on ThT concentration. To study this, absorbance kinetics in the range of ThT concentration generally employed in fibrillation studies (10-100 μM) have been performed [18, 19, 21, 23]. For three ThT concentrations (10, 40, 100 μM at pH 8.9 and 50°C), the reactions show the same time-dependent behavior (Figure 5.3a, log-lin plot) with essentially identical decay times of $\sim$ 2 h, as obtained by single-exponential fits of the progress curves (see Table 5.1 for the dependence of decay times on temperature and pH). Furthermore, when properly normalized (see equation in Figure 5.3b), the data show the same kinetic profile (Figure 5.3b), confirming the same features at different ThT concentrations. This independence on ThT concentration was a general result obtained for all of the pH values and temperatures investigated. Only at very high dye concentration (>>100 μM), incubation of ThT at 50°C and at pH 8.9 for 18 hours did not result in a color change, but, instead, macroscopic yellow particles appeared as precipitate in solution. Interestingly, it has been proposed that different spatial arrangement of the ThT ion may also occur in aqueous solution. In particular, ThT seems able to form micelles leading to changes in conductivity of the solution as well as in the emission spectra [80, 82]. Probably, for ThT concentration >>100 μM, the ThT ions may not only undergo reversible hydroxylation, but other processes may also take place, e.g.

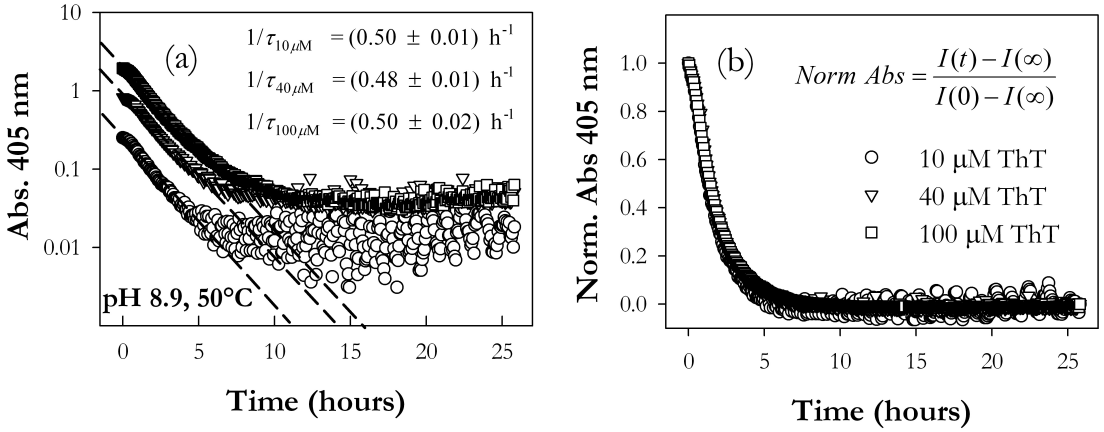

Figure 5.3: (a) Log-lin plot of absorbance signal at 405 nm of 10, 40, and 100 μM ThT in 0.1 M phosphate buffer (pH 8.9) at 50°C as a function of incubation time. Dashed lines represent linear fittings of early stages of the processes. (b) Normalization of the kinetics using the inserted equation.

Table 5.1: Absorbance decay times (h) and k_1 values for ThT hydroxylation

	pH 8.9	pH 8.6	pH 8.3	pH 8.1	pH 7.7	pH 7.3	$k_1 \cdot 10^{-2}$ [$\mu M^{-1}\ h^{-1}$]
35°C	15 h	30 h	62 h	89 h	164 h	370 h	0.40±0.03
40°C	8 h	14 h	29 h	42 h	83 h	200 h	0.55±0.09
45°C	3 h	7 h	14 h	21 h	38 h	100 h	0.95±0.06
50°C	2 h	3 h	7 h	11 h	21 h	53 h	1.14±0.24
55°C	1 h	2 h	4 h	6 h	11 h	33 h	1.81±0.24

micelle formation, resulting in a different degradation mechanism.

In the range of 10-100 μM, experimental results suggest a process fully controlled by ThT-solvent coupling and not dependent on possible association between dye ions. According to Cundall and coworkers (1981)[70], a reversible hydroxylation process may trigger the loss of yellow color, being induced by the solvent and dependent on the OH^- concentration (see Figure 5.2a). Moreover, this process includes a loss of the positive charge [70] present when the dye is dissolved in solutions with pH ranging from 2 to 7 [80]. Therefore the process is likely to be based on the following reaction:

$$ThT^+ + OH^- \underset{k_2}{\overset{k_1}{\rightleftharpoons}} ThTOH \tag{5.1}$$

where k_1 and k_2 are the hydroxylation and dehydration rate constants, respectively. From equation 5.1, an exponential decay of ThT concentration is predicted

$$[ThT^+] = \frac{[ThT^+]_{t=0}}{1 + \frac{k_1}{k_2} \cdot [OH^-]} + (k_1 \cdot [OH^-] + [ThT^+]_{t=0}) \cdot e^{-(k_1 \cdot [OH^-] + k_2) \cdot t} \tag{5.2}$$

being such behavior in accordance with the single-wavelength kinetics in Figure 5.2a.

Further, from equation 5.2 the theoretical equilibrium values for hydroxylated ThT (hereafter ThTOH) at the end of the process can be obtained:

$$[ThTOH]_{eq} = [ThT^+]_{t=0} \cdot \frac{\frac{k_1}{k_2} \cdot [OH^-]}{1 + \frac{k_1}{k_2} \cdot [OH^-]} \tag{5.3}$$

The same kind of kinetic study as shown in Figure 5.2a have been carried out in a range of incubation temperatures (35-55°C). The experimental equilibrium data for the ThTOH concentration after a 18 hours-incubation of 100 μM ThT (temperature range 35-55°C) are plotted as a function of the OH^- concentration in solution (Figure 5.4). As can be seen, at increased OH^- concentration, the data show an increase in the final amount of ThTOH up to an almost total conversion of ThT species to the hydroxylated form at higher OH^- concentrations. Such behavior is very well described by the equilibrium expression of equation 5.3 (solid line in Figure 5.4) for all the temperatures investigated. From these curve fits, the ratio between rate constants at equilibrium has been estimated to be 1.2 μM^{-1} (k_1/k_2, see equation 5.3). This ratio turns out to be almost unaffected by changes in the temperature,

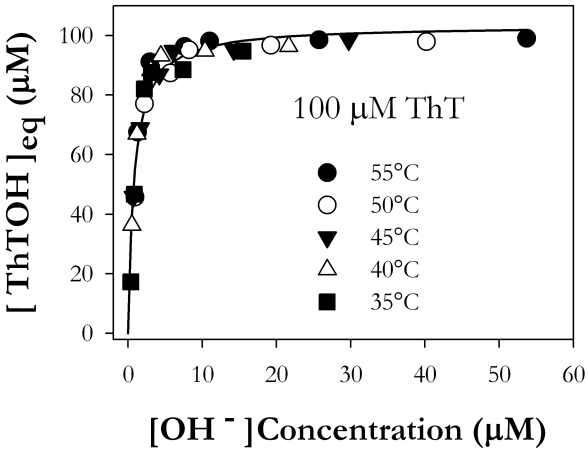

Figure 5.4: Experimental equilibrium values for the amount of ThTOH as a function of OH^- concentration. The ThTOH concentration was estimated at the end of the thermal treatment of 100 μM ThT for each pH (7.3-8.9) and temperature (35-55°C). Solid line represents fitting function as obtained using equation 5.3 (see text).

indicating that the equilibrium is essentially determined only by the concentration of OH^- in solution. Moreover, kinetics rate constants of the process (K_{meas}) predicted from equation 5.1 are linearly dependent on the OH^- concentration (equation 5.4).

$$K_{meas} = k_1 \cdot [OH^-] + k_2 \tag{5.4}$$

The linearity of the rate constant K_{meas} as a function of OH^- shown in equation 5.4 has been experimentally confirmed in Figure 5.5a, where the experimental rate constants of the processes (100 μM ThT, pH $>$ 7.33) are reported as a function of the OH^- concentration for all the temperatures. In accordance with the theoretical prediction, a linear relationship between the two parameters has been obtained, the correlation being temperature-dependent. For calculation of the activation energy of the hydroxylation process, we used k_1 values (see Table 5.1) obtained from the linear fits in Figure 5.5a, and an effective activation enthalpy of ~ 63 kJ $\cdot$ mol^{-1} was subsequently determined from the Arrhenius plot (Figure 5.5b, see also Section 5.2.2 for details on structural changes of the molecule).

5.2.2 Chemical structure of hydroxylated ThT

In view of all the data in section 5.2.1, the hydroxylation reaction shown in equation 5.1 seems to be the main process occurring at basic pH and in the range of the

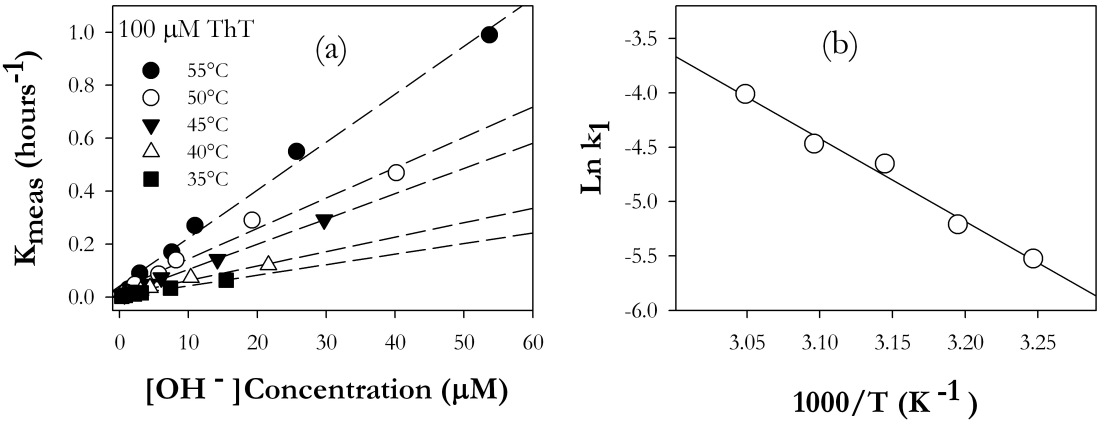

Figure 5.5: (a) Rate constant as a function of OH^- concentration for the kinetics at 100 μM of ThT. Dashed lines represent linear fits at each temperature; (b) Arrhenius plot for the rate constant k_1 (see text) of the kinetics at 100 μM of ThT in the pH range 7.3 to 8.9. The temperature range is 35-55°C.

ThT concentrations used in this study. Cundall and coworkers (1981) proposed a theoretical ThTOH structure, suggesting that the thiazole group is involved in the process with a loss of charge of the nitrogen and OH^- binding to the nearest carbon [70](see Section 2.1.1). With the aim of experimentally confirming the proposed molecular structure, an analysis based on a theoretical and experimental ^{1}H-NMR was carried out on the ThT and the proposed ThTOH species. In Figure 5.6, experimental NMR spectra of 100 μM ThT at pH 8.9 in deuterium phosphate buffer as detected before (black line) and after 15 hours incubation at 50°C (red line) are shown. The ^{1}H-NMR spectrum of ThT is in agreement with the calculated chemical shifts from the geometry optimized ThT structure (Figure 5.7a). Theoretically, the hydrogen atoms in the aromatic rings (IV and V) generally have a chemical shift in the range 7-8 ppm and such prevision is confirmed by the obtained NMR signals (chemical shift, intensities as well as splitting caused by scalar coupling). The signal from the dimethylamino group (I) and the two methyl groups (II and III) are found in the range 2-4 ppm, with the dimethylamino peak as the most intense. Moreover, the calculated chemical shifts of ThT (Figure 5.7a) allow to accurately assign each CH_3 group to a specific experimental NMR signal. Thus, the chemical shift of the methyl group on the aromatic ring (III) is 2.556 ppm, whereas the peak at 4.252 ppm comes from the CH_3 bound to the positively charged nitrogen (II).

After 15 hours of incubation at 50°C (red line in Figure 5.6), the NMR spectrum of the ThT sample shows a global shift towards lower ppm values (higher field) for all

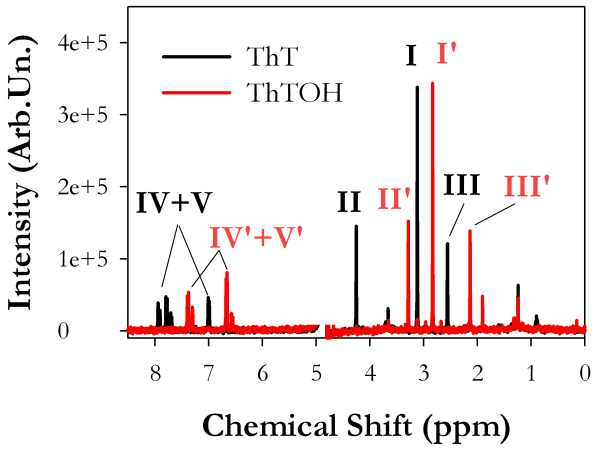

Figure 5.6: Experimental ^{1}H-NMR spectra of 100 μM ThT at pH 8.9 in deuterium phosphate buffer as detected before (black line) and after 15 hours incubation at 50°C (red line). Roman numerals are related to hydrogen atoms belonging to different chemical groups in the molecules (see also Figures 5.7a and 5.7b).

the peaks involved, with the largest change for the methyl-N group (II'). Following the suggestion of Cundall and coworkers (1981) for the hydroxylated chemical structure, DFT calculations on ThT with OH^- (red and grey atoms in Figure 5.7b) bound to the carbon in the thiazole group have been carried out. It is also worthy of note that, besides the OH^- group binding and the loss of charge on the nitrogen, the geometry optimized structure of ThTOH (Figure 5.7b) differs from that of ThT also in the mutual position between fragment I-V and fragment II-III-IV, with a huge variation of the dihedral angle S-C-C-C (referred in literature as φ angle) from ∼33°(ThT, Figure 7a) to ∼101° (ThTOH, Figure 5.7b).

The calculated chemical shifts of each hydrogen atom were estimated and compared to the experimental values from NMR. The plot in Figure 5.8 shows a good agreement between theoretical prediction and experimental data for ThT (open circles), and also for ThTOH (open triangles) a satisfying linear correlation is observed. Moreover, the DFT calculations also allow for prediction of the electronic excited states for both the involved species, providing theoretical insights into the absorbance properties of the molecules. These calculations show that ThT has one transition with a significant oscillator strength centered at ∼ 409 nm, whereas only an UV signal (∼ 290-297 nm) for ThTOH with a weaker intensity is predicted (Table 5.2). These results are in full agreement with the experimental UV-Vis spectra (see spectra at the beginning and at the end of the kinetics, Figure 5.1b). Moreover,

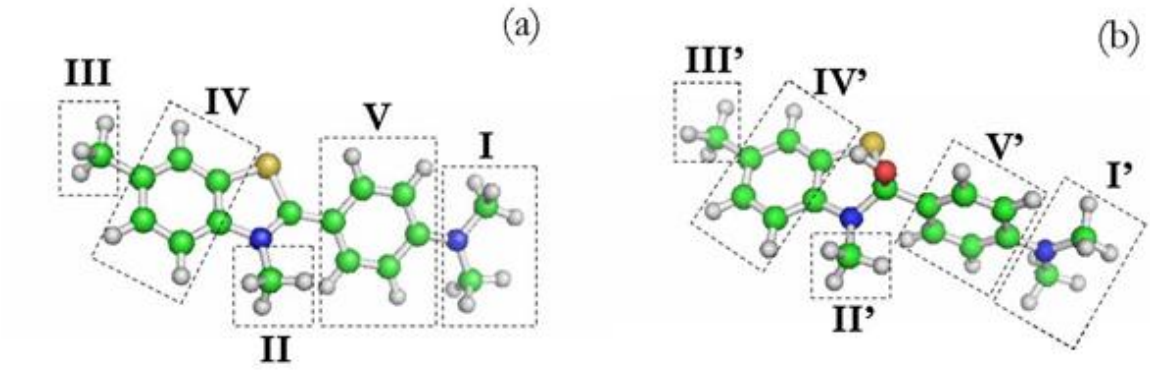

Figure 5.7: Geometry optimized structures of (a) ThT and (b) ThTOH. Roman numerals are related to hydrogen atoms belonging to different chemical groups in the molecules (see also Figure 5.6). Atom color: hydrogen (gray), carbon (green), nitrogen (blue), sulphur (yellow) and oxygen (red).

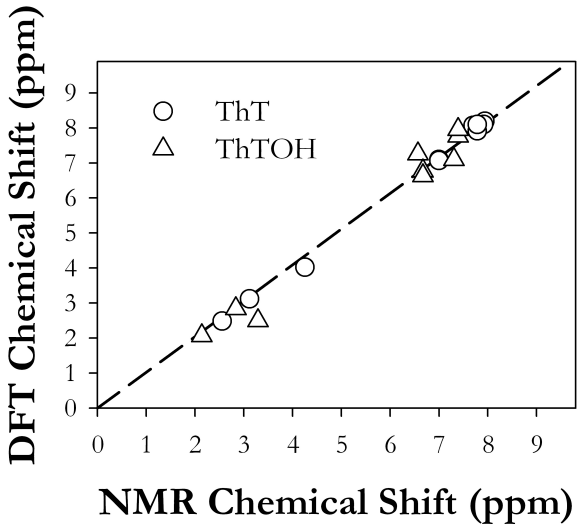

Figure 5.8: Chemical shifts of the hydrogen atoms in ThT and ThTOH calculated for the geometry optimized structures (Figures 5.7a and 5.7b) as a function of experimental NMR chemical shifts. Calculated chemical shielding constants were compared to chemical shifts by means of a linear regression referring to the experimental NMR data.

Table 5.2: Theoretical Transition Wavelength (λ_{trans}) and Oscillator Strength (f) for ThT and ThTOH based on structures in Figure 5.7.

λ_{trans} ThT	f	λ_{trans} ThT	f	λ_{trans} ThTOH	f	λ_{trans} ThTOH	f
409 nm	0.94	279 nm	0.04	316 nm	0.02	281 nm	0.04
305 nm	0.03	264 nm	0.02	297 nm	0.15	278 nm	0.01
299 nm	0.01	259 nm	0.02	295 nm	0.12	274 nm	0.01
290 nm	0.07	253 nm	0.02	290 nm	0.13	264 nm	0.05
284 nm	0.03	237 nm	0.01	284 nm	0.04	259 nm	0.02

NMR spectra of ThT pH 8.9 during incubation at 50°C for a period of 1 day were also recorded (data not shown). After a total conversion to the hydroxylated form, further storage at high temperature results in a decay in the intensity of all the NMR peaks. This result suggests that, after a long incubation at high temperature, a further chemical degradation of ThTOH may also occur.

5.2.3 ThT hydroxylation on amyloid detection

ThT is usually employed for *in situ* detection of amyloid fibrils. It has been reported that ThT emission intensity is, in a good approximation, linearly dependent on the amount of aggregates [73]; however, as recently shown for different types of glucagon [81] and insulin fibrils [56], its quantum yield may vary considerably depending on the morphology of the amyloid aggregates. With the aim to ascertain how the presence of ThTOH in solution may affect amyloid detection, firstly, emission spectra of the two ThT species in presence of fibrils have been compared. For such experiment, Succinyl Concanavalin A (S-Con A) has been employed as a model system for the growth of fibrillar aggregates because of its capability to form fibrils in experimental conditions in which ThTOH may occur. In fact, S-Con A forms amyloid fibrils at basic pH at temperatures between 37°C and 45°C and the rate of aggregates formation increases with temperature, without any change in the aggregation mechanisms [23, 28]. After inducing fibrils formation on two identical S-Con A samples (see Section 2.4.2), we added aliquots of (a) fresh ThT and (b) ThT after 15 hours of incubation at 50°C (pH 8.9), respectively, in a final concentration of 40 μM. As expected from the different absorbance spectra of the two species (for example, see spectra at the beginning and at the end of kinetics, Figure 5.1b), upon an excitation at 440 nm and in presence of amyloid aggregates ThT brightly fluoresces, whereas ThTOH presents a lower emission intensity (Figure 5.9). Such result is not surprising by itself,

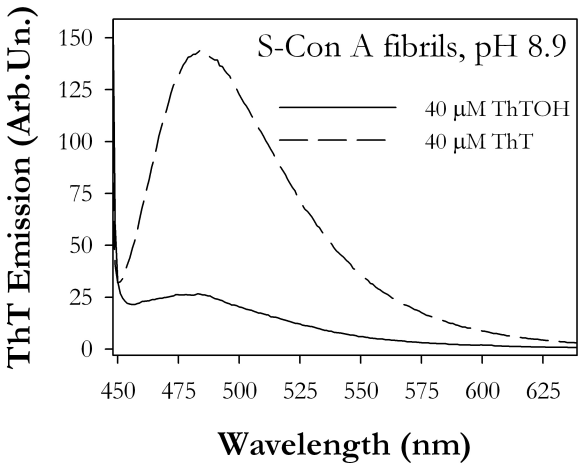

Figure 5.9: Fluorescence emission spectra (λ_{exc} = 440 nm) of Succinyl Concanavalin A fibrils after addition of 40 μM of fresh ThT pH 8.9 (dashed line) and 40 μM of ThT pH 8.9 treated for 15 hours at 50°C (solid line).

but it has to be considered in view of the *in situ* fibrils detection. Fibrils staining by ThT depends on the active-dye concentration employed and, as a consequence, modification of the amount of amyloid-sensitive ThT during the aggregation kinetics may generally affect the overall fibril detection. If ThT hydroxylation takes place during the fibril formation, chemical equilibrium between the two species changes, a large amount of ThTOH occurs in solution and, simultaneously, ThT concentration decreases, so that a reliable evaluation of fibrils concentration can not be obtained. In this respect, aggregation kinetics of S-Con A at pH 8.9 and 50°C in presence of ThT have been performed; in Figure 5.10a the absorbance intensity at 440 nm (excitation wavelength used) both for ThT free in solution and ThT during S-Con A fibrillation has been reported. In both cases, ThT hydroxylation takes place, being the process slowed down in presence of native protein and aggregates. Furthermore, during S-Con A amyloid aggregation, emission signal at 480 nm (λ_{exc} = 440 nm) increases and it reaches a maximum value in $\sim$ 70 minutes (open triangles in Figure 5.10b); afterwards a decay of emitted intensity occurs, being such decrease mainly related to the change in the absorbance signal at 440 nm (open triangles in Figure 5.10a). For comparison, the same fibrillation kinetics has been also followed by an *ex situ* ThT experiment (black triangles in Figure 5.10b); in this case, by adding freshly prepared ThT before each fluorescence detection (see Section 2.4.2), ThT hydroxylation is prevented and no artifacts ascribable to such process can occur in the fibrils detection. *Ex situ* data show a prompt increase of fluorescence signal which reaches

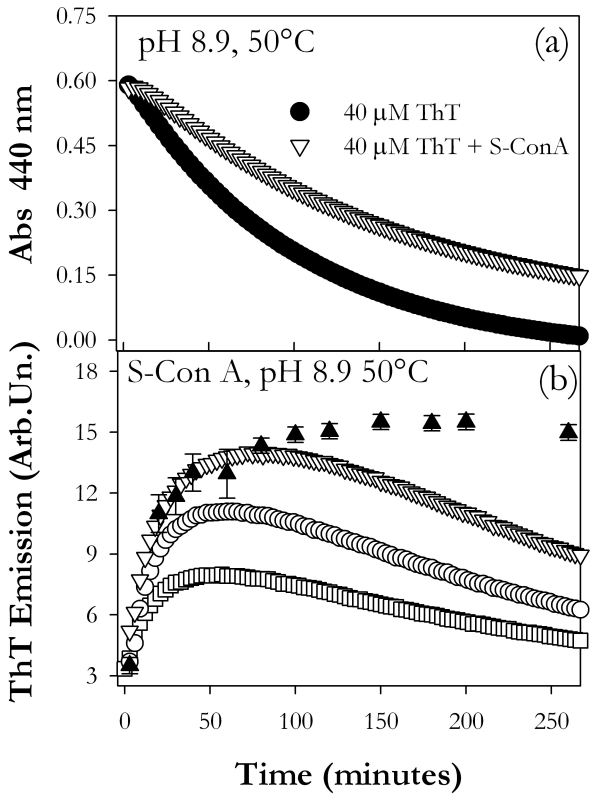

Figure 5.10: (a) Absorbance signal of 40 μM ThT at 440 nm and 50°C as a function of incubation time; in buffer solutions pH 8.9 (black circles) and in buffer solution pH 8.9 with 0.5 mg/ml of Succinyl Concanavalin A (S-Con A) (open triangles). (b) *In situ* fluorescence emission (λ_{exc}=440 nm and λ_{em}=480 nm) of S-Con A fibrils with 40 μM (open triangles), 15 μM (open circles) and 5 μM (open square) of ThT at pH 8.9 as a function of incubation time (50°C). *Ex situ* fluorescence emission (λ_{exc}=440 nm and λ_{em}=480 nm) of S-Con A fibrils with 40 μM of ThT at pH 8.9 as a function of incubation time (50°C) (black triangles). In the *ex situ* experiment, data were scaled and error bars represent absolute deviations observed on four replicates.

a maximum in $\sim$ 100 minutes followed by a plateau where fluorescence values keep almost unvaried. At least in the first 70 minutes of the kinetics, *in situ* data at 40 μM of ThT do match quite well with the *ex situ* results, whereas such agreement ceases when hydroxylation process makes the concentration of active-ThT insufficient to bind to all the sites. As a consequence, lowering the initial amount of ThT in the *in situ* experiment should in principle lead to further changes in the fibril detection; with the aim of confirming such prevision, we performed analogous *in situ* kinetics in presence of two different amounts of ThT (5 μM and 15 μM) and data are also reported in Figure 5.10b. By lowering ThT concentration, kinetic profiles drastically change and disagreement between *ex situ* and *in situ* data appears more pronounced as initial ThT concentration is lower; as a consequence, a dramatic mistake in the evaluation of the effective rate constant occurs and percentage error up to $\sim$60% and $\sim$34% have been estimated for kinetics at 5 μM and 15 μM, respectively. Interestingly, measurements up to 13 hours show a total disappearance of both the absorbance and fluorescence signal, indicating a complete conversion of all the ThT molecules (unbounded, bounded/previously bounded) into ThTOH species. All these results together suggest that, during thermally induced fibrillation at alkaline pH, *in situ* ThT fluorescence is determined by at least two different processes: hydroxylation and fibrils growth. Consequently, besides the initial dye concentration, rate of ThT hydroxylation compared to the rate of aggregates formation has to be taken into account for a reliable evaluation of fibrils formation.

5.3 Conclusions

At alkaline pH and high temperature (35-55°C), the ThT solutions rapidly lose their normal yellow color. By means of UV-Vis absorbance, the time-dependent and thermodynamic properties of these kinetics in a wide range of pH, temperature and ThT concentrations were characterized, proposing a hydroxylation reaction for the ThT ion. The process is reversible, independent of the dye concentration with an effective activation energy barrier of $\sim$63 kJ $\cdot$ mol^{-1} and a rate constant proportional to the OH^- concentration in the solution. To describe all the experimental results, a theoretical reaction between ThT ions and OH^- has been proposed (equation 5.1), leading to a good agreement with the experimental data. Moreover, on the basis of experimental ^{1}H-NMR and DFT calculations, the structure of hydroxylated ThT most likely corresponds to ThT with OH^- bound to the benzothiazole group, involving also a loss of a positive charge and a mutual rotation of the different fragments. Finally, data show that hydroxylation may dramatically affect the fluorescence intensity of ThT in detecting amyloid fibrils. These results thus provide new insights

on the sensitivity and reliability of the ThT as an *in situ* tool for amyloid detection at basic pH and high temperature. In particular, Table 5.1 could represent a general reference to roughly calculate whether problems related to the hydroxylation of ThT can occur during fibrillation measurements, provided that the fibrillation temporal profile is already known by some other techniques. Moreover, if the necessary active-dye concentration for a specific fibrillation detection is already known, it is also possible to evaluate if a reasonable initial ThT concentration can be used to overcome the problems related to hydroxylation during *in situ* measurements.

Conclusions and perspectives

In this work different aspects related to the *in vitro* insulin fibrils formation have been taken into account.

Thioflavin T fluorescence has been largely employed in this Thesis as a detection tool to specifically stain amyloid fibrils. Such tool has been used to characterize the kinetic profile of insulin fibrillogenesis occurring at low pH and high temperature. In these conditions, ThT fluorescence can lead to reliable results for quantitative evaluation of fibrils. In particular, insulin fibril formation has been investigated for both the human and bovine type in two different solutions.

Firstly, in collaboration with Novo Nordisk A/S (Denmark) studies on human insulin fibrillation have been carried out starting from acetic acid solutions and inducing amyloid aggregation at 45°C. The main purpose was studying the effect of insulin concentration (1-20 mg/mL) by *in situ* ThT on two meaningful parameters of the process: the inverse of the time necessary to reach the 50% of the kinetics ($1/t_{50\%}$) and the fluorescence final value (FFV). The former parameter is a sort of overall rate constant accounting both for the nucleation and the growth time, whereas the latter could be considered as a rough estimation of fibril concentration. Both of these parameters show a linear dependence on insulin concentration up to 5 mg/mL and afterwards a sort of saturation occurs. Interestingly, the two parameters result linearly dependent each other. On the basis of these data and taking into account the secondary nucleation mechanisms recently proposed for insulin together with the surface-dependent ThT-fibrils binding, the interaction *via* fibrils surface (heterogenous nucleation) among the different and possible secondary mechanisms has been suggested. Moreover, the reproducibility of the kinetics has been taken into account and such analysis shows that the progress curves result more reproducible at high concentration pointing out, at least in early stages, an inherent stochasticity of the process.

Amyloid fibril formation from bovine insulin samples has been also studied in HCl solution inducing aggregation at 60°C. Using ThT fluorescence the kinetic profiles in a wide range of bovine insulin concentration (0.5-10 mg/mL) have been characterized showing the occurrence of a double-sigmoidal process at 3.5-4 mg/mL in

which different morphologies occur, as revealed by AFM images. Further, in the low concentration regime (< 2.5 mg/mL) both the ThT and light scattering signals show a slight increase in the intensity since the first instants of incubation. Then, ThT and scattering data display large intensity fluctuations dependent on insulin concentration and afterwards signals increase of several orders of magnitude. Such sequence of events suggests a scenario in which a primary (homogeneous) nucleation takes place in the early stages of the process followed by stochastic (temporally and spatially) formation of the first stable aggregates that, diffusing through the solution, produces the detected intensity fluctuations. Finally, such stable aggregates likely promote the formation of amyloid fibrils in the whole sample volume by secondary nucleation mechanisms, determining the exponential growth of the detected signals.

Because of the so wide use of ThT, a characterization of its spectroscopic features has been carried out (Chapter 5). In particular, the effect of pH and temperature on the spectroscopic properties of ThT in phosphate buffer solution has been considered. At basic pH and in a wide range of temperature, ThT solution does not preserve its absorbance spectrum and simultaneously it loses its peculiar yellow color. Also on the basis of previous theoretical suggestion, a hydroxylation process in which an OH^- binds to the ThT ion has been supposed. To prove such suggestion, a theoretical and experimental NMR study has been performed. The geometry optimized structure for both of the species (ThT and ThTOH) and their theoretical shielding constants have been obtained by Density Functional Theory calculations. Then, the latter values have been related to the experimental chemical shifts obtained by NMR spectra of the two species, confirming the hypothesis. Such characterization introduces to a practical problem in detecting amyloid fibrils by *in situ* ThT staining. In fact changing the absorbance spectrum of ThT can dramatically affect the quantum yield of fluorescence producing artifacts in the quantitative detection of amyloid aggregates. As regard this subject, a comparative study of the fluorescence activity of both ThT and ThTOH in presence of succinyl Concanavalin A (S-Con A) fibrils has been performed showing an almost absent fluorescence signal of the complex ThTOH-fibrils. Moreover, during kinetics at high temperature and basic pH, i.e. when hydroxylation is favored, occurrence of ThTOH during the *in situ* detection can lead to an erroneous evaluation of fibrils presence, drastically changing the kinetic profile of the reaction.

In the still poorly understood variety of mechanisms occurring in the formation of insulin amyloid fibrils, this work strongly supports the presence of secondary mechanisms as the *main director* leading to the characteristic exponential temporal profile. Moreover, the crucial role of the fibrils surface as nucleation point has been elucidated together with the pronounced spatial heterogeneity that characterizes the early stages of the process. Not less important, some hint on the ThT-fibrils bin-

ding has been pointed out. First of all, the dependence of the characteristic ThT fluorescence on the morphologies of the fibril surely represents one of the point that need to be taken into account for a reliable evaluation of the data. More general, the study on ThT stability (Chapter 5) represents a systematic report on the optical and structural features of this dye in conditions generally used to study *in vitro* fibrillation.

Clearly, the results here presented leave different and general open problems that need to be dealt with. First of all, at present very little is understood about the details of the molecular mechanism behind this ThT-response, and the study presented in Chapter 5 further indicated that a deeper knowledge needs to be gained for a proper evaluation of the ThT assay. This is important both for a better understanding of the experiments which are monitored by ThT and for a future development of improved probes, markers and/or inhibitors of protein fibrillation. In particular, further investigation needs to be addressed to the following points:

1. Localization on the fibrils surface of the binding sites for ThT.

2. Molecular mechanism leading to the enhanced fluorescence quantum yield when ThT is bound to fibrils.

3. Dependence of ThT fluorescence on different morphologies and geometrical arrangement of fibrils.

4. High resolution characterization of ThT binding to amyloid probes.

In this sense, some ideas have been already considered. Using insulin as a model system, thereby ensuring maximum output from the studies presented in this work, it should be interesting to investigate different morphologies of mature protein fibrils. To clarify the above mentioned points 1, 2, 3, challenging information can be obtained by comparison of the characteristics of ThT fluorescence and attempting isothermal titration calorimetry analysis of ThT binding to mature fibrils with different morphologies. It should also be possible to combine this with X-ray fibre diffraction analysis of the same fibril morphologies, in the presence of ThT, supplemented with transmission electron microscopy for direct three-dimensional verification of the morphologies. Moreover, attempting high resolution crystal structure determination of peptides in amyloid-like conformation in the presence of ThT [104] should be particularly useful. In fact, such a structure would yield hitherto unprecedented information about the underlying molecular mechanisms behind ThT-binding, and thus provide the first basis for structure-based design of improved probes of amyloid fibrils.

Bibliography

[1] Vendruscolo M., Zurdo J., MacPhee C.E. and Dobson C.M. "Protein folding and misfolding: a paradigm of self-assembly and regulation in complex biological systems" *Phil. Trans. R. Soc. Lond. A* **361**, 1205–1222, 2003.

[2] Dobson C.M. "Protein folding and misfolding" *Nature* **426**, 884–890, 2003.

[3] Anfinsen C.B. "Principles that govern the folding of protein chains" *Science* **181**, 223–230, 1973.

[4] Dobson C.M., Sali A. and Karplus M. "Protein folding: a perspective from theory and experiment" *Angew. Chem. Int. Ed. Eng.* **37**, 868–893, 1998.

[5] Bryngelson J.D. and Wolynes P.G. "Spin glasses and the statistical mechanics of protein folding" *Proc Natl Acad Sci U S A* **84**, 7524–7528, 1987.

[6] Bryngelson J.D., Onuchic J.N., Socci N.D. and Wolynes P.G. "Funnels, pathways, and the energy landscape of protein folding: a synthesis" *Proteins* **21**, 167–195, 1995.

[7] Dill K.A. and Chan H.S. "From Levinthal to pathways to funnels" *Nature Struct. Biol.* **4**, 10–19, 1997.

[8] Dinner A.R., Sali A., Smith L.J., Dobson C.M. and Karplus M. "Understanding protein folding via free energy surfaces from theory and experiment" *Trends Biochem. Sci.* **25**, 331–339, 2000.

[9] Wolynes P.G., Onuchic J.N. and Thirumalai D. "Navigating the folding routes" *Science* **267**, 1619–1620, 1995.

[10] Ellis R. "Macromolecular crowding: an important but neglected aspect of the intracellular environment" *Curr. Opin. Struct. Biol.* **11**, 114–119, 2001.

[11] Bukau B. and Horwich A.L. "The Hsp70 and Hsp60 chaperone machines" *Cell* **92**, 351–366, 1998.

[12] Hartl F.U. and Hayer-Hartl M. "Molecular chaperones in the cytosol: from nascent chain to folded protein" *Science* **295**, 1852–1858, 2002.

[13] Horwich A. "Protein aggregation in disease: a role for folding intermediates forming specific multimeric interactions" *J. Clin. Invest.* **110**, 1221–1232, 2002.

[14] Thomas P.J., Qu B.H. and Pedersen P.L. "Defective protein folding as a basis of human disease" *Trends Biochem. Sci.* **20**, 456–459, 1995.

[15] Dobson C.M. "The structural basis of protein folding and its links with human disease" *Phil. Trans. R. Soc. Lond. B* **356**, 133–145, 2001.

[16] Stefani M. "Protein misfolding and aggregation: new examples in medicine and biology of the dark side of the protein world" *Biochim. Biophys. Acta* **1739**, 5–25, 2004.

[17] Jansen R., Dzwolak W. and Winter R. "Amyloidogenic self-assembly of insulin aggregates probed by high resolution atomic force microscopy" *Biophys. J.* **88**, 1344–1353, 2005.

[18] Nielsen L., Khurana R., Coats A., Frokjaer S., Brange J., Vyas S., Uversky V.N. and Fink A.L. "Effect of environmental factors on the kinetics of insulin fibril formation: elucidation of the molecular mechanism" *Biochemistry* **40**, 6036–6046, 2001.

[19] Nielsen L., Frokjaer S., Brange J., Uversky V.N. and Fink A.L. "Probing the mechanism of insulin fibril formation with insulin mutants" *Biochemistry* **40**, 8397–8409, 2001.

[20] Groenning M., Olsen L., van de Weert M., Flink J.M., Frokjaer S. and Jorgensen F.S. "Study on the binding of Thioflavin T to β-sheets-rich and non-β-sheet cavities" *J. Struct. Biol.* **158**, 358–369, 2007.

[21] Groenning M., Norrman M., Flink J.M., van de Weert M., Bukrinsky J.T., Schluckebier G. and Frokjaer S. "Binding mode of Thioflavin T in insulin amyloid fibrils" *J. Struct. Biol.* **159**, 483–497, 2007.

[22] Dzwolak W., Jansen R., Smirnovas V., Loksztejn A., Porowski S. and Winter R. "Template-controlled conformational patterns of insulin fibrillar self-assembly reflect history of solvation of the amyloid nuclei" *Phys. Chem. Chem. Phys.* **7**, 1349–1351, 2005.

[23] Vetri V., Canale C., Relini A., Librizzi F., Militello V., Gliozzi A. and Leone M. "Amyloid fibrils formation and amorphous aggregation in Concanavalin A" *Biophys. Chem.* **125**, 184–90, 2007.

[24] Uversky V.N. and Fink A.L. "Conformational constraints for amyloid fibrillation: the importance of being unfolded" *Biochim. Biophys. Acta* **1698**, 131–153, 2004.

[25] Militello V., Vetri V. and Leone M. "Conformational changes involved in thermal aggregation processes of Bovine Serum Albumin" *Biophys. Chem.* **105**, 133–141, 2003.

[26] Militello V., Casarino C., Emanuele A., Giostra A., Pullara F. and Leone M. "Aggregation kinetics of Bovine Serum Albumin studied by FTIR spectroscopy and light Scattering" *Biophys. Chem.* **107**, 175–187, 2004.

[27] Vetri V. and Militello V. "Thermal induced conformational changes involved in the aggregation pathways of beta-lactoglobulin" *Biophys. Chem.* **113**, 83–91, 2005.

[28] Vetri V. *Conformational changes involved in protein aggregation* Dipartimento di Scienze Fisiche ed Astronomiche, 2008.

[29] Sipe J.D. and Cohen A.S. "History of the amyloid fibril" *J. Struct. Biol.* **130**, 88–98, 2000.

[30] Attanasio F., Cascio C., Fisichella S., Nicoletti V.G., Pignataro B., Savarino A. and Rizzarelli E. "Trehalose effects on α-crystallin aggregates" *Biochem. Biophys. Res. Commun.* **354**, 899–905, 2007.

[31] Giuffrida M.L., Grasso G., Ruvo M., Pedone C., Saporito A., Marasco D., Pignataro B., Copani A. and Rizzarelli E. "Aβ(25-35) and its C-and/or N-blocked derivatives: copper driven structural features and neurotoxicity" *Journal Neuroscience Research* **85**, 623–633, 2007.

[32] Coelho T. "Familial amyloid polyneuropathy: new developments in genetics and treatment" *Curr. Opin. Neurol.* **9**, 355–359, 1996.

[33] Lansbury P.T.J. "A Reductionist View of Alzheimer's Disease" *Acc. Chem. Res.* **29**, 317–321, 1996.

[34] Fandrich M. "On the structural definition of amyloid fibrils and other polypeptide aggregates" *Cell. Mol. Life Sci.* **64**, 20662078, 2007.

[35] Nelson R., Sawaya M.R., Balbirnie M., Madsen A.., Riekel C., Grothe R. and Eisenberg D. "Structure of the cross-beta spine of amyloid-like fibrils" *Nature* **435**, 773–778, 2005.

[36] Chothia C. "Conformation of twisted-pleated sheets in proteins" *J. Mol. Biol.* **75**, 295302, 1973.

[37] Rochet J.C. and Lansbury P.T.J. "Amyloid fibrillogenesis: themes and variations" *Curr. Opin. Struct. Biol.* **10**, 60–68, 2000.

[38] Nilsson M.R. and Raleigh D.P. "Analysis of amylin cleavage products provides new insights into the amyloidogenic region of human amylin." *J. Mol. Biol.* **294**, 1375–1385, 1999.

[39] DeLellis R.L. and Bowlings M.C. "The use of Sirius red and Congo red staining in routine histopathology" *Human Pathol.* **1**, 655, 2006.

[40] Turnell W.G. and Finch J.T. "Binding of the Dye Congo red to the amyloid protein pig insulin reveals a novel homology amongst amyloid-forming peptide sequences" *J. Mol. Biol. ,* **227**, 1205–1223, 1992.

[41] Khurana R., Uversky V.N., Nielsen L. and Fink A.L. "Is Congo red an amyloid-specific dye?" *J. Biol. Chem.* **276**, 22715–22721, 2001.

[42] Christopeit T., Hortschansky P., Schroeckh V., Guhrs K., Zandomeneghi G. and Fandrich M. "Mutagenic analysis of the nucleation propensity of oxidized alzheimer's beta-amyloid peptide" *Prot. Sci.* **14**, 2125–2131, 2005.

[43] Zandomeneghi G., Krebs M.R., McCammon M.G. and Fandrich M. "FTIR reveals structural differences between native beta-sheet proteins and amyloid fibrils" *Prot. Sci.* **13**, 3314–3321, 2004.

[44] Nilsson M.R. "Techniques to study amyloid fibril formation in vitro" *Methods* **34**, 151–160, 2004.

[45] Ferrone F.A., Hofrichter J., Sunshine H.R. and Eaton W.A. "Kinetic studies on photolysis-induced gelation of sickle cell hemoglobin suggest a new mechanism" *Biophys. J.* **32**, 361–380, 1980.

[46] Ferrone F.A., Hofrichter J. and Eaton W.A. "Kinetics of sickle hemoglobin polymerization. II. A double nucleation mechanism" *J. Mol. Biol.* **183**, 611–631, 1985.

[47] Ferrone F. "Analysis of protein aggregation kinetics" *Methods Enzymol.* **309**, 256–274, 1999.

[48] Oosawa F. and Asakura S. *Thermodynamics of the polymerization of protein* Academic Press, London, 1975.

[49] Goldstein R.F. and Stryer L. "Cooperative polymerization reactions: analytical approximations, numerical examples, and experimental strategy" *Biophys. J.* **50**, 583–599, 1986.

[50] Powers E.T. and Powers D.L. "The kinetics of nucleated polymerizations at high concentrations: amyloid fibril formation near and above the supercritical concentration" *Biophys. J.* **91**, 122–132, 2006.

[51] Smith M.I., Sharp J.S. and Roberts C.J. "Nucleation and growth of insulin fibrils in bulk solution and at hydrophobic polystyrene surfaces" *Biophys. J.* **93**, 2143–2151, 2007.

[52] Knowles T.P., Shu W., Devlin G.L., Meehan S., Auer S., Dobson C.M. and Welland M.E. "Kinetics and thermodynamics of amyloid formation from direct measurements of fluctuations in fibril mass" *Proc. Natl. Acad. Sci. U S A.* **104**, 10016–10021, 2007.

[53] Waugh D.F. "A fibrous modification of insulin. The heat precipitate of insulin" *J. Am. Chem. Soc.* **68**, 247–250, 1946.

[54] Waugh D.F., Wilhelmson D.F., Commerford S.L. and Sackler M.L. "Studies of the nucleation and growth of selected types of insulin fibrils" *J. Am. Chem. Soc.* **75**, 2592–2600, 1953.

[55] Librizzi F. and Rischel C. "The kinetic behavior of insulin fibrillation is determined by heterogeneous nucleation pathways" *Prot. Sci.* **14**, 3129–3134, 2005.

[56] Manno M., Craparo E., Podestá A. Bulone D., Carrotta R., Martorana V., Tiana G. and San Biagio P.L. "Kinetics of different processes in human insulin amyloid formation" *J. Mol. Biol.* **366**, 258–274, 2007.

[57] Grudzielanek S., Smirnovas V. and Winter R. "Solvation-assisted pressure tuning of insulin fibrillation: from novel aggregation pathways to biotechnological applications" *J. Mol. Biol.* **356**, 497–509, 2006.

[58] Rogers S.S., Krebs M.R.H., Bromley E.H.C., van der Linden E. and Donald A.M. "Optical microscopy of growing insulin amyloid spherulites on surfaces in vitro" *Biophys. J.* **90**, 1043–1054, 2006.

[59] Vestergaard B., Groenning M., Roessle M., Kastrup J.S., van de Weert M., Flink J.M., Frokjaer S., Gajhede M. and Svergun D.I. "A helical structural nucleus is the primary elongating unit of insulin amyloid fibrils" *PLoS Biology* **5**, 1089–1097, 2007.

[60] Smith M.I., Sharp J.S. and Roberts C.J. "Insulin fibril nucleation: the role of prefibrillar aggregates" *Biophys. J.* **95**, 3400–3406, 2008.

[61] Vetri V., Librizzi F., Militello V. and Leone M. "Effects of succinylation on thermal induced amyloid formation in Concanavalin A" *Eur. Biophys. J.* **36**, 733–741, 2007.

[62] Hawe A., Sutter M. and Jiskoot W. "Extrinsic fluorescent dyes as tools for protein characterization" *Pharm. Res.* **25**, 1487–1498, 2007.

[63] Voropai E.S., Samtsov M.P., Kaplevskii K.N., Maskevich A.A., Stepuro V.I., Povarova O.I., Kuznetsova M., Turoverov K.K., Fink A.L. and Uverskii V.N. "Spectral properties of Thioflavin T and its complexes with amyloid fibrils" *J. Appl. Phys.* **70**, 868–874, 2003.

[64] Vassar P.S. and Culling C.F.A. "Fluorescent stains, with special reference to amyloid and connective tissues" *Arch. Pathol.* **68**, 487–498, 1959.

[65] Kelényi G. "Thioflavin S fluorescent and Congo red anisotropic stainings in the histologic demonstration of amyloid" *Acta Neuropathol.* **7**, 336–348, 1967.

[66] Raj Retna C. and Ramaraj R. "Emission of Thioflavin T and its off-on control in polymer membranes" *Photochem Photobiol.* **74**, 752–759, 2001.

[67] Parker A. and Joyce T.A. "Prompt and delayed fluorescence of some DNA dynamics" *Photochem. Photobiol.* **18**, 467–474, 1973.

[68] Shirra R. "Dye aggregation in freezing aqueous solutions" *Chem. Phys. Lett.* **119**, 463–466, 1985.

[69] Margulis L., Rozen H. and Nir S. "Model for competitive adsorption of organic cations on clays" *Clays Clay Miner.* **36**, 270–276, 1988.

[70] Cundall R.B., Davies A.K., Morris P.G. and Williams J. "Factors influencing the photosensitizing properties and photoluminescence of Thioflavin T" *J. Photochemistry* **17**, 369–376, 1981.

[71] Stsiapura V.I., Maskevich A.A., Kuzmitsky V.A., Turoverov K.K. and Kuznetsova I.M. "Computational study of Thioflavin T torsional relaxation in the excited state" *J. Phys. Chem. A* **111**, 4829–4835, 2007.

[72] Maskevich A.A., Stsiapura V.I., Kuzmitsky V.A., Kuznetsova I.M., Povarova O.I., Uversky V.N. and Turoverov K.K. "Spectral properties of Thioflavin T in solvents with different dielectric properties and in a fibril-incorporated form" *J. Proteome Res.* **6**, 1392–1401, 2007.

[73] Naiki H., Higuchi K., Hosokawa M. and Takeda M. "Fluorometric determination of amyloid fibrils in vitro using the fluorescent dye Thioflavin T" *Anal. Biochem.* **177**, 244–249, 1989.

[74] Levine III H. "Thioflavine T interaction with synthetic Alzheimer's disease beta-amyloid peptides: detection of amyloid aggregation in solution" *Prot. Sci.* **2**, 404–410, 1993.

[75] Stsiapura V.I., Maskevich A.A., Kuzmitsky V.A., Uversky V.N., Kuznetsova I.M. and Turoverov K.K. "Thioflavin T as a molecular rotor: fluorescent properties of Thioflavin T in solvents with different viscosity" *J. Phys. Chem. B* **112**, 15893–15902, 2008.

[76] Serpell L.C., Blake C.C. and Fraser P.E. "Molecular structure of a fibrillar Alzheimer's A beta fragment" *Biochemistry* **39**, 13269–13275, 2000.

[77] Jiménez J.L., Nettleton E.J., Bouchard M., Robinson C.V., Dobson C.M. and Saibil H.R. "The protofilament structure of insulin amyloid fibrils" *Proc. Natl. Acad. Sci. USA* **99**, 9196–9201, 2002.

[78] Khurana R., Ionescu-Zanetti C., Pope M., Li J., Nielson L., Ramrez-Alvarado M., Regan L., Fink A.L. and Carter S.A. "A general model for amyloid fibril assembly based on morphological studies using atomic force microscopy" *Biophys. J.* **85**, 1135–1144, 2003.

[79] Krebs M.H.R., Bromley E.H.C. and Donald A.M. "The binding of Thioflavin T to amyloid fibrils: localisation and implications" *J. Struct. Biol.* **149**, 30–37, 2005.

[80] Sabaté R., Lascu I. and Saupe S.J. "On the binding of Thioflavin T to HET-s amyloid fibrils assembled at pH 2" *J. Struct. Biol.* **162**, 387–396, 2008.

[81] Pedersen J.S., Dikov D., Flink J.L., Hjuler H.A., Christiansen G. and Otzen D.E. "The changing face of glucagon fibrillation: structural polymorphism and conformational imprinting" *J. Mol. Biol.* **355**, 501–523, 2006.

[82] Khurana R., Coleman C., Ionescu-Zanetti C., Carter S.A., Krishna V., Grover R.K., Roy R. and Singh S. "Mechanism of Thioflavin T binding to amyloid fibrils" *J. Struct. Biol.* **151**, 229–238, 2005.

[83] Lakowicz J.R. *Principles of fluorescence spectroscopy* Kluwer Academic New York, 1999.

[84] Blanchard C.R. *Atomic Force Microscopy* Springer New York, 1996.

[85] Pignataro B., Sardone L. and Marletta G. "Dynamic Scanning Force Microscopy investigation of nanostructured spiral-like domains in Langmuir-Blodgett monolayers" *Nanotechnology* **14**, 245–249, 2003.

[86] Porter R.R. "Partition chromatography of insulin and other proteins" *Biochem. J.* **53**, 320–328., 1953.

[87] Ahmad A., Uversky V., Hong D. and Fink A. "Early events in the fibrillation of monomeric insulin" *The Journal of Biological Chemistry* **280**, 42669–42675, 2005.

[88] Manno M., Craparo E.F., Martorana V., Bulone D. and San Biagio P.L. "Kinetics of insulin aggregaytion: disentanglement of amyloid fibrillation from large-size cluster formation" *Biophys. J.* **90**, 4585–4591, 2006.

[89] Waugh D.F. "A mechanism for the formation of fibrils from protein molecules" *J. Cell. Physiol.* **49**, 145–164, 1957.

[90] Fandrich M. "Absolute correlation between lag time and growth rate in the spontaneous formation of several amyloid-like aggregates and fibrils" *J. Mol. Biol.* **365**, 1266–1270, 2007.

[91] Ruschak A.M. and Miranker A.D. "Fiber-dependent amyloid formation as catalysis of an existing reaction pathway" *Proc. Natl. Acad. Sci. U.S.A.* **104**, 12341–12346, 2007.

[92] Bishop M.F. and Ferrone F.A. "Kinetics of nucleation-controlled polymerization. A perturbation treatment for use with a secondary pathway" *Biophys. J.* **46**, 631–644, 1984.

[93] Linse S., Cabaleiro-Lago C., Xue W.F., Lynch I., Lindman S., Thulin E., Radford S.E. and Dawson K. "Nucleation of protein fibrillation by nanoparticles" *Proc. Natl. Acad. Sci. U.S.A.* **104**, 8691–8696, 2007.

[94] Grudzielanek S., Velkova A., Shukla A., Smirnovas V., Tatarek-Nossol M., Rehage H., Kapurniotu A. and Winter R. "Cytotoxicity of insulin within its self-assembly and amyloidogenic pathways" *J. Mol. Biol.* **370**, 372–384, 2007.

[95] Grudzielanek S., Jansen R. and Winter R. "Solvational tuning of the unfolding, aggregation and amyloidogenesis of insulin" *J. Mol. Biol.* **351**, 879–894, 2005.

[96] Krebs M.R.H., MacPhee C.E., Miller A.F., Dunlop I.E., Dobson C.M. and Donald A.M. "The formation of spherulites by amyloid fibrils of bovine insulin" *Proc. Natl. Acad. Sci. U.S.A.* **101**, 14420–14424, 2004.

[97] Dzwolak W., Smirnovas V., Jansen R. and Winter R. "Insulin forms amyloid in a strain-dependent manner: an FT-IR spectroscopic study" *Prot. Sci.* **13**, 1927–1932, 2004.

[98] Dzwolak W., Grudzielanek S., Smirnovas V., Ravindra R., Nicolini C., Jansen R., Loksztejn A., Porowski S. and Winter R. "Ethanol-perturbed amyloidogenic self-assembly of insulin: looking for origins of amyloid strains" *Biochemistry* **44**, 8948–8958, 2005.

[99] Hortschansky P., Schroeckh V., Christopeit T., Zandomeneghi G. and Fandrich M. "The aggregation kinetics of Alzheimer's beta-amyloid peptide is controlled by stochastic nucleation" *Prot. Sci.* **14**, 1753–1759, 2005.

[100] Hofrichter J. "Kinetics of sickle hemoglobin polymerization. III. Nucleation rates determined from stochastic fluctuations in polymerization progress curves" *J. Mol. Biol.* **189**, 553–571, 1986.

[101] Brown W. *Light Scattering, principles and development* Oxford, 1996.

[102] Frid P., Anisimov S.V. and Popovic N. "Congo red and protein aggregation in neurodegenerative diseases" *Brain Res. Rev.* **53**, 135–160, 2007.

[103] Mera S.L. and Davies J.D. "Differential Congo red staining: the effects of pH, non-aqueous solvents and the substrate" *Histochem J.* **16**, 195–210, 1984.

[104] Sawaya M.R., Sambashivan S., Nelson R., Ivanova M.I., Sievers S.A., Apostol M.I., Thompson M.J., Balbirnie M., Wiltzius J.J., McFarlane H.T., Madsen A., Riekel C. and Eisenberg D. "Atomic structures of amyloid cross-beta spines reveal varied steric zippers." *Nature* **447**, 453–457, 2007.

Scientific activity

Publications

- Librizzi F., Vetri V., Foderá V., Militello V., Navarra G., Leone M. The role of conformational changes in the aggregation process of proteins, *Curr. Prot. Pept. Sci.*, submitted.

- Foderá V., Cataldo S., Librizzi F., Pignataro B., Spiccia P., Leone M. Self-organization pathways and spatial heterogeneity in insulin amyloid fibrils formation, *J. Phys. Chem. B*, submitted.

- Foderá V., Groenning M., Vetri V., Librizzi F., Spagnolo S., Cornett C., Olsen L., van de Weert M., Leone M. **2008** Thioflavin T hydroxylation at basic pH and its effect on amyloid fibril detection, *J. Phys. Chem. B*, **112** (47) 15174−15181.

- Militello V. Navarra G., Foderá V., Librizzi F., Vetri V., Leone M. **2008** Thermal aggregation of proteins in the presence of metal ions *Biophysical Inquiry into Protein Aggregation and Amyloid Diseases*, **Chapter 7**, 181−232 Editors P.L. San Biagio and D. Bulone, Research Signpost, Kerala, India.

- Foderá V., Librizzi F., Groenning M., van de Weert M., Leone M. **2008** Secondary Nucleation and Accessible Surface in Insulin Amyloid Fibril Formation, *J. Phys. Chem. B* **112** (12) 3853−3858.

- Librizzi F., Foderá V., Vetri V., Lo Presti C., Leone M., **2007** Effects of confinement on insulin amyloid fibrils formation, *European Biophysics Journal* **36** (7) 711−15.

Communications to congresses: talks

- Foderá V., Groenning M., Vetri V., Librizzi F., Spagnolo S., Cornett C., Olsen L., van de Weert M., Leone M. *Thioflavin T hydroxylation kinetic at basic pH*

and its effect on amyloid fibril detection XIX SIBPA Congress Roma Italy, September **2008**.

Communications to congresses: posters

- Foderá V., Librizzi F., Vetri V. and Leone M. *Early stages and spatial heterogeneity in insulin amyloid fibrils formation* XIX SIBPA Congress, Roma Italy, September **2008**.

- Vetri V., Foderá V., D′Amico M., Leone M. and Militello V. *Thermally induced Fibrillar Aggregation of Bovine Serum Albumin* XIX SIBPA Congress, Roma Italy, September **2008**.

- Vetri V., Librizzi F., Militello V., Foderá V. and Leone M. *Molecular mechanisms involved in thermally induced amyloid formation of Concanavalin A*, 2nd International Conference on Molecular Perspectives on Protein−Protein Interactions, Croatia Hotel, Dubrovnik, June 27-July 1, **2008**.

- Foderá V., F. Librizzi, M. Groenning, M. van de Weert, V. Vetri and M. Leone *Nucleation mechanism and spatial heterogeneity in Insulin Amyloid Fibril Formation*, 2nd International Conference on Molecular Perspectives on Protein-Protein Interactions Croatia Hotel, Dubrovnik, June 27-July 1, **2008**.

- Ricca M., Buscarino G., Amenta M., Vetri V., Foderá V., Leone M., *Thermal induced oxidative process in Sicilian olive oil investigated by optical and EPR spectroscopy*, Food and Chemistry Congress, Praga, Czech Republic, November **2007**.

- Librizzi F., Foderá V., Groenning M., van de Weert M. and Leone M. *Secondary Nucleation and Accessible Surface in Insulin Amyloid Fibril Formation*, 12th ECSBM Bobigny (Paris Region) France, September **2007**.

- Foderá V., F. Librizzi, V. Vetri, C. Lo Presti and M. Leone *Effects of confinement on insulin amyloid fibrils formation*, XVIII SIBPA Congress, Terrasini (Palermo) Italy, September **2006**.

- Foderá V., Lo Presti C., Librizzi F., Vetri V., Dispensa C., Spadaro G. and Leone M. *Internal properties of $\gamma-$irradiated polymeric hydrogels studied by means of fluorescent probes*, XVIII SIBPA Congress, Terrasini (Palermo) Italy, September **2006**.

- Foderá V., Lo Presti C., Librizzi F., Vetri V., Dispensa C., Spadaro G. and Leone M. *Internal properties of $\gamma-$irradiated polymeric hydrogels studied by means of fluorescent probes*, 11th Tihany Symposium on Radiation Chemistry, Eger, Hungary, August **2006**.

Stages

- **November 2007-March 2008:** Fellowship for Guest PhD student (Drug Research Academy) at the Department of Pharmaceutics and Analytical Chemistry, University of Copenhagen, Denmark. Supervisor: Prof. Marco van de Weert.
- **March-May 2007**: Stage at the Department of Pharmaceutics and Analytical Chemistry, University of Copenhagen, Denmark. Supervisor: Prof. Marco van de Weert.
- **January-July 2006:** Fellowship for a stage at the Department of Pharmaceutics and Analytical Chemistry (DFU), Copenhagen, Denmark. Supervisor: Prof. Marco van de Weert.

Awards

- Prize *Sergio Ciani* for the best poster *Effects of confinement on insulin amyloid fibrils formation* XVIII SIBPA Congress Terrasini (Palermo) Italy, September **2006**.

Attended schools

- Multidimensional Optical Fluorescence Microscopy towards Nanoscopy, 19−29 April 2008, Erice, Italy.
- Probing the Nanoworld: Microscopies, Scattering and Spectroscopies of the Solid State, 12−23 March 2007, Julich Germany.
- Research with Neutron and Synchrotron Radiation, 5−9 March 2007, Sportheim Planneralm Styria, Austria.

Attended courses

- Raman spectroscopy applied to amorphous systems, Palermo 2007.

- Thermodynamic Statistics at Equilibrium, Palermo 2007.
- Statistical Physics, Palermo 2006.
- Radiation−Matter interactions, Palermo 2006.
- Receptor Structure and Function, Copenhagen 2006

Acknowledgments

Humans use to meet each others in very strange and accidental circumstances, through unimaginable connections and with unpredictable ending. Scientific research groups are generally composed by humans and, as a consequence, may also start randomly collaborating with each others without really knowing the kind of final results they can reach together. Sometimes humans involved in such scientific collaborations are also lucky, and this was exactly my case.

This work is the result of an intense and incessant collaboration between my group at the Department of Physical and Astronomical Sciences of the University of Palermo and the Faculty of Pharmaceutical Sciences, University of Copenhagen. Working in two different places makes difficult, and maybe behind my possibilities, listing and properly thanking the huge number of people that has been involved in different extent in my PhD project.

Firstly, I sincerely thank my supervisor Prof. Maurizio Leone, for his guidance and for the uncommon opportunity he gave me to experience new scientific reality. His suggestions and exhortations will be precious reference points in whatever I'll do in my future.

Working in a lab for many hours per day and sitting on a chair looking for the interpretation of the data are things that need to be learned and you can not know them *a priori*. For this, I'm particularly grateful to my friends Dr. Valeria Vetri and Dr. Fabio Librizzi. They carefully introduced me to the scientific world, being a support and an inexhaustible source of experience and knowledge during my entire stay in the laboratories in Palermo. I will always be indebted to them.

I would also like to thank the two others members of the group, Prof. Valeria Militello and Dr. Giovanna Navarra and the people at the Biophysics Institute (National Council of the Research) in Palermo.

Flying to the northern part of Europe: I will always be indebted also to the people of the Biomacromolecules Group at the Department of Pharmaceutics and Analytical Chemistry of Copenhagen. First of all, I have to address my gratitude to Prof. Sven Frokjær for his kindness to give me the opportunity to be in touch with a such challenging research group. Without him, this collaboration would have never

started.

Working at BMM meant to closely meet two brilliant and acute persons: Prof. Marco van de Weert and Dr. Minna Groenning Jensen. Both of them helped me in getting used to work and live in another country. Their scientific and human support will always have a special place in my mind.

A special thank to Prof. Bente Vestergaard (Department of Medicinal Chemistry, University of Copenhagen) for her capacity to continuously transfer to me joy of living and her uncommon will to overcome any difficulty.

I am also grateful to the Danish company Novo Nordisk A/S and, in particular, to Morten Schlein for his care and professionalism during our scientific collaboration.

I also thank Prof. Lorenzo Cordone (University of Palermo) and Prof. Daniel Otzen (University of Århus) for kindly reviewing this thesis.

Taking care of a laboratory and of the instrumentation is always a quite important job: I thank Daniele Francofonte and Gianluca Napoli (University of Palermo) and Karina Juul Vissing (University of Copenhagen) for their careful technical assistance.